RE – OS AND PGE GEOCHEMISTRY OF ORGANIC-RICH SEDIMENTARY ROCKS AND PETROLEUM

ALEXANDER JAMES FINLAY

RE – OS AND PGE GEOCHEMISTRY OF ORGANIC-RICH SEDIMENTARY ROCKS AND PETROLEUM

ALEXANDER JAMES FINLAY

A THESIS SUBMITTED IN PARTIAL FULFILMENT OF THE REQUIREMENTS FOR THE DEGREE OF DOCTOR OF PHILOSOPHY AT DURHAM UNIVERSITY.

DEPARTMENT OF EARTH SCIENCES
DURHAM UNIVERSITY
2010

ABSTRACT

The research in this thesis is presented in paper format with each of four chapters representing one complete study. Chapter two presents Re–Os and geochemical fingerprint data for UK Atlantic margin oils. organic and $\delta^{13}C$ geochemical data demonstrate that the oil is sourced from Upper Jurassic marine shales and the Re–Os data yields an age of 68 ± 13 Ma. Comparison of this date with published basin histories and Ar-Ar geochronology demonstrate that Re–Os ages correspond with the timing of oil generation. Furthermore the similarities between oil and source rock $^{187}Os/^{188}Os$ at the time of oil generation (Os_g) indicates that Os_g can be used to identify oil source units.

Chapter three demonstrates, through the analysis of Kimmeridge Clay Fm. core and North Sea oil, that unradiogenic mantle like values within oils from wells in the Viking Graben and East Shetland Basin cannot be inherited from source. It is hypothesised that they are caused by contamination by a hydrothermal fluid sourced from either Cenozoic intrusive units or the mantle. Strain localisation is suggested to have caused the main basin bounding faults within the Viking Graben and East Shetland Basin to be of sufficient depth to act as conduits for hydrothermal fluid to propagate through and contaminate oils within reservoirs.

Chapter four investigates how Os_i values across the Ordovician/Silurian boundary GSSP at Dob's Linn, Scotland, tracks the Hirnantian glaciation within a globally important source unit: the Ordovician/Silurian "Hot" Shales. During the Late Katian, Os_i values increase from 0.28 – 1.08, providing evidence for increased silicate weathering of radiogenic continental crust. A decrease to less radiogenic Os_i (~0.60) occurs at the base Hirnantian and marks the onset of the Hirnantian Glaciation. This is ascribed to Hirnantian ice cover and reduced chemical weathering rates cutting the supply of radiogenic material. In the Late Hirnantian an abrupt increase in Os_i values to ~1.1 over 19 cm of stratigraphy, is attributed to the leaching of exposed radiogenic glacial deposits and increased weathering of silicate terrane during deglaciation.

Chapter five applies the Platinum Group Elements, specifically Pt/Pd ratios, to identify oil source units. It is demonstrated that asphaltenes from the well constrained UK Atlantic margin petroleum system contain similar Pt/Pd and Os_g values to the known source unit. A further study of the poorly constrained West Canadian Tar Sands demonstrates that Pt/Pd ratios in source rocks are not affected by hydrocarbon maturation and are distinct between differing potential source units. Comparison of the Tar Sands with potential source units demonstrates that the Tar Sands are mainly sourced from the Lower Jurassic Gordondale Fm., with minor input from the Devonian/Mississippian Exshaw Fm.

DECLARATION

I declare that this thesis, which I submit for the degree of Doctor of Philosophy at Durham University, is my own work and not substantially the same as any which has previously been submitted at this or any other university.

Alexander Finlay
Durham University
May 2010

ACKNOWLEDGEMENTS

I would like to thank my main supervisor, Dave Selby, firstly for taking me on to do this PhD and then for putting up with me for the last three and a half years. You have been a great boss and golfing buddy, especially when I manage to win. Although possibly one of the most annoying things to hear from you, "just run a few more samples" has made this a much better thesis. Here's to two more years! Thanks also to my supervisor at BP, Mark Osborne, for getting the CASE funding sorted out. Also may thanks for having me down to BP a few times to chat about what my research really means outside of academia. The idea that this thesis may have some industrial use has been a real help over the last 3 years. Many thanks have to go to Graham for also supervising me. Although actual supervision has not been too interactive, when ever I have turned up with a question the feed back has been extremely helpful.

I also need to thank all of those who have been unfortunate enough to share a lab with me. Geoff Nowell and Chris Ottley need a special mention for their help on the Mass Spectrometry side of things. The Chris's Ottley and Dale are also especially thanked with their help with the PGE study, whether it involved number crunching, chemistry or trying to get an asher to work! Gary Wilkinson and Dave Stevenson are also thanked for their help with computers.

This thesis is comprised of 4 papers and I would like to thank John Gluyas, Jonny Imber, Howard Armstrong, Richard Davies and Chris Dale for there advice on manuscript preparation. Tom Challands is also thanked for his assistance in the field at Dob's Linn. From BP I would also like to thank Dan Finucane and Stephen Crawley for providing biostratigraphical and C isotope data for this project.

Importantly I need to especially thanks my parents for there constant support and help. Although not surprisingly you both admit to struggle a wee bit with isotope geochemistry, having a place to go and relax when needed, and even get fed, was invaluable. Also to my friends who have been helped, either unwinding over the occasional Friday night pint or cup of tea, cheers.

Finally, thanks to everyone who help me in any way but I have not mentioned specifically. I'm sure that if you are reading this and have written a thesis yourself you will understand that all I want to do now is get this submitted, if you haven't yet, you will. So I'm sorry if I have forgotten to mention you, give me a kick and I'll get you a beer to make up.

TABLE OF CONTENTS

LIST OF ABBREVIATIONS

CBM – Ceramic Building Material
$\delta^{13}C$ – Carbon isotope value reported in standard delta notation relative to the VPDB scale
ESB – East Shetland Basin
GC – Gas chromatography
GCMS – High-resolution gas chromatography mass spectrometry
GSSP – Global Stratotype Section and Point
HICE – Hirnantian isotopic carbon excursion
HPLC – High performance liquid chromatography
HSE – Highly siderophile element
I/S – Illite/Smectite ratio
KCF – Kimmeridge Clay Formation
MF – Moray Firth
MSWD – Mean standard weighted distribution
NCIET – Northern Centre for Isotopic and Elemental Tracing
ORS – Organic rich shale
Os_g – $^{187}Os/^{188}Os$ at the time of oil generation
Os_i – Initial $^{187}Os/^{188}Os$ calculated at the time of deposition
PGE – Platinum group element
Ph – Phytane
ppb – Part per billion (ng/g)
ppt – Part per trillion (pg/g)
Pr – Prystane
SDO-1 – USGS Devonian Ohio Shale standard
TOC – Total organic carbon
UCC – Upper continental crust
UKAM – United Kingdom Atlantic margin
VG – Viking Graben
VPDB – Vienna Pee Dee Belemnite
WCSB – West Canadian Sedimentary Basin
WCTS – West Canadian Tar Sands
WMFZ – Western margin fault zone

1. INTRODUCTION

A common problem for petroleum exploration is understanding the spatial and temporal controls on hydrocarbon formation. Dating the timing of hydrocarbon generation in petroleum exploration has mainly been carried out through the use of basin modelling often with enigmatic parameters (e.g. Lamers and Carmichael, 1999 and Scotchman et al., 2006 for the UK Atlantic Margin). Therefore knowing the absolute age of petroleum generation provides vital information and controls on the understanding of a petroleum system. Furthermore knowing the source of petroleum can provide invaluable data to model migration pathways and so identify possible undiscovered traps.

Rhenium – Osmium geochronology is based on the β decay of ^{187}Re to ^{187}Os over a half life of ~44Ga (Cohen, 2004) and is dissimilar to other lithopyllic geochronometers (e.g. Rb-Sr, U-Pb, Sm-Nd, Lu-Hf) in that Re and Os are siderophillic. Furhtermore, both Re and Os have an "organophyllic" affinity meaning that they are enriched in organic rich sedimentary units (e.g. black shales, the main source of oil) relative to Upper Continental Crust (UCC; Pegram et al., 1992; Esser and Turekian, 1993; Peucker-Ehrenbrink and Jahn, 2001; Ravizza and Peucker-Ehrenbrink, 2003; Sun et al., 2003; Dalai et al., 2006; Oxburgh et al., 2007). Assuming that the $^{187}Os/^{188}Os$ composition at the time of deposition is constant, and the sample Re – Os systematics are undisturbed, the $^{187}Re/^{188}Os$ and $^{187}Os/^{188}Os$ ratios of samples will positively correlate and form an isochron age using the following equation;

$$\left(\frac{^{187}Os}{^{188}Os}\right)_{present} = \left(\frac{^{187}Os}{^{188}Os}\right)_{initial} + \left(\frac{^{187}\mathrm{Re}}{^{188}Os}\right) * \left(e^{\lambda t} - 1\right)$$

where λ is the ^{187}Re decay constant ($1.666 \times 10^{-11} a^{-1}$; Smoliar et al., 1996) and t is the age (e.g. Dickin 1995). Therefore, by using this isochron dating technique, the depositional age of black shales can be calculated (Ravizza and Turekian, 1989; Cohen et al., 1999; Peucker-Ehrenbrink and Hannigan, 2000; Creaser et al., 2002; Jaffe et al., 2002; Selby and Creaser, 2003; Kendall et al., 2004; Selby and Creaser, 2005; Hannah et al., 2004; Yang et al., 2004; Selby, 2007; Turgeon et al., 2007; Azmy et al., 2008; Selby et al., 2009; Kendall et al., 2009a&b).

There are three sources of Re and Os in a black shale, hydrogenous, detrital and extraterrestrial. Under oxic conditions both Re and Os are soluble in sea water, however, under anoxic conditions Re and Os become insoluble. Therefore, in anoxic

marine conditions, sediment at the sea-floor/seawater interface become enriched in hydrogenous Re and Os, with the $^{187}Os/^{188}Os$ composition reflecting seawater conditions at the time of deposition (e.g. Cohen 2004). When the sediment is cut off from interacting with anoxic sea water the Re – Os system becomes closed and the isotopic clock commences recording the age of deposition. Like the majority of metals it is uncertain in which organic fraction Re and Os reside, however it is likely that they are contained within metalloporphyins and heteratomic ligands (Selby et al., 2007). The Carius tube Cr-H2SO4 digestion method, utilised in this thesis for Re – Os analysis (see below), has been demonstrated to digest the organic fraction of black shale, with minimal detrital and extraterrestrial input (Selby and Creaser, 2003). Therefore by analysing the hydrogenous Re – Os composition of shale it is possible to not only provide a depositional age, but also calculate the sea water Os isotopic composition at the time of deposition.

The four dominant sources of Os to the oceans are riverine and aeolian input from denuded continental crust, cosmic material and hydrothermal fluids. Hydrothermal fluids and cosmic material have unradiogenic Os isotopic compositions of 0.127 (Peucker-Ehrinbrink and Ravizza 2000; Cohen, 2004) where as continental crust varies from unradiogenic (~0.13; young) to radiogenic (~1.9; ancient) with an average value of ~1.4 (Peucker-Ehrinbrink and Ravizza 2000; Cohen, 2004). Therefore the Os isotopic composition of sea water is controlled by the differing fluxes of each source. For example, if there is increased mafic volcanism (e.g. from a large igneous province) or a meteorite event the Os isotopic composition of sea water will be unradiogenic (i.e. low $^{187}Os/^{188}Os$), whereas if there is increased denudation of cratonic crustal material sea water will be radiogenic (i.e. high $^{187}Os/^{188}Os$; Peucker-Ehrinbrink and Ravizza 2000; Cohen, 2004).

Petroleum maturation has been demonstrated to not observably disturb source rock Re – Os systematics (Selby et al., 2007 and references there in), likely due to the minor amounts of Re and Os being transferred to the generated oil (e.g. ~1-5 ppb Re). Re and Os have been demonstrated to be enriched in the asphaltene fraction of oil and, importantly, both the Re and Os isotopic compositions of an asphaltene are similar to those of the oil it is separated from (Selby et al., 2007). Therefore it is possible to analyse the asphaltene fraction of oil (and so have larger sample Re and Os) and be confident that the Re – Os isotopic compositions reflect that of whole oil. To date only two petroleum Re – Os studies have been undertaken, firstly on the West Canadian Tar Sands (111.6 ± 5.3 Ma; Selby and Cohen, 2005) and Bitumin from the Polaris

Mississippi Valley Type Deposit (374.9 ± 9 Ma; Selby et al., 2005). The 111.6 ± 5.3 Ma age of the West Canadian Tar Sands agrees with proposed basin models (Barson et al., 2000; Riediger et al., 2000) and 374.9 ± 9 Ma age of Polaris bitumen agrees within uncertainty of previous Rb – Sr sphalerite ages (~366; Christensen et al., 1995). Therefore, it is hypothesised that Re – Os Petroleum ages record the timing of generation (Selby and Creaser, 2005; Selby et al., 2005; Selby et al., 2007). However, the source of both the WCTS and Polaris bitumens are highly debated (e.g. generation of WCTS at 60 Ma, Cao and Bachu, 1992, as opposed to ~110 Ma, Barson et al., 2000; Riediger et al., 2000), consequently, we can not be certain if the Re – Os ages record petroleum generation, migration or emplacement.

Oil – source fingerprinting is commonly carried out through utilising C isotopes, the *n*-alkanes, Hopane and Sterane biomarker analysis (e.g. Peters et al., 1999). When oils have been severely biodegraded these methods can not be utilised as biodegradation mainly affects the light organic fraction and increases the asphaltene fraction (e.g. Speight, 1998; Peters et al., 2005). Greater than 90 % of Re and Os are found in the asphaltene fraction of an oil and it has been hypothesised that the $^{187}Os/^{188}Os$ of oil at the time of generation (Os_g) is inherited from the source rock $^{187}Os/^{188}Os$ at the time of generation (Os_g; Selby and Creaser, 2005; Selby et al., 2005; Selby et al., 2007). Therefore if this hypothesis is correct, Os isotopes can be used to fingerprint both biodegraded and unbiodegraded oils. Furthermore the Platinum Group Elements (PGE; Pt, Ir and Pd) are enriched in ORS and oil (Coveney et al., 1992 Colodner et al., 1992; Over et al., 1997; Sawlowics, 1999; Pearson and Woodland, 2000 Jaffe et al., 2002; Juvonen et al., 2002; Pasava et al., 2003; Meisel and Moser, 2004; Siebert et al., 2005; Schmitz et al., 2006; Fedorov et al., 2006; Jiang et al., 2006; Wille et al., 2007; Qi and Gao, 2008) Therefore as the PGEs share the same organophyllic and siderophillic characteristics as Re and Os it is possible that they can also provide an oil – source fingerprinting tool.

Rhenium and Os analysis is complex and time consuming. All Re – Os analysis in this thesis is a was conducted at the Northern Centre for Isotopic and Elemental Tracing facility at Durham University following the analytical protocols of Selby and Creaser (2003); Selby (2007) and Selby et al. (2007).

Oils and oils and asphaltenes were digested, using the carius tube technique (Shirey and Walker, 1995). ~0.1 – 0.2 g of asphaltene was dissolved with a known volume of ^{190}Os and ^{185}Re spike solution in 9 ml of inverse *aqua regia* (6 ml of 16 N HNO_3 and 3 ml of 12 N HCl) at 220°C for 24 hrs. Osmium was purified from the

inverse *aqua regia* solution using solvent extraction ($CHCl_3$) and micro-distillation methods. After the removal of Os, the Re bearing inverse *aqua regia* solution was evaporated to dryness at 80˚C and then re-dissolved in 3 ml 0.2 N HNO_3 in preparation for Re anion exchange chromatography (e.g. Selby and Creaser 2003).

Shale samples were prepared by removing any drill core marks with a diamond polishing wheel, to avoid surface contamination, and then powdered in a ceramic mill to ensure Re and Os sample homogenisation. The analytical methodology varies from that of oil with ~0.5 g of whole rock powder was dissolved with a known volume of ^{190}Os and ^{185}Re mixed tracer (spike) solution in 8 ml of 0.25 g/g CrO_3 in 4N H_2SO_4 at 220°C for 48 hrs in carius tubes. Osmium was purified from the CrO_3-H_2SO_4 solution using solvent extraction ($CHCl_3$) and micro–distillation methods (e.g. Selby and Creaser 2003). After the removal of Os, 1 ml of the CrO_3–H_2SO_4 was mixed with 1 ml of Milli–Q water and reduced from Cr^{6+} to Cr^{3+} by sparging with SO_2 in preparation for Re anion exchange chromatography. After chromatography the Re fraction was then further purified by single bead anion extraction.

The purified Re and Os from both asphaltene and shale samples were loaded onto a Ni and Pt filaments respectively, and analysed for their isotopic compositions using Negative Thermal Ionisation Mass Spectrometry (NTIMS; Creaser et al., 1991) on a ThermoElectron (TRITON) mass spectrometer. Re was measured using Faraday collectors and Os in peak hopping mode using a secondary electron multiplier.

This thesis aims to utilise a suite of the Highly Siderophile Elements (Re, Os, Pt, Pd and Ir) to further our understanding of petroleum systems through:

1. Identifying if Re – Os oil ages are dating petroleum generation, migration or emplacement.
2. Investigating how the Re – Os petroleum system can be disturbed naturally
3. Investigating palaeoclimatic effects on sea water Os isotope composition and therefore variability in source rock Os_i.
4 Investigating the applicability of applying other HSEs (Pt, Ir and Pd) as an oil to source fingerprint.

The research in this thesis is presented in paper format with each chapter representing 1 complete study. Chapter 2 presents a geochronological study of the UK Atlantic Margin oil fields entitled “Rhenium-Osmium geochronology of UK Atlantic Margin oil: Implications for global petroleum systems”. A version of this chapter has

been submitted for publication in the journal *Geology* co-authored by Selby (supervisor) and Osborne (BP Supervisor). Finlay undertook project setup, sample preparation, geochemical analysis and data interpretation and manuscript composition. Selby provided supervision and manuscript editing advice. Osborne provided petroleum samples for analysis, supervision and manuscript editing advice.

Chapter 3 presents a geochemical study of North Sea oil and source rock and is entitled "Fault charged hydrothermal fluid contamination of U.K. North Sea oils: Insights from Re-Os isotopes." A version of this chapter has been accepted for publication in the journal *Geology*, co-authored by Selby, Osborne and Finucane. Finlay undertook project setup, sample preparation, Re – Os analysis, geochemical data interpretation and manuscript composition. Selby provided supervision and manuscript editing advice. Osborne provided samples for analysis, $\delta^{13}C$ data from BP, supervision and manuscript editing advice. Finucane provided biostratigraphical analysis and interpretation.

Chapter 4 presents a Re – Os and $\delta^{13}C$ investigation of the basal Silurian GSSP entitled "Tracking the Hirnantian glaciation using Os isotopes." A version of this chapter has been accepted for publication in the journal *Earth and Planetary Science Letters*, co-authored by Selby and Gröcke. Finlay formulated the project, undertook fieldwork, sample preparation, Re – Os analysis, multi isotope data interpretation and manuscript composition. Selby provided supervision and manuscript editing advice. Gröcke provided $\delta^{13}C$ analysis and manuscript editing advice.

Chapter 5 presents the use of the PGEs as an oil source tracer entitled "PGE fingerprinting of oils to source in world wide petroleum systems". A version of this chapter is in preparation for submittal to Science, co-authored by Selby and Osborne. Finlay undertook project set up, sample preparation, geochemical analysis, data interpretation and manuscript composition. Selby provided WCTS and WCSB samples for analysis, Re – Os data for the UK Atlantic margin shales, supervision and manuscript editing advice. Osborne provided UK Atlantic Margin petroleum samples for analysis, supervision and manuscript editing advice.

The objective of chapter 2 is to understand if Re – Os petroleum geochronology is dating the timing of oil generation, migration or emplacement. Previous Re – Os petroleum studies suggest that the ages produced date generation and migration (Alberta Tar sands; Selby and Creaser, 2005; Polaris Mississippi Valley Type deposit; Selby et al., 2005). However, these studies have been undertaken on areas with ambiguous source units, therefore leaving this question open to debate. The UK Atlantic Margin

(Fig. 1.1) is predominantly sourced from an Upper Jurassic, marine, organic rich shale (equivalent to the North Sea Kimmeridge Clay Fm.) with a slight input from Mid-Jurassic shallow marine/terrestrial shale (Spencer et al., 1999; Mark et al., 2008; Scotchman et al., 2006; Leach et al., 1999; Lamers and Carmichael, 1999; Scotchman and Carr, 2005; Parnell et al., 2005; Hols et al., 1999; Rooney et al., 1998; Cornford et al., 1998; Scotchman et al., 1998; Mark et al., 2005; Scotchman et al., 2006), therefore analysis of oils from this area can answer this question. This study presents Re–Os data for 18 oils from the Clair, Schiehallion, Cuillin and Foinaven fields of the UK Atlantic margin. This study also present a geochemical fingerprint of the oils utilised in this study which confirms an Upper Jurassic marine shale source. When compared to published basin histories and absolute geochronology (Mark et al., 2005; Scotchman et al., 2006; Lamers and Carmichael 1999) we demonstrate that Re-Os ages correspond with the timing of oil generation in the UK Atlantic margin. Our data confirms the hypothesis that Re–Os oil geochronology records the timing of petroleum generation. Furthermore, we build on the hypothesis of Selby and Creaser (2005), Selby et al. (2005) and Selby et al. (2007) that the Os isotopic composition of oil is related to the source unit and can therefore act as a fingerprint.

Chapter 3 tests a controversial hypothesis that unradiogenic Os isotope values reported from the Brent Oil Field (UK North Sea; Fig. 1.1.) are inherited from an unknown late Jurassic source (Graham et al., 2006). This is carried out through the analysis of thirteen oils sourced from throughout the Northern North Sea and a Kimmeridge Clay Formation core, the known major source of North Sea oil, to produce Os isotope compositions calculated at the timing of generation. Eight oils from the Moray Firth and Central Graben contain radiogenic Os isotope compositions as expected from the Kimmeridge Clay Formation source, however, five oils sourced from the Viking Graben and East Shetland Basin contain unradiogenic, mantle like, Os values similar to those reported for the Brent Oil Field. This study proposes an alternative hypothesis in that the unradiogenic Os isotopic values from the Viking Graben and East Shetland Basin are caused by contamination from hydrothermal fluids either sourced from intrusive mafic units or the mantle, not inheritance from an unknown source. The Viking Graben and East Shetland Basin have undergone increased crustal thinning and strain localisation, compared to the Moray Firth and Central Graben, allowing and increased intrusive mafic volcanism and boundary faults to propagate to sufficient depth to act as conduits for hydrothermal fluids to interact and contaminate oils in the Viking Graben and East Shetland Basin. This hypothesis is

supported by published studies of the Miller, Sleipner and Magnus oil fields which record mantle like $\delta^{13}C_{CO2}$, He and Ne isotopic values (James 1990; Ballentine et al., 1996; Lu et al., 2009)

Both Chapters 2 and 3 demonstrate that the Osmium isotopic composition of undisturbed oil is inherited from source. Chapter 4 investigates to what extent and over what time the initial $^{187}Os/^{188}Os$ Os isotope composition at the time of deposition (Os_i) can vary within a shale section at the Ordovician/Silurian Global Stratotype Section and Point (GSSP), Dob's Linn, Scotland. Ordovician/Silurian organic rich marine shales form major global source units (e.g. Lunig et al., 2000). The climate changed from greenhouse to icehouse over the Late Ordovician – Early Silurian, resulting in glaciation and the second largest recorded mass extinction, followed by a return to greenhouse conditions (Trotter et al., 2008). Furthermore as this section contains a GSSP it has been heavily studied and has excellent biostratigraphic constraints, making it an ideal section to test. We present Re – Os and $\delta^{13}C$ data which track geodynamic processes throughout this period. The new Os_i data provides evidence for a period of increased silicate weathering of radiogenic continental crust, most likely from the Caledonian Orogeny (the likely driving mechanism for the drawdown in atmospheric CO_2 and global cooling that resulted in the onset of the Hirnantian Glaciation). This is followed by a decrease to less radiogenic Os_i at the base Hirnantian which coincides with the trend to more positive $\delta^{13}C_{org}$ values that mark the onset of the Hirnantian Glaciation. The Os_i stays constant during the glacial maximum, followed by a rapid increase in Os_i which coincides with the deglacial limb of the $\delta^{13}C_{org}$ profile (0.5 Os_i units over 19 Cm). This study demonstrates the first use of $^{187}Os/^{188}Os$ chemostratigraphy for the Paleozoic as a proxy for reconstructing the Earth's climate system, particularly palaeoceanography and demonstrates that Os_i can be highly variable in a short amount of stratigraphy.

Chapters 2, 3 and 4 have all dealt with the Re – Os system to provide further information on the spatial and temporal constraints of petroleum systems. Chapter 5 tests if other Platinum Group Elements (PGEs), specifically Pt and Pd, can be used to further spatial constraints on petroleum systems by being used as an oil source fingerprint. A study of the UK Atlantic Margin oils and the known Kimmeridge Clay Fm. source unit demonstrate that Pt/Pd values are similar in oil sand source. Therefore it is likely that Pt/Pd values in oils are inherited from source. A further study of the West Canadian Tar Sands and potential oil source units, demonstrates that Pt/Pd ratios in source rocks are; not affected by hydrocarbon maturation; similar within the same

source unit; and that Pt/Pd values between differing source units are distinct. Therefore by combining Pt/Pd with the $^{187}Os/^{188}Os$ composition at the time of hydrocarbon generation (Os_g), within oils and source units of the West Canadian Tar Sands, the Gordondale Fm. is demonstrated to be the main source with a minor input from the Exshaw Fm.

References

Azmy, K., Kendall, B., Creaser, R.A., Heaman, L, de Oliveira, T.F. 2009. Global Correlation of the Vazante Group, Sao Francisco Basin, Brazil: Re-Os and U-Pb radiometric age constraints. Precamb. Res. 164, 160 – 172.

Ballentine, C.J., O'Nions, R.K., Coleman, M.L. 1996. A Magnus opus: Helium, neon, and argon isotopes in a North Sea oilfield. Geochim. Cosmochim. Acta 60, 831-849.

Barson, D., et al., Hydrogeology of heavy oil and tar sand deposits: Water flow and supply, migration and degradation, Field Trip Notes (Geological Survey of Canada, 2000), Open File Report 3946.

Cao, S., Bachu, S. 1992. Use of a quantitive basin analysis system in the evalution of hydrocarbon generation, migration and accumulation (Proceedings of the world petroleum congress, Wiley).

Cohen, A.S., 2004 The rhenium-osmium isotope system: applications to geochronological and palaeoenvironmental problems. J. Geol. Soc. Lond. 161, 729 – 734.

Cohen, A.S., Coe, A.L., Bartlett, J.M., Hawkesworth, C.J. 1999. Precise Re–Os ages of organic-rich mudrocks and the Os isotope composition of Jurassic seawater. Earth Planet. Sci. Lett 167, 159 – 173.

Colodner, D.C., Boyle, E.A., Edmond, J.M., Thomson, J. 1992 Post-depositional mobility of Platinum, iridium and rhenium in marine sediments. Nature, 358, 402 – 404.

Cornford, C., 1998. Source rocks and hydrocarbons of the North Sea. In Glennie, K.W. (Editor), Petroleum Geology of the North Sea. Blackwell Science, Oxford, p. 376-462.

Coveney, R.M., Murowchick, J.B., Grauch, R.I., Glascock, M.D., Denison, J.R., 1992. Gold and platinum in shales with evidence against extraterrestrial sources of metals. Chem. Geol. 99. 101-114

Creaser, R.A., Sannigrahi, P., Chacko, T., Selby, D. 2002. Further evaluation of the Re-Os geochronometer in organic-rich sedimentary rocks: A test of hydrocarbon maturation effects in the Exchaw Formation, Western Canada Sedimentary Basin. Geochim. Cosmochim. Acta 66, 3441 – 3452.

Dalai, T.K., Ravizza, G.E., Peucker-Ehrenbrink, B., 2006. The Late Eocene 187Os/188Os excursion: Chemostratigraphy, cosmic dust flux and the Early Oligocene glaciation. Earth Planet. Sci. Lett. 241, 477–492.

Dickin, A.P., 1995.Radiogenic isotope geology. (Cam. Uni. Press)

Esser, B.K., Turekian, K.K. 1993. The osmium isotopic composition of the continental crust. Geochim. Cosmochim. Acta 57, 3093–3104

Fedorov, Y.N., Ivanov,K.S. Erokhin, Y.V., Ronkin, Y.L. 2007, Inorganic Geochemistry of the Oil of West Siberia: First ICP-MS Data Doklady Akademii Nauk, 414, 385–388.

Graham, S., Karlsen, D.A., Dypvik, H., Andersen, T., Backer-Owe, K. 2006. Re–Os variations in North Sea shales and oils. Geochim. Cosmochim. Acta 70, A211.

Hannah, J.L., Bekker, A., Stein, H.J., Markey, R.J., Holland, H.D. 2004. Primitive Os and 2316 Ma age for marine shale: implications for Paleoproterozoic glacial events and the rise of atmospheric oxygen. Earth Planet. Sci. Lett. 225, 43 – 52.

Holmes, A.J. 1999. The Jurassic petroleum system of the West of Britain Atlantic margin – an integration of tectonics, geochemistry and basin modelling. In: Fleet, A.J. & Boldy, S.A.R. (eds) Petroleum Geology of Northwest Europe: Proceedings of the 5th Conference, 1351-1365. (Geol. Soc. Lon. 1999).

Jaffe, L.A., Peucker-Ehrenbrink, B., Petsch, S.T. 2002. Mobility of rhenium, platinum group elements and organic carbon during black shale weathering. Earth Planet. Sci. Lett. 198, 339-353.

James, A.T. 1990.. Correlation of reservoired gases using the carbon isotopic compositions of wet gas components. AAPG Bull. 74, 1441 – 1458.

Jiang, S-Y., Yang, J-H., Ling, H-F., Chen, Y_Q., Feng, H_Z., Zhao, K-D., Ni, P., 2007. Extreme enrichment of polymetallic Ni–Mo–PGE–Au in lower Cambrian black shales of South China: An Os isotope and PGE geochemical investigation. Palaeogeog., Palaeoclim., Palaeoecol., 254, 217–228.

Lu, J. Wilkinson, M., Haszeldine, S., Fallick, A.E. 2009. Long-term performance of a mudrock seal in natural CO2 storage. Geology 37, 35-38

Juvonen, R., Lakomaa, T., Soikkeli, L. 2002. Determination of gold and the platinum group elements in geological samples by ICP-MS after nickel sulphide fire assay: difficulties encountered with different types of geological samples. Talanta 58 595-603

Kendall, B.S., Creaser, R.A., Ross, G.M., Selby, D.S. 2004. Constraints on the timing of Marinoan "Snowball Earth" glaciation by 187Re–187Os dating of a Neoproterozoic, post-glacial black shale in Western Canada. Earth Planet. Sci. Lett. 222, 729–740.

Kendall, B., Creaser, R.A., Selby, D. 2009a. 187Re – 188Os geochronology of Precambrian organic-rich sedimentary rocks. Geol. Soc. (Lond.)Spec. Pub. 362. 85 – 107.

Kendall, B., Creaser, R.A., Calver, C.R., R, T.D., Evans, D.A.D. 2009b Correlation of Sturtian diamictite successions in southern Australia and northwestern Tasmania by Re – Os black shale geochronology and the ambiguity if "Sturtian" – type diamictite – cap carbonate pairs as chronostratigraphic marker horizons. Precamb. Res. 172, 301 – 310.

Lamers, E., Carmichael, S.M.M. 1999. The Palaeocene deepwater sandstone play West of Shetland. In: Fleet, A.J. & Boldy, S.A.R. (eds) Petroleum Geology of Northwest Europe: Proceedings of the 5th Conference, 645-659. (Geol. Soc. Lon.).

Leach, H.M., Herbert, N., Los, A., Smith, R.L. 1999. The Schiehallion development. . In: Fleet, A.J. & Boldy, S.A.R. (eds) Petroleum Geology of Northwest Europe: Proceedings of the 5th Conference, 683-692. (Geol. Soc. Lon. 1999).

Luning, S., Craig, J., Loydell, D.K., Storch, P., Fitches, B. 2000. Lower Silurian Hot Shales in North Africa and Arabia: Regional distribution and depositional model. Earth Sci. Rev. 49, 121-200.

Mark, D.F., Parnell, J., Kelley, S.P., Lee, M., Sherlock, S.C., Carr, A. 2005 Dating of Multistage Fluid Flow in Sandstones. Science, 309, 2048-2051.

Mark, D.F., Green, P.F., Parnell, J., Kelley, S.P., Lee, M., Sherlock, S.C. 2008 Late Palaeozoic hydrocarbon migration through the Clair field, West of Shetland, UK Atlantic margin. Geochim. Cosmochim. Acta 72, 2510-2533

Meisel, T., Moser, J. 2004 Platinum group elements and rhenium abundances in low abundance reference material. Geostand. Geoanal. Res. 28, 288-250

Over, D.J., Conaway, C.A., Katz, D.J., Goodfellow, W.D., Gregoire, D.C. 1997 Platinum group element enrichments and possible chondritic Ru:Ir across the Fransnian-Famennian boundary, western New York State. Palaeogeog. Palaeoclimate. Palaeoecol. 132 399-410.

Oxburgh, R., Pierson-Wickmann, A.C., Reisberg, L., Hemming, S. 2007. Climate-correlated variations in seawater 187Os/188Os over the past 200,000 yr: Evidence from the Cariaco Basin, Venezuela. Earth Planet. Sci. Lett. 263, 246–258.

Parnell, J., Green, P.F., Watt, G., Middleton, D. 2005. Thermal history and oil charge on the UK Atlantic margin. Pet. Geosci. 11, 99-112.

Pasava, J., Barnes, S-J., Vymazalovia, A. 2003. The use of mantle normalization and metal ratios in the identification of the sources of platinum-group elements in various metal-rich black shales. Min. Dep. 38, 775 – 783.

Pearson D.G., Woodland, S.J. 2000. Solvent extraction/anion exchange separation and determination of PGE's (Os, Ir, Pt, Pd, Ru) and Re-Os isotopes in geological samples by isotope dilution ICP-MS. Chem. Geol. 165, 87-107.

Pegram, W.J., Krishnaswami, S., Raviza, G.E.. Turekian, K.K. 1992. The record of sea water 187Os/186Os variation through the Cenozoic. Earth Planet. Sci. Lett. 113, 569 - 576.

Peters, K. E., Walters, C.C., Moldowan, J. M. 2005. The Biomarker Guide Volume 1: Biomarkers and Isotopes in the Environment and Human History (Cambridge University Press. 2005).

Peters, K.E., Fraser, T.H., Amris, W. Rustanto, B., Hermanto, E. 1999. Geochemistry of Crude Oils from Eastern Indonesia. AAPG Bull. 83, 1927-1924.

Peucker-Ehrenbrink, B., Hannigan, R.E. 2000. Effects of black shale weathering on the mobility of rhenium and platinum group elements. Geology, 28, 475-478.

Peucker-Ehrenbrink, B., Jahn, B. 2001. Rhenium-osmium isotope systematics and platinum group element concentrations: Loess and the upper continental crust, Geochem. Geophys. Geosyst., 2, 1061.

Qi, J., Gao, J. 2008. Revisiting platinum group elelments of Late Permian coals from western Guizhou Province, SW China. Int. J. Coal Geol. 75, 189 – 193.

Ravizza, G., Peucker-Ehrenbrink, B. 2003. The marine 187Os/188Os record of the Eocene-Oligocene transition: the interplay of weathering and glaciation. Earth Planet. Sci. Lett. 210, 151–165.

Ravizza, G., Turekian, K. K., 1989. Application of the 187Re-187Os system to black shale geochronometry. Geochim. Cosmochim. Acta 53, 3257 – 3262.

Riediger, C., Ness, S., Fowler, M., Akpulat, T. 2000. Timing of oil Migration, Palaeozoic and Cretaceous bitumen and heavy oil deposits, eastern Alberta. GeoCanada (2000) CD Archive.

Rooney, M.A., Vuletich, A.K., Griffith, C.E. 1998. Compound-specific isotope analysis as a tool for characterising mixed oils: an example from the East of Shetland area. Org. Geochem. 29, 241- 254.

Sawlowicz, Z. 1993. Iridium and other platinum-group elements as geochemical markers in sedimentary environments. Palaeogeog. Palaeoclim. Palaeoecol. 104, 253 – 270.

Schmitz, B., Ellwood, B.B., Peucker-Ehrenbrink, B., El Hassani, A., Bultynek, P. 2006. Platinum group elements and 187Os/188Os in a purported impact ejecta layer near the Eifelian-Givetian stage boundary, Middle Devonian. Earth Planet. Sci. Lett. 249 162 – 172.

Scotchman, I.C., Carr, A.D. 2005. Modelling the effects of transient overpressure on the petroleum systems of the UK North East Atlantic Margin and northern North Sea areas: implications for the deep water South Atlantic and Gulf of Mexico. In: Dore, A.G. & Vining, B.A. (eds) Petroleum Geology; North-West Europe and Global perspectives – Proceedings of the 6th Petroleum Geology Conference, 1274-1265 (Geol. Soc. Lon. 2005)

Scotchman, I.C., Griffith, C.E., Holmes, A.J., Jones, D.M. 1998. The Jurassic petroleum system north and west of Britain; a geochemical oil-source correlation study. Org. Geochem. 29, 671-700.

Scotchman, I.C., Carr, A.D., Parnell, J. 2006. Hydrocarbon generation modelling in a multiple rifted and volcanic basin: a case study in the Foinaven Sub-basin, Faroe-Shetland Basin, UK Atlantic margin. Scot. J. Geol. 42, 1-19.

Seibert, C., Kramers, J.D, Meisel, T.H., Morel, P.H., Nagler, T.H. 2005. PGE, Re-Os and mo isotope systematics in Archaean and early Proterozoic sedimentary systems as proxies for redox conditions of the early earth. Geochim. Cosmochim. Acta. 69, 1787 – 1801.

Selby, D. 2007. Direct Rhenium-Osmium age of the Oxfordian-Kimmeridgian boundary, Staffin bay, Isle of Skye, U.K., and the Late Jurassic time scale. Norwegian J. Geol. 87, 291-299.

Selby, D., Creaser, R. A. 2003. Re-Os geochronology of organic rich sediments: an evaluation of organic matter analysis methods. Chem. Geol. 200, 225 – 240.

Selby, D., Creaser, R.A. 2005. Direct radiometric dating of the Devonian-Mississippian time-scale boundary using the Re-Os black shale geochronometer. Geology. 33, 545 – 548.

Selby, D., Creaser, R.A., Dewing, K., Fowler, M. 2005. Evaluation of bitumen as a 187Re–187Os geochronometer for hydrocarbon maturation and migration: A test case from the Polaris MVT deposit, Canada. Earth Planet. Sci. Lett 235. 1– 15

Selby, D., Creaser. R.A., Fowler, MG. 2007. Re-Os elemental and isotopic systematics in crude oils. Geochim. Cosmochim. Acta 71, 378 – 386.

Selby, D., Mutterlose, J., Condon, D.J., 2009. U–Pb and Re–Os geochronology of the Aptian/Albian and Cenomanian/Turonian stage boundaries: Implications for timescale calibration, osmium isotope seawater composition and Re–Os systematics in organic-rich sediments. Chem. Geol. 265, 394 – 409.

Smoliar, M. I., Walker, R. J., Morgan, J. W., 1996. Re-Os ages of group IIA, IIIA, IVA, and IVB iron meteorites. Science 271, 1099 – 1102.

Speight, J.G. 1998. The chemistry and Technology of petroleum. Marcel Dekker, Inc., New York.

Spencer, A.M., Birkeland, Ø., Knag, G.Ø., Fredsted, R. 1999. Petroleum systems of the Atlantic margin of northwest Europe. In: Fleet, A.J. & Boldy, S.A.R. (eds) Petroleum Geology of Northwest Europe: Proceedings of the 5th Conference, 231-246. (Geol. Soc. Lon. 1999).

Sun, W., Bennett, V.C., Eggins S, M., Kamenetsky, V.S., Arculus R.J., 2003. Enhanced mantle-to-crust rhenium transfer in undegassed arc magmas. Nature 422 294–297

Trotter, J.A., Williams, I.S., Barnes, C.R., Lecuyer, C., Nicoll, R.S., 2008. Did cooling oceans trigger Ordovician biodiversification? Evidence from conodont thermometry. Science 321, 550–554.

Turgeon, S.C., Creaser, R.A., Algeo, T.J. 2007. Re-Os depositional ages and seawater Os estimates for the Frasnian-Famennian boundary: Implications for weathering rates, land plant evolution, and extinction mechanisms. Earth Planet. Sci. Lett. 261, 649 – 661.

Willi, M., Kramers, J.D., Voegelin, A.R., Beukes, N.J., Schröder, S., Lacassie, J.D., Meisel, T. 2007 Evidence for a gradual rise of oxygen between 2.6 and 2.5Ga from Mo isotopes and Re-PGE signatures in shales. Geochim. Cosmochim. Acta 71 2417 – 2435.

Yang, G., Chen, J., Du, A., Qu, W., Yu, G. 2004. Re-Os dating of Mo-bearing black shale of the Laoyaling deposit, Tongling, Anhui Province, China. Chin. Sci. Bull. 49. 1396 – 1400.

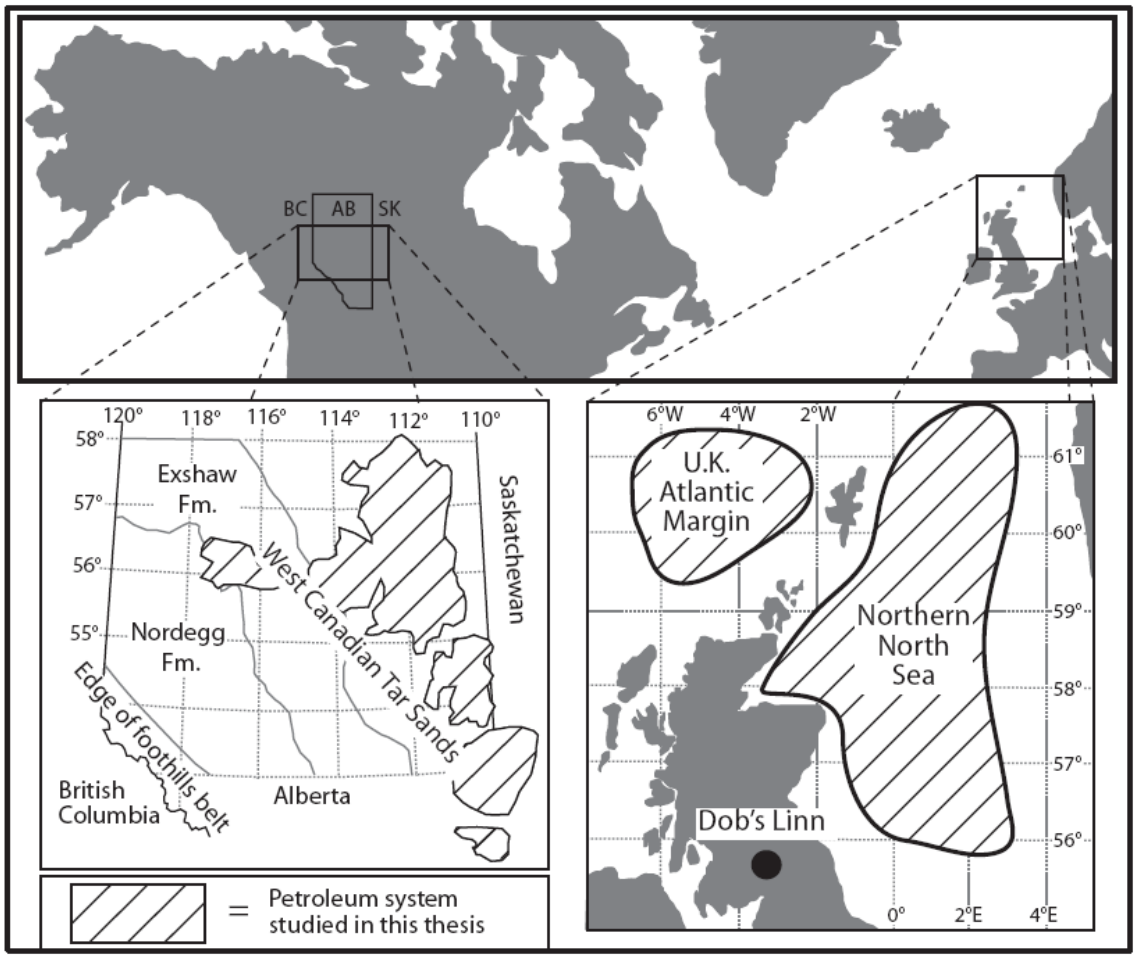

Figure 1.1. Location map of areas studied in this thesis: U.K. Atlantic Margin, the Northern North Sea, Dob's Linn, the Canadian Tar Sands, the Exshaw Fm. and the GordondaleFm.

2: RE-OS GEOCHRONOLOGY OF UK ATLANTIC MARGIN OIL: IMPLICATIONS FOR GLOBAL PETROLEUM SYSTEMS.

A version of this chapter is in review with Geology, co–authored by David Selby (Durham University) and Mark Osborne (BP).

2.1 Introduction

Hitherto Re–Os geochronology studies of petroleum systems are suggested to record the timing of hydrocarbon generation and migration (West Canadian Tar Sands; Selby and Creaser, 2005; Polaris Mississippi Valley Type deposit; Selby et al., 2005). However, these studies have focused on petroleum systems in which both the timing of petroleum generation, and the identity of the source unit, is either unknown or highly debated. Therefore, it is uncertain if the Re–Os ages record the timing of oil generation, migration, emplacement or another geological process. The UK Atlantic Margin (Fig. 2.1) is a well understood petroleum system, predominantly sourced from an Upper Jurassic, marine, organic-rich shale (equivalent to the North Sea Kimmeridge Clay Fm.) with a minor input from Mid-Jurassic shallow marine/terrestrial shale (Spencer et al., 1999; Leach et al., 1999; Lamers and Carmichael, 1999; Scotchman and Carr, 2005; Parnell et al., 2005; Holmes et al., 1999; Rooney et al., 1998; Cornford et al., 1998; Scotchman et al., 1998; Mark et al., 2005; Scotchman et al., 2006). Therefore, comparison of Re–Os ages from UK Atlantic margin oil with basin models and absolute (Ar-Ar) geochronology will identify if Re–Os petroleum geochronology records the timing of oil generation, migration or emplacement.

This study presents Re–Os data for 18 oils from the Clair, Schiehallion, Cuillin and Foinaven fields of the UK Atlantic Margin. This study also presents a geochemical fingerprint of the oils utilised in this study that confirms an Upper Jurassic marine shale source. When compared to published basin histories, that model the timing of generation, and absolute geochronology, that dates migration, (Mark et al., 2005; Scotchman et al., 2006; Lamers and Carmichael, 1999) we demonstrate that Re-Os ages correspond with the timing of oil generation in the UK Atlantic margin at 68 ± 13 Ma. This confirms the hypothesis that Re–Os oil geochronology records the timing of petroleum generation. Furthermore, we demonstrate that the hypothesis that the Os isotopic composition of oil is related to the source unit and can therefore act as a fingerprint is valid (Selby and Creaser, 2005; Selby et al., 2005; Selby et al., 2007).

2.2 Geological Setting

The West of Shetland Basin petroleum system is a rifted fault block and graben province of Tertiary to Mesozoic age running along the UK Atlantic margin between the West Shetland platform and Faeroe Islands (Carruth et al 2003; Mark 2010; Spencer et al 1999). A large body of geochemical and basin modelling research indicate a significant Upper Jurassic marine source with minor Middle Jurassic terrestrial input for UK Atlantic margin oils (Spencer et al., 1999; Mark et al., 2008; Scotchman et al., 2006; Leach et al., 1999; Lamers and Carmichael, 1999; Scotchman and Carr, 2005; Parnell et al., 2005; Hols et al., 1999; Rooney et al., 1998; Cornford et al., 1998; Scotchman et al., 1998; Mark et al., 2005; Scotchman et al., 2006). Reservoirs are found in fractured basement, Devonian (e.g. structural trapped Clair field; Spencer et al., 1999; Carruth et al., 2003), Jurassic and Palaeogene sediments (e.g. Stratigraphically trapped Foinaven and Schiehallion fields; Fig. 2.1; Fig. 2.2; Spencer et al., 1999; Mark et al., 2010).

The Devonian and Early Carboniferous collapse of the Caledonian orogenic belt formed deep, sinistral transtensional basins. Faulting reversed in the Carboniferous and transpression, lead to basin inversion (De Paola et al., 2005; Carruth et al 2003). Boreal rifting in the Permian and Triassic reactivated existing faults and lead to the deposition of fluvial clastics and evaporates. Jurassic marine transgression lead to localised early Jurassic deposition, however, the majority of Middle Jurassic costal sediments lie uncomfortably on Triassic deposits. Late Jurassic/ Early Cretaceous central Atlantic rifting formed the Westray, Flett and Rona Ridge fault blocks and surrounding sub-basins (Fig. 2.1). Continued transgression lead to anoxic conditions within these sub-basins and the deposition of an organic rich marine shale, equivalent to the North Sea Kimmeridge Clay Formation (Carruth et al., 2003; Spencer et al.,1999; Scotchman et al., 2006). Thermal subsidence ensured continued sediment deposition which, by the end of the Cretaceous, caused buried Jurassic sediments to become mature (Carruth et al., 2003, Spencer et al., 1999, Scotchman et al., 2006). The Early Palaeocene Icelandic plume led to the formation of the Faeroes Platform through flood volcanism as well as uplift of the Shetland Platform. Denudation of the Shetland Platform formed coarse turbidites in the Foinaven Sub-basin and periodic deposition, during marine lowstands, in the Flett Sub-basin (Carruth et al., 2003). Decreased subsistence rates in the Late Palaeocene / Eocence drove marine regression which, combined with filling of accommodation space, lead to the deposition of fluvial / deltaic sediments sourced from

the eroding east Shetland Platform (Carruth et al., 2003). These sediments form a ~3 km thick Palaeocene sedimentary succession containing present day reservoirs (Spencer et al., 1999). Oligocene/Miocene north-south compressions reactivated major NW/SE trending faults and inverted Palaeocene basins. Miocene thermal cooling lead to the subsidence and collapse of the Atlantic margin and present day deep sea floor levels (Carruth et al., 2003; Spencer et al., 1999; Mark 2010).

2.3 Re – Os analytical methodology

Rhenium and Os analysis was conducted at the Northern Centre for Isotopic and Elemental Tracing facility at Durham University following the analytical protocols of Selby and Creaser (2003); Selby (2007) and Selby et al. (2007).

Asphaltene was separated for from 18 oils from the UK Atlantic Margin (Fig. 2.1) using the *n*–heptane based methodology of Speight (1998) and Selby et al. (2007), because Re and Os in oil is principally complexed within the asphaltene fraction and the Re–Os asphaltene isotope compositions approximate that of the whole oil (Selby et al., 2007). In summary, in a 60 ml glass vial, 40 ml of *n*–heptane was added to 1 g of oil. The contents were thoroughly mixed and agitated for ~12 hrs. The contents of the vial were then transferred to a 50 ml centrifuge tube and centrifuged at 4000 rpm for 5 minutes to ensure complete separation of the soluble maltene and insoluble asphaltene fractions. The maltene fraction was decanted to waste and the asphaltene fraction was dried on a hot plate at ~60˚C.

Using the carius tube technique (Shirey and Walker, 1995) ~0.1 – 0.2 g of asphaltene was dissolved with a known volume of ^{190}Os and ^{185}Re spike solution in 9 ml of inverse *aqua regia* (6 ml of 16 N HNO_3 and 3 ml of 12 N HCl) at 220°C for 24 hrs. Osmium was purified from the inverse *aqua regia* solution using solvent extraction ($CHCl_3$) and micro-distillation methods. After the removal of Os, the Re bearing inverse *aqua regia* solution was evaporated to dryness at 80˚C and then re-dissolved in 3 ml 0.2 N HNO_3 in preparation for Re anion exchange chromatography. The purified Re and Os were loaded onto a Ni and Pt filaments respectively, and analysed for their isotopic compositions using Negative Thermal Ionisation Mass Spectrometry (NTIMS; Creaser et al., 1991) on a ThermoElectron (TRITON) mass spectrometer. Re was measured using Faraday collectors and Os in peak hopping mode using a secondary electron multiplier.

Total procedural blanks for Re and Os 2.4 and <0.7 pg, respectively, with $^{187}Os/^{188}Os$ value of ~0.18 (n = 2). Raw Re and Os oxide values were corrected for

oxygen contribution and mass fractionation. The Re and Os isotopic values and elemental abundances are calculated by full propagation of uncertainties from Re and Os mass spectrometer measurements, blank abundance and isotopic composition, spike calibration and sample and spike weights. Throughout the period of this study, in house Re and Os standard solutions were repeatedly analysed to monitor instrument reproducibility. The Re standard runs produced average $^{185}Re/^{187}Re$ values of 0.59838 ± 0.00185 (1S.D. n = 41) indistinguishable from the reported values of Selby (2007; 0.5977 ± 0.0012). The NCIET Re standard is made from zone-refined Re ribbon in the same way to the in house Re standard (AB1) of the Department of Earth Sciences, University of Alberta, and the $^{185}Re/^{187}Re$ values are indistinguishable from AB1 values reported by Selby and Creaser (2003; 0.59863 ±0.00062) and Selby et al. (2005; 0.5986 ± 0.0006). The measured difference between our reported $^{185}Re/^{187}Re$ values and the accepted $^{185}Re/^{187}Re$ value (Gramlich et al., 1973) is used to correct for sample mass fractionation. The Os (AB2) standard is made from ammonium hexachloro-osmate. The average $^{187}Os/^{188}Os$ AB2 ratio, using the electron multiplier, is 0.10678 ± 0.00037 (1 S.D. n = 45), indistinguishable from AB2 values reported by Selby and Creaser (2003; 0.106838 ±0.000029), Selby et al. (2005; 0.10684 ± 0.00009) and Selby (2007; 0.10679 ± 0.00007).

2.4 UK Atlantic margin source rock identification

To confirm the oils analysed in this study are sourced from the Kimmeridge Clay Fm (KCF), high performance liquid chromatography (HPLC), carbon isotope ($\delta^{13}C$), gas chromatography (GC) and high-resolution gas chromatography mass spectrometry (GCMS) analysis was undertaken (Table 2.1). The $\delta^{13}C$ and organic geochemical analysis were determined using the standard ENV/E1-1003, ENV/E1-2002, ENV/E1-3008 and ENV/E1-3017 protocols at the Laboratory of the Government Chemist, Teddington (Table 2.1). The HPLC analysis demonstrates that oils utilized in this study are composed of 39.6 – 70.1 % saturates, 25.5 – 42.7 % aromatics and 4.4 – 21.0 % residual (NSOs). $\delta^{13}C$ analysis of whole oil ($\delta^{13}C_{WO}$), saturate ($\delta^{13}C_{sat}$) and aromatic ($\delta^{13}C_{aro}$ fractions range from -29.8 to -29.7 ‰, -29.7 to -30.3 ‰ and -28.8 to -29.3 ‰, respectively. GC analysis of isoprenoids and *n*-alkanes produced Pr/Ph values ranging between 1.4 and 1.9. The Pr/nC_{17} and Ph/nC_{18} results positively correlate ($R^2 = 0.97$) and range from 0.5 to 1.6 and 0.3 and 1.0 respectively. GCMS oil analysis provides C_{27}, C_{28} and C_{29} sterane biomarker values, that when normalised to 100 %, range from 29.5 -

35 % (mean 33.1; S.D. 1.7), 26.6 – 36.4 % (mean 30.0; S.D. 3.0) and 32.2 to 40.4 % (mean 36.9 %; S.D. 2.4), respectively.

The $\delta^{13}C$ data shows very little spread in $\delta^{13}C_{WO}$ (mean, -29.5; S.D. 0.1), $\delta^{13}C_{sat}$ (mean, -30.1; S.D. 0.2) and $\delta^{13}C_{aro}$ (mean, -29.0; S.D. 0.2) values, demonstrating the oils are all from the same source (Fig. 2.3a). The $\delta^{13}C_{aro}/\delta^{13}C_{sat}$ (~1) suggests the source organic matter was predominantly marine with a minor component of mixed terrigenous material (Sofer, 1984; Peters et al., 1999) as expected from an Upper Jurassic marine source (Cornford, 1998). The HPLC data indicate that oils from within the same oil field possess a similar composition; however, the four different oil fields have distinct compositions (Fig. 2.3b). Previous studies of UK Atlantic margin oils suggest biodegradation as a control (e.g. Rooney et al., 1998), with the Clair field being the least biodegraded and the Cuillin, Schiehallion and Foinaven fields show increased levels biodegradation. The isoprenoid data confirms this increase in biodegradation from Clair to Foinaven fields (Fig. 2.3c). Furthermore the isoprenoid data demonstrates that all samples contain a similar mix of Type II and III oils, supporting their formation from a single source unit. The C_{28} sterane data are all similar and therefore further support a single source unit and also suggest that the oil was mainly from a mixed planktonic-bacterial source with some terrigenous material (Fig. 2.3d). Therefore, as expected, these oils are sourced from Upper Jurassic marine shales (KCF equivalent; e.g. Cornford, 1998).

2.5 Re – Os dating of UK Atlantic Margin oil

Rhenium-Os isotope data for the asphaltene fraction of oil from the Clair, Schiehallion, Cuillin and Foinaven fields are presented because Re and Os are predominantly complexed within the asphaltene fraction of oil. Furthermore Re–Os isotope data of the asphaltene fraction of oil approximate that of the whole oil (Table 2.2; Selby et al., 2007). These asphaltene fractions contain 0.74 – 20.77 ppb Re and 54.6 – 316.9 ppt Os. The $^{187}Re/^{188}Os$ (35.1 – 673.0) and $^{187}Os/^{188}Os$ (1.037 – 1.340) positively correlate and yield an date of 68 ± 13 Ma (Fig. 2.4a), which is similar to generation and charging ages produced by basin modelling (Late Cretaceous – Palaeogene; Scotchman et al. 2006).

To produce a reliable Re–Os age, three criteria must be met. 1) Re–Os isotopic systematics must remain undisturbed, 2) there must be a sufficient range in $^{187}Re/^{188}Os$ and 3) the $^{187}Os/^{188}Os$ at the time of oil generation (Os_g) must be similar (Cohen et al., 1999). Our Re–Os date has a large mean standard weighted distribution (MSWD) of 20,

suggesting that one of these criteria has not been met. Given the Re–Os date is in agreement with the basin models it is unlikely that the Re–Os isotope systematics have been disturbed. Our data have a significant spread in both $^{187}Re/^{188}Os$ and $^{187}Os/^{188}Os$ (637.8 and 0.7523 units, respectively; Fig. 2.4a). However, the majority of the samples have similar $^{187}Re/^{188}Os$ values (35.1–158), with two samples possessing higher $^{187}Re/^{188}Os$ (G2762, 581; G2750, 673) and more radiogenic $^{187}Os/^{188}Os$ (G2762, 1.808; G2750, 1.741; Fig. 2.4a). Without regressing G2750 and G2762 the spread of $^{187}Re/^{188}Os$ is limited (122), but it is greater than that used to date the Aptian/Albian boundary (Selby et al., 2009). Regression of all Re–Os data without samples G2762 and G2750 yields an imprecise age of 59 ± 66 Ma (MSWD = 19). This Re-Os date is similar to the original age, albeit with a large uncertainty, suggesting that the age is not forced by the spread of data between G2750, G2762 and the main data cluster. Furthermore, as this subset of data has a smaller MSWD to that produced by all the data, the spread in $^{187}Re/^{188}Os$ can not be accountable for the large MSWD of the full dataset.

The majority of the Os_g (calculated at 68 Ma) form two distinct groups, ~1.01 (n = 10) and 1.12 (n = 6), with two samples contain an Os_g of 0.92 and 1.25 (Fig. 2.4b). Individual regressions of the Re–Os data for the 2 groups yield Re–Os dates of 71.9 ± 5 Ma (MSWD = 1.02; Os_g = 1.11 ± 0.02; Fig. 2.4c) and 64.3 ± 3.4 Ma (MSWD = 2.1; Os_g = 1.02 ± 0.01; Fig. 2.4d). Therefore it is possible that the high MSWD given for the regression of all the Re–Os data is a product of combining Re–Os data that possess distinct Os_g. A possible explanation for this is that different kerogen types undergo catagenesis at different pressure – temperature conditions. The oils reported here are mixed type II and III oils (Fig. 2.3c) and the oils comprising the 64.3 Ma isochron contain a slightly greater proportion of terrigenous material than the 71.9 Ma isochron (Fig. 2.3d). Therefore, as typical marine organic matter will expel petroleum at lower temperatures than terrestrial organic matter (~110°C compared to ~135°C; Ruble et al., 2001), it is possible that the older pulse is mainly sourced from marine kerogen and the younger mainly from terrestrial kerogen (e.g. Fig. 2.3d). It is important to note that the 71.9 ± 5 and 64.3 ± 3.4 Ma ages are within uncertainty of each other and therefore must be treated with caution. Therefore only the 68 Ma age is considered for the rest of this study

A oil generation age of 68 Ma is supported by published $^{40}Ar/^{39}Ar$ geochronology and basin modelling of oil generation and charging in the UK Atlantic Margin (Lamers and Carmichael., 1999; Mark et al., 2005; Scotchman et al., 2006; Fig. 2.5). $^{40}Ar/^{39}Ar$ geochronology of K-feldspar cement that contain mixed aqueous fluid

and hydrocarbon fluid inclusions has identified three periods of fluid flow within the Victory Field, UK Atlantic margin (Mark et al., 2005). Two charges of oil are recognised at 80.1 ± 5.6 Ma and 71.6 ± 7.1 Ma (indistinguishable by age but of different temperatures, ~115°C and ~94°C respectively). A third migration phase occurred at 62.7 ± 8.6 Ma, which was only associated with an aqueous fluid charge (Mark et al., 2005). The Re–Os date presented here overlaps within uncertainty with the two $^{40}Ar/^{39}Ar$ dates associated with UK Atlantic margin oil charging, therefore supporting the hypothesis that Re–Os oil analysis yields the timing of petroleum generation within the UK Atlantic Margin (Selby and Creaser, 2005; Selby et al., 2005).

Hydrocarbon generation and migration models (BasinMod 1-D; TemisPack 2-D and PresRo), which take into account the multiple rifting and igneous events in the Faroe-Shetland Basin as well as P-T conditions derived from fluid inclusion studies, further support our Re–Os dates (Scotchman et al., 2006; Fig. 2.5). This modelling suggests that 3 separate oil charges occurred; 1) during the Late–Cretaceous as subsiding source rocks in the Foinaven sub basin started to generate hydrocarbons and ceased in response to the End–Cretaceous uplift; 2) during the Palaeocene as a result of sudden renewed subsidence and 3) during the Oligocene/Miocene driven by basin inversion and a reduction in overpressure rather than increased generation (Scotchman et al., 2006). Our Re–Os date (68 ± 13 Ma) agrees with the modelled timing of the Late Cretaceous and Palaeocene charges, which may suggest that, in part, oil generation and migration was semi-contemporaneous. However, no evidence of the Oligocene/Miocene charge is observed in the Re–Os dates. The Oligocene/Miocene charge was produced by reduction of overpressure rather than increased oil generation, therefore, suggesting that the Re–Os dates solely record oil generation events. A separate study of 3D, 2D seismic and exploration wells confirms that oil generation commenced during the Late Cretaceous, with major expulsions occurring as a result of rapid burial during the Late Cretaceous and Early Palaeocene (Lamers and Carmichael, 1999).

A further $^{40}Ar/^{39}Ar$ K feldspar cement date bearing oil and aqueous fluid inclusions, from a single Foinaven well, records an earlier oil charge at 113 ± 3.5 Ma (Mark et al., 2010). No oil to source correlation was undertaken in this study and therefore these oils could be sourced from deeper units than the Jurassic. Furthermore, the $^{40}Ar/^{39}Ar$ date is produced from a single well in the Foinaven field and has not been recorded in other UK Atlantic Margin $^{40}Ar/^{39}Ar$ studies (Mark et al., 2005), suggesting it is from a very minor generation event. It is possible that the 113 Ma charges (Mark et

al., 2010) are recorded by the two Foinaven samples that possess distinct Os_g (G2075 and G2763), and hence do not form part of either the 72 Ma or 64 Ma Re–Os isochrons.

In addition, the Re–Os data can also provide information on the oil source unit as the produced oil will inherit the $^{187}Os/^{188}Os$ of the source rock (Selby and Creaser 2005; Selby et al., 2007). Published Re–Os data for sections of the KCF (Cohen et al., 1999; Selby, 2007) suggest that at 68 Ma the $^{187}Os/^{188}Os$ for the KCF would have been between ~0.9 and 2.4. The Os_g for oil of the Atlantic margin are 0.92–1.12 and therefore provide further evidence that the oil was sourced from the Upper Jurassic KCF equivalent marine shale.

2.6 Conclusions

This is the first Re–Os study of a petroleum system with a clearly defined source and good understanding of the timing of petroleum generation events. Organic geochemistry of eighteen asphaltenes from the Clair, Schiehallion, Cuillin and Foinaven fields of the UK Atlantic margin demonstrate that they were sourced from Upper Jurassic marine shales, in agreement with published literature (e.g. Holmes, 1999). The agreement of the Re-Os date produced from these oils (68 ± 13 Ma) with both Ar-Ar geochronology (Mark et al., 2005) and basin models (e.g., Scotchman et al., 2006) provides the first clear evidence that Re–Os petroleum analysis yields the timing of oil generation within a petroleum system. Furthermore, we demonstrate that the hypothesis that the Os isotopic composition of asphaltenes is inherited from the source unit and, therefore can be used to fingerprint an oil to its source, is valid (Selby and Creaser, 2005; Selby et al., 2005; Selby et al., 2007). Thus we demonstrate how Re–Os petroleum geochronology can increase both our understanding of the temporal and spatial aspects of petroleum system evolution.

References

Carruth, A.G. 2000. The Foinaven field, Blocks 204/19 and 204/24a, UK North Sea. In: Gluyas, J.G. & Hichens, H.M. (eds) United Kingdom Oil and Gas Fields, Commemorative Millennium Volume. (Geological Society, London, Memoir 20, 121-130).

Cohen, A.S., Coe, A.L., Bartlett, J.M. Hawkesworth, C.J. 1999. Precise Re–Os ages of organic-rich mudrocks and the Os isotope composition of Jurassic seawater. Earth and Planetary Science Letters 167, 159 – 173.

De Paola, N., Holdsworth, R.E., McCaffrey, K.J.W. Barchi, M.R. 2005. Partitioned transtension: an alternative to basin inversion models. J, Struct. Geol. 27, 607 – 625

Cornford, C. 1998. Source rocks and hydrocarbons of the North Sea. In Glennie, K.W. (Editor), Petroleum Geology of the North Sea. Blackwell Science, Oxford.

Gramlich, J.W., Murphy, T.J., Garner, E.L. and Shields, W.R. Absolute isotopic abundance ratio and atomic weight of a reference sample of rhenium. J. Res. Nat. Bur. Stand. 77, 691 – 698. (1973)

Holmes, A.J. 1999. The Jurassic petroleum system of the West of Britain Atlantic margin – an integration of tectonics, geochemistry and basin modelling. In: Fleet, A.J. & Boldy, S.A.R. (eds) Petroleum Geology of Northwest Europe: Proceedings of the 5th Conference, 1351-1365. (Geological Society of London).

Lamers, E., Carmichael, S.M.M. 1999. The Palaeocene deepwater sandstone play West of Shetland. In: Fleet, A.J. & Boldy, S.A.R. (eds) Petroleum Geology of Northwest Europe: Proceedings of the 5th Conference, 645-659. (Geological Society of London).

Leach, H.M., Herbert, N., Los, A., Smith, R.L. 1999. The Schiehallion development. . In: Fleet, A.J. & Boldy, S.A.R. (eds) Petroleum Geology of Northwest Europe: Proceedings of the 5th Conference, 683-692. (Geological Society of London).

Mark, D.F., Parnell, J, Kelley, S.P Lee, M.R. & Sherlock, S.C, Carr. A. 2005. Dating of Multistage Fluid Flow in Sandstones. Science, 309, 2048-2051

Mark, D.F., Parnell, J., Kelley, S.P., Lee, M.R. & Sherlock, S.C. 2010. 40Ar/39Ar dating of oil generation and migration at complex continental margins. Geology 38, 75 – 78.

Parnell, J., Green, P.F., Watt, G., Middleton, D. 2005. Thermal history and oil charge on the UK Atlantic margin. Pet. Geosci. 11, 99-112.

Peters, K.E., Fraser, T.H., Amris, W. Rustanto, B., Hermanto, E. 1999. Geochemistry of Crude Oils from Eastern Indonesia. AAPG Bulletin. 83, 1927-1924.

Rooney, M.A., Vuletich, A.K.. Griffith, C.E. 1998. Compound-specific isotope analysis as a tool for characterising mixed oils: an example from the East of Shetland area. Org. Geochem. 29, 241- 254.

Ruble, T.E., Lewan, M.D., Philip, R.P. 2001. New insights on the Green River petroleum system in the Uinta basin from hydrous pyrolysis experiments. AAPG Bulletin 85 1333–1371.

Scotchman, I.C.,Carr, A.D. 2005. Modelling the effects of transient overpressure on the petroleum systems of the UK North East Atlantic Margin and northern North Sea areas: implications for the deep water South Atlantic and Gulf of Mexico. In: Dore, A.G. & Vining, B.A. (eds) Petroleum Geology; North-West Europe and Global perspectives – Proceedings of the 6th Petroleum Geology Conference, 1274-1265 (Geological Society of London)

Scotchman, I.C., Carr, A.D., Parnell, J. 2006. Hydrocarbon generation modelling in a multiple rifted and volcanic basin: a case study in the Foinaven Sub-basin, Faroe-Shetland Basin, UK Atlantic margin. Scot. J. Geol. 42, 1-19.

Scotchman, I.C., Griffith, C.E., Holmes, A.J., Jones, D.M. 1998. The Jurassic petroleum system north and west of Britain; a geochemical oil-source correlation study. Org. Geochem. 29, 671-700.

Selby, D. 2007. Direct Rhenium-Osmium age of the Oxfordian-Kimmeridgian boundary, Staffin bay, Isle of Skye, U.K., and the Late Jurassic time scale. Nor. J. Geol. 87, 291-299.

Selby, D., Creaser, R. A. 2003. Re-Os geochronology of organic rich sediments: an evaluation of organic matter analysis methods. Chem. Geol. 200, 225 – 240.

Selby, D., Creaser, R.A. 2005. Direct radiometric dating of hydrocarbon deposits using Rhenium-Osmium isotopes. Science. 308, 1293 – 1295.

Selby, D., Creaser, R.A., Dewing, K., Fowler, M. 2005. Evaluation of bitumen as a 187Re–187Os geochronometer for hydrocarbon maturation and migration: A test case from the Polaris MVT deposit, Canada. Geochim. Cosmochim. Acta.. 235. 1– 15.

Selby, D., Creaser. R.A., Fowler, MG. 2007. Re-Os elemental and isotopic systematics in crude oils. Earth Planet. Sci. Lett. 71, 378 – 386.

Selby, D., Mutterlose, J., Condon, D.J. 2009. U–Pb and Re–Os geochronology of the Aptian/Albian and Cenomanian/Turonian stage boundaries: Implications for timescale calibration, osmium isotope seawater composition and Re–Os systematics in organic-rich sediments. Chem. Geol. 265, 394 – 409.

Shirey, S.B. Walker, R.J. 1995. Carius Tube Digestion for Low-Blank Rhenium-Osmium Analysis. Anal. Chem. 67, 2136 – 2141.

Sofer, Z. 1984. Stable Carbon isotope compositions of crude oils: Application to source depositional environments and Petroleum alteration. AAPG Bull. 68, 31-49.

Spencer, A.M., Birkeland, Ø., Knag, G.Ø., 1999. Fredsted, R. Petroleum systems of the Atlantic margin of northwest Europe. In: Fleet, A.J. & Boldy, S.A.R. (eds) Petroleum Geology of Northwest Europe: Proceedings of the 5th Conference, 231-246. (Geological Society of London)

Table 2.1 Geochemical data for UK Atlantic margin oil.

Well[a]	206/8-2	206/8-2	206/8-3A	206/8-3A	204/20-5	204/20-5	204/19-3A	204/19-3A	204/19-3A	PFJ-1160	PFJ-1187	PFJ-1247	204/24A-1	204/24A-1	Mean	S.D.	Range for KCF sourced oilsg
G Number[bc]	G5400[c]	G5401[c]	G0124[b]	G0123[b]	G2851[c]	G2851[c]	G2749[c]	G2750[c]	G2762[c]	G5234[c]	G5271[c]	G5306[c]	G2075[b]	G2763[b]			
Oil field			Clair			Schiehallion		Cuillin				Foinaven					
Saturates (%)	39.6	39.8	46.5	39.0	59.9	70.1	47.3	51.5	54.2	62.0	N.D.[f]	61.8	63.9	58.6	53.4	10.3	N.D.[f]
Aromatics (%)	41.4	42.7	37.1	40.0	30.9	25.5	42.0	39.6	37.7	34.3	N.D.[f]	34.9	32.7	37.1	36.6	4.9	N.D.[f]
Residual (%)	19.1	17.5	16.4	21.0	9.2	4.4	10.7	8.9	8.1	3.7	N.D.[f]	3.3	3.4	4.3	10.0	6.4	N.D.[f]
Saturates/Aromatics	1.0	0.9	1.3	1.0	1.9	2.8	1.1	1.3	1.4	1.8	N.D.[f]	1.8	2.0	1.6	1.5	0.48	0.6 - 8.0
$d^{13}C$ Whole Oil	-29.5	-29.5	-29.5	-29.7	-29.5	-29.5	-29.4	-29.4	-29.4	-29.6	N.D.[f]	-29.6	-29.6	-29.5	-29.5	0.1	-27.1 - -30.4
$d^{13}C$ Saturates	-30.2	-30.3	-30.2	-30.2	-30.3	-30.1	-29.7	-30.0	-30.1	-30.2	N.D.[f]	-30.1	-30.1	-30.1	-30.1	0.2	N.D.[††]
$d^{13}C$ Aromatics	-29.0	-29.0	-28.8	-28.9	-29.1	-29.3	-29.1	-28.9	-29.2	-29.0	N.D.[f]	-28.9	-28.8	-28.8	-29.0	0.2	N.D.[††]
Pr^d/Ph^e	1.9	1.9	N.D.[f]	N.D.[f]	1.5	1.4	[h]	1.9	1.5	1.7	N.D.[f]	1.6	N.D.[f]	N.D.[f]	1.7	0.2	0.6 - 1.9
Pr^d/nC_{17}	0.5	0.5	N.D.[f]	N.D.[f]	1.0	1.0	[h]	0.8	0.7	1.6	N.D.[f]	1.4	N.D.[f]	N.D.[f]	0.9	0.4	0.3 - 1.0
Ph^e/nC_{18}	0.3	0.3	N.D.[f]	N.D.[f]	0.7	0.7	[h]	0.5	0.5	1.0	N.D.[f]	0.9	N.D.[f]	N.D.[f]	0.6	0.2	0.2 - 1.1
C_{27} sterane (%)	N.D.[f]	N.D.[f]	29.5	33.0	35.0	33.7	33.7	N.D.[f]	31.4	N.D.[f]	35.0	N.D.[f]	33.1	33.7	33.1	1.7	N.D.[f]
C_{28} sterane (%)	N.D.[f]	N.D.[f]	33.0	26.6	29.0	29.6	28.7	N.D.[f]	36.4	N.D.[f]	30.0	N.D.[f]	28.3	27.9	30.0	3.0	N.D.[f]
C_{29} sterane (%)	N.D.[f]	N.D.[f]	37.5	40.4	36.0	36.7	37.6	N.D.[f]	32.2	N.D.[f]	35.0	N.D.[f]	38.6	38.4	36.9	2.4	N.D.[f]

[a] UK grid
[b] BP Unpublishe data
[c] Data from this study
[d] Pristane
[e] Phytane
[f] No Data
[g] Cornford et al. (1998)
[h] To biodegraded for analysis

Table 2.2 Re-Os Asphaltene data for UK Atlantic margin oil.

Well[a]	"G" Number	Field	Asphaltene content %	Re (ppb)			Os (ppt)			$^{187}Re/^{188}Os$			$^{187}Os/^{188}Os$			rho	Os_g [b]		
206/8-2	G5399	Clair	3.5	2.18	±	0.01	294.7	±	3.5	40.0	±	0.9	1.079	±	0.031	0.684	1.03	±	0.02
206/8-2	G5400	Clair	1.9	2.24	±	0.01	312.0	±	2.8	38.7	±	0.6	1.037	±	0.021	0.656	0.99	±	0.01
206/8-2	G5401	Clair	1.6	2.32	±	0.01	316.9	±	2.8	39.6	±	0.6	1.062	±	0.021	0.656	1.02	±	0.01
206/8-2	G5402	Clair	3.1	2.18	±	0.01	295.9	±	2.7	39.8	±	0.6	1.067	±	0.021	0.654	1.02	±	0.01
206/8-2	G5403	Clair	3.1	2.64	±	0.02	349.2	±	3.1	40.9	±	0.6	1.068	±	0.021	0.653	1.02	±	0.01
206/8-2	G5404	Clair	4.5	1.83	±	0.01	260.8	±	2.4	38.0	±	0.6	1.054	±	0.022	0.658	1.01	±	0.01
206/8-3A	G0124	Clair	8.0	1.39	±	0.04	68.76	±	1.67	111	±	6	1.221	±	0.081	0.688	1.09	±	0.05
206/8-3A	G0123	Clair	4.3	1.47	±	0.04	226.8	±	2.8	35.1	±	1.2	1.055	±	0.032	0.485	1.02	±	0.02
204/20-5	G2851	Schiehallion	1.2	2.80	±	0.02	180.3	±	3.8	84.7	±	3.7	1.140	±	0.068	0.719	1.04	±	0.04
204/19-3A	G2749	Cuillin	1.7	6.00	±	0.04	208.4	±	1.5	158	±	2	1.163	±	0.016	0.627	0.98	±	0.01
204/19-3A	G2750	Cuillin	1.6	20.8	±	0.1	180.0	±	1.6	673	±	9	1.741	±	0.026	0.740	0.98	±	0.01
204/19-3A	G2762	Cuillin	2.8	4.49	±	0.03	45.43	±	0.67	581	±	16	1.808	±	0.056	0.852	1.15	±	0.02
PFJ-1160	G5234	Foinaven	0.4	2.58	±	0.04	182.6	±	2.0	77.7	±	1.9	1.222	±	0.028	0.589	1.13	±	0.02
PFJ-1187	G5271	Foinaven	0.4	2.57	±	0.04	176.8	±	1.9	79.6	±	1.8	1.188	±	0.027	0.598	1.10	±	0.02
PFJ-1247	G5306	Foinaven	0.4	2.74	±	0.04	182.6	±	1.9	82.4	±	1.8	1.212	±	0.027	0.604	1.12	±	0.02
PFJ-1246	G5307	Foinaven	-	18.6	±	0.1	151.4	±	1.7	74.4	±	2.0	1.200	±	0.029	0.574	1.12	±	0.02
204/24A-1	G2075	Foinaven	1.2	1.63	±	0.04	62.12	±	1.18	142	±	7	1.084	±	0.050	0.731	0.92	±	0.03
204/24A-1	G2763	Foinaven	0.8	0.74	±	0.04	54.61	±	1.53	75.6	±	6.3	1.340	±	0.100	0.597	1.25	±	0.07

All uncertainties shown are 2σ.

[a]UK North Sea grid.

[b] Os_g = 187Os/188Os calculated at the time of oil generation (68 Ma).

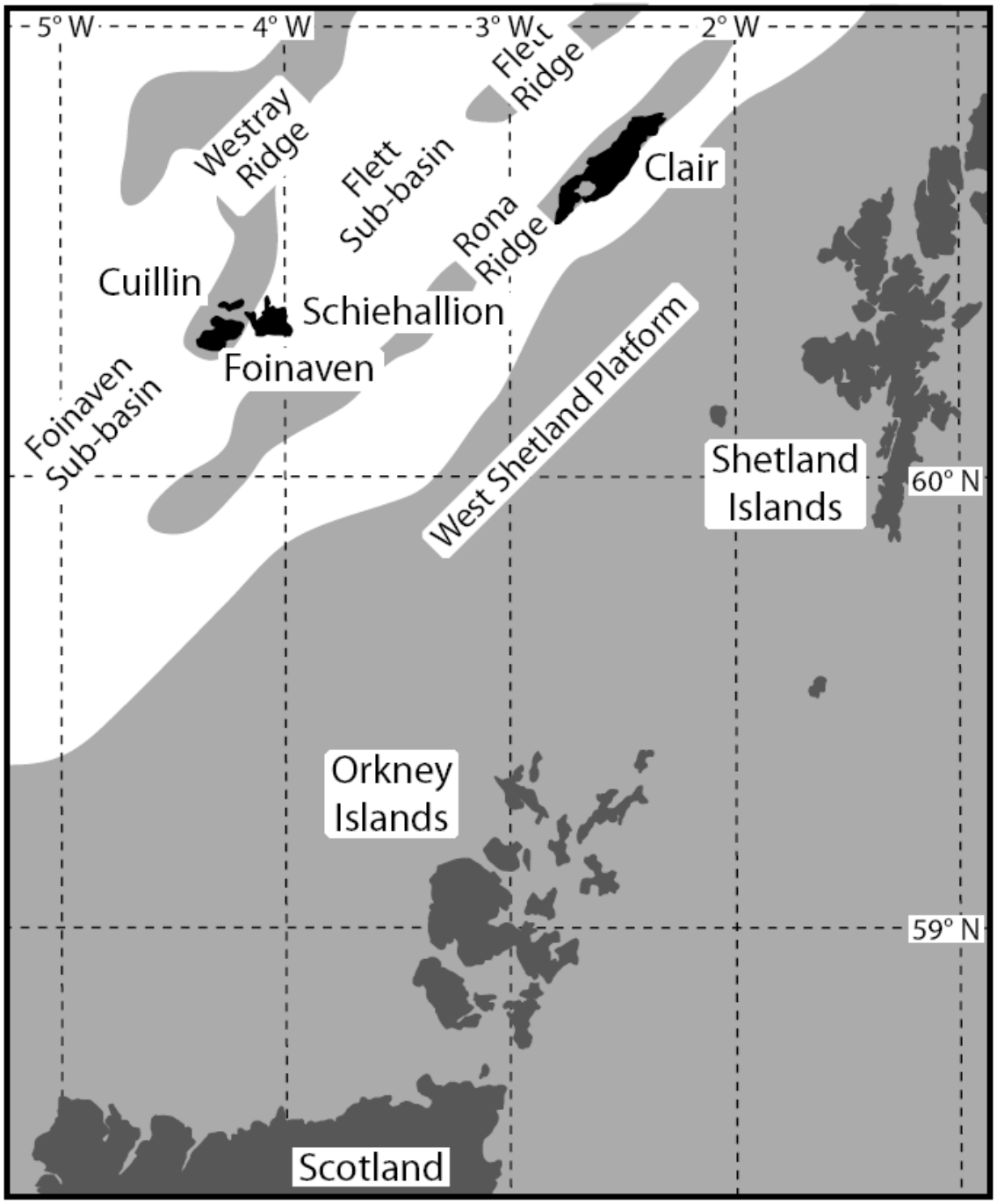

Figure 2.1. Location map of fields used in this study (Carruth, 2000; Scotchmann et al., 2006)

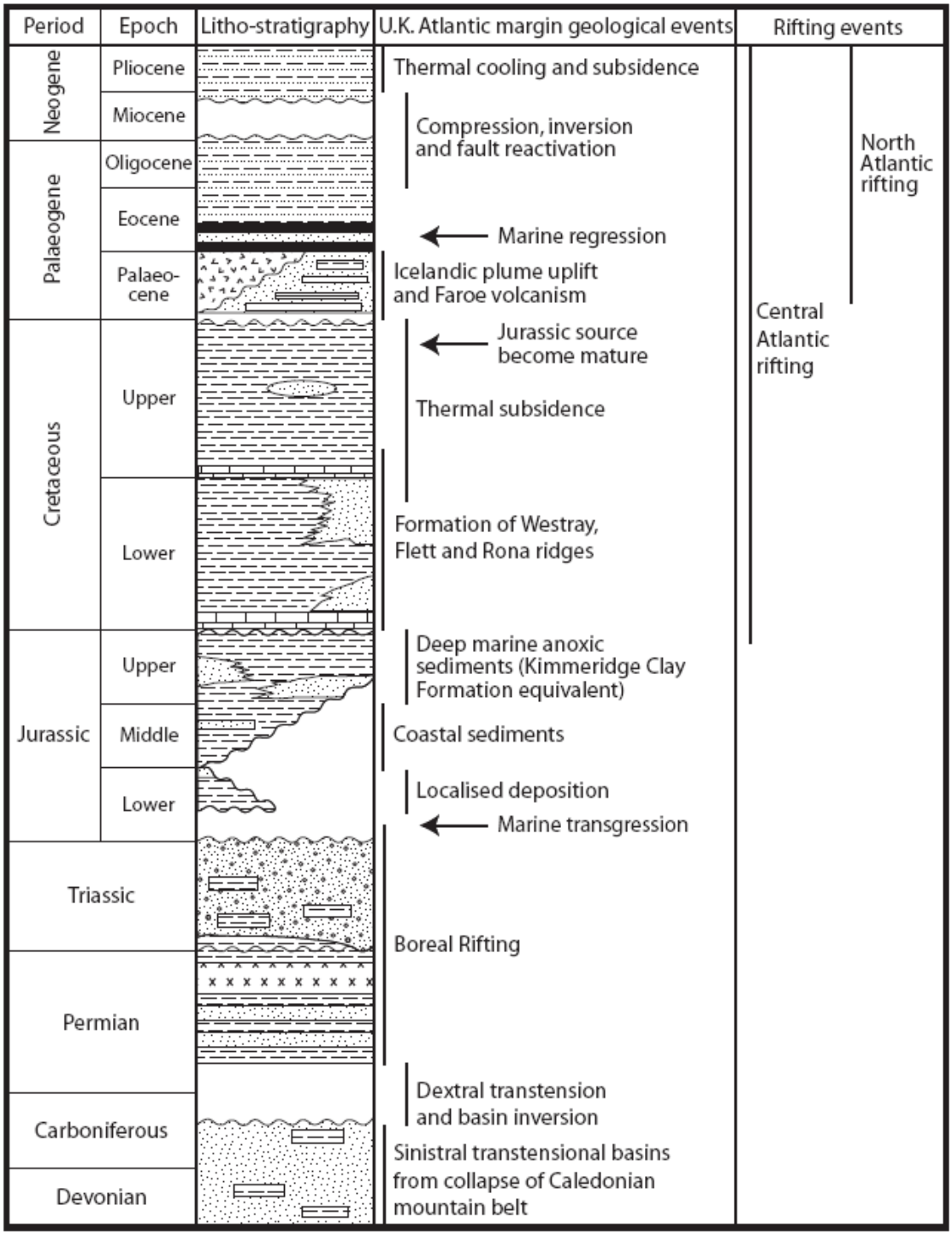

Figure 2.2. Geological column for the UK Atlantic margin compiled from Nadin et al., 1997; Spencer et al., 1999; Carruth, 2003; Scotchman et al., 2006; Mark et al., 2010.

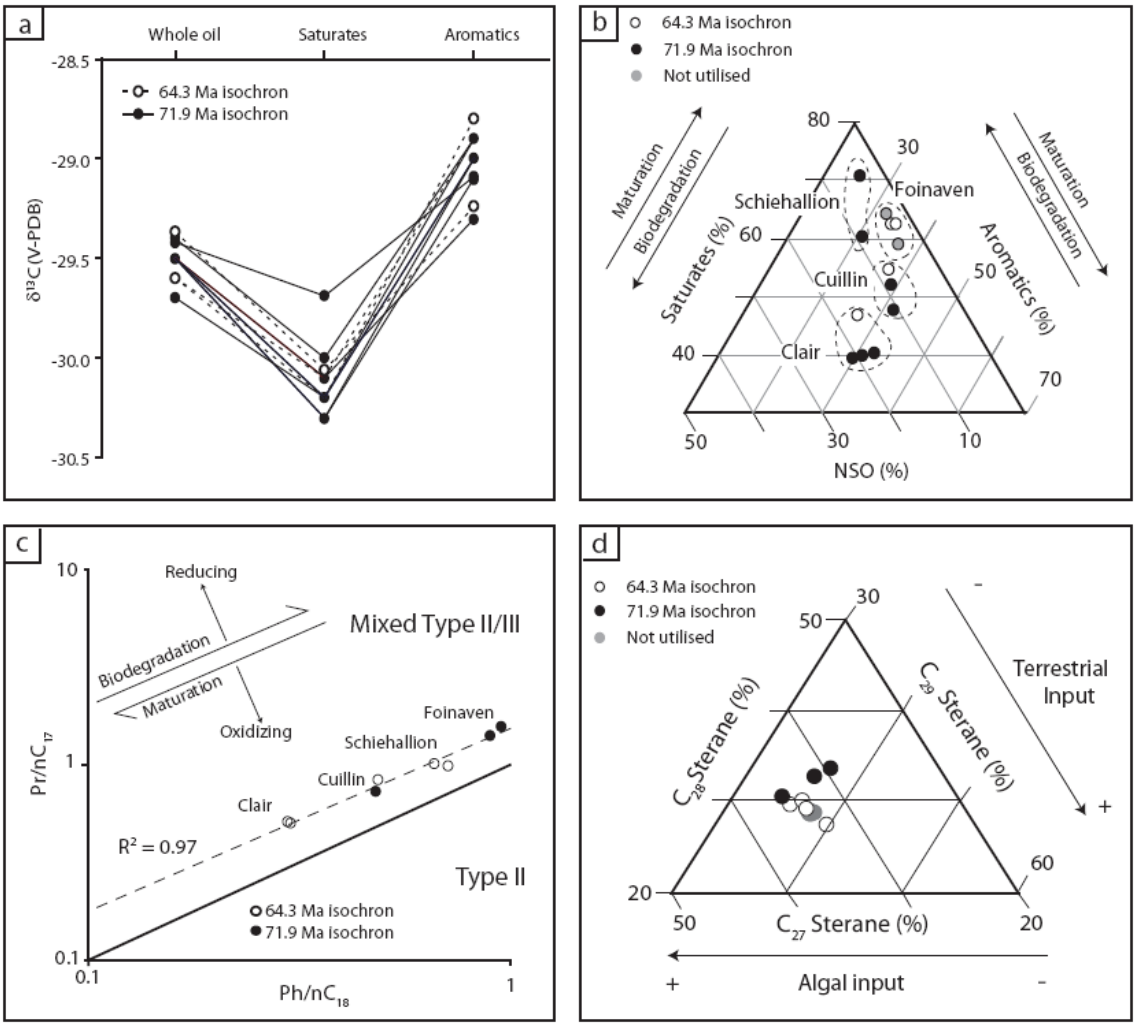

Figure 2.3. Geochemical fingerprint data for oils from the Clair, Foinaven, Schiehallion and Cuillin oil fields. Fig. 2.3a – HPLC data; Fig. 2.3b – $\delta^{13}C_{WO}$, $\delta\ ^{13}C_{sat}$ and $\delta\ ^{13}C_{aro}$ results; Fig. 2.3c - Pr/nC$_{17}$ and Ph/nC$_{18}$ data, Type II and mixed type II/III lines from Peters et al. (1999); Fig. 2.3d – Sterane biomarker data, Middle and Upper-Jurassic grouping (Cornford, 1998), Planktonic and terrestrial enrichments (Peters et al., 1999). See text for discussion.

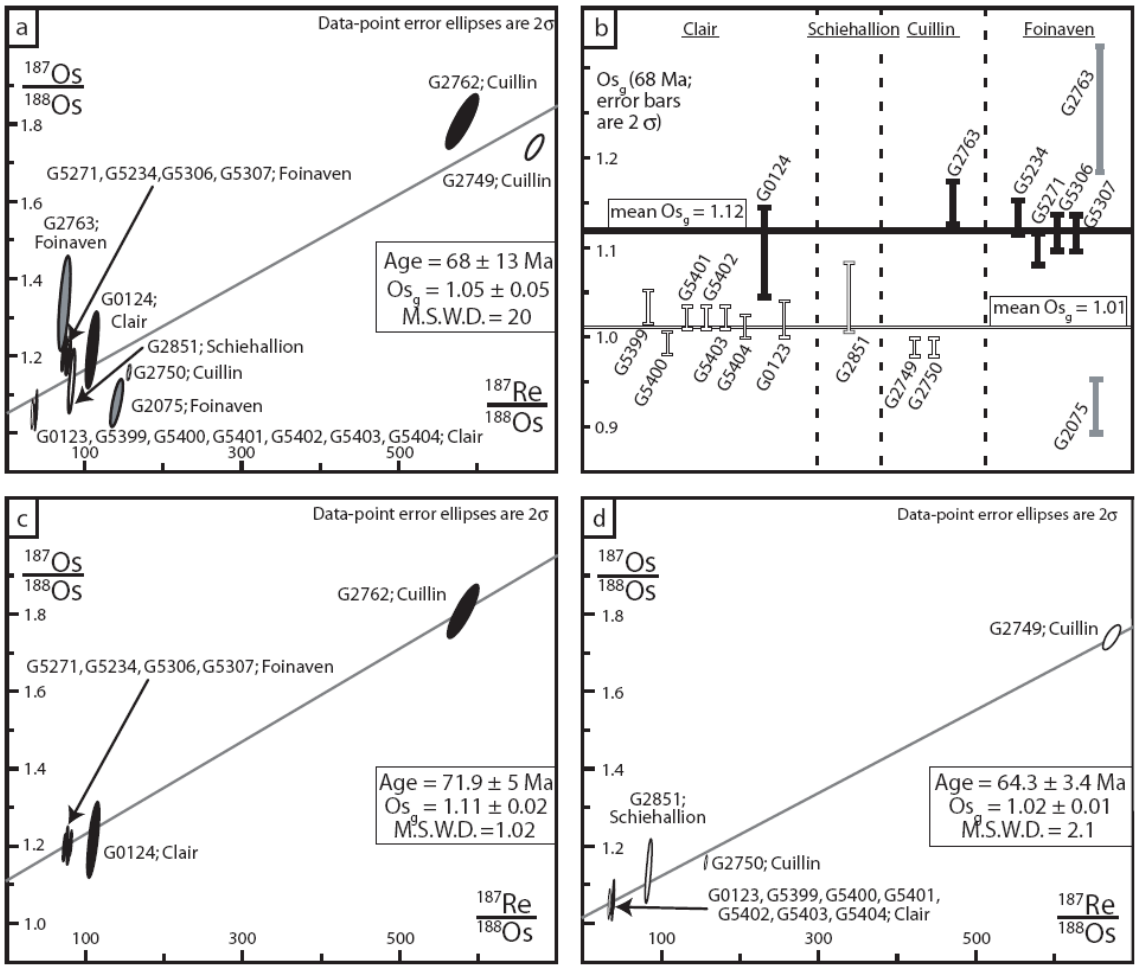

Figure 2.4. Re–Os isochrons for asphaltene from the Clair, Foinaven, Schiehallion and Cuillin oil fields. Fig. 2.4a - formed by all data; Fig. 2.4b – groupings of similar Os_g; Fig. 2.4c - Re–Os isochron for oils with an Os_g of ~1.12; Fig. 2.4d - Re–Os isochron for oils with an Os_g of ~1.12. See text for discussion.

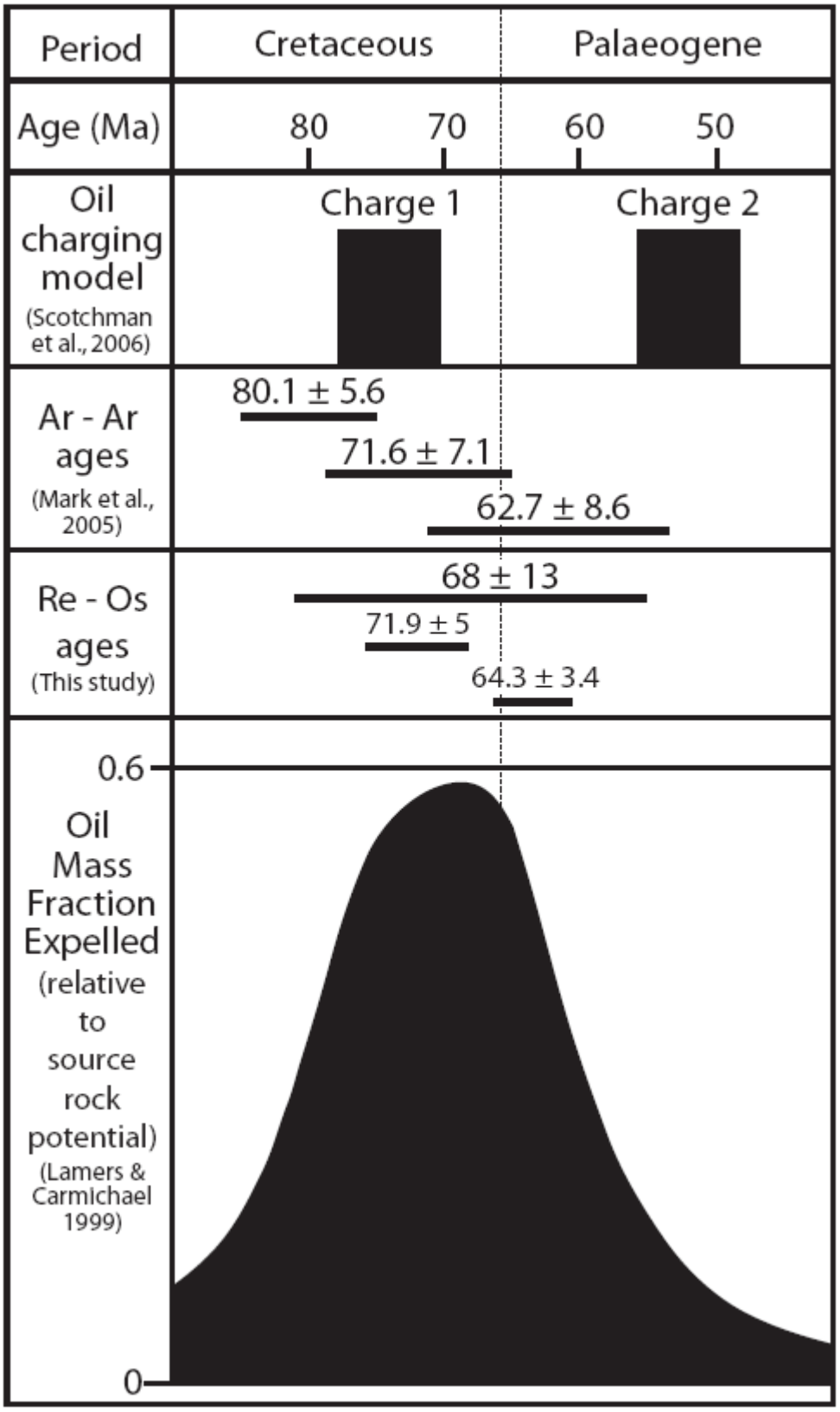

Figure 2.5. Comparison of Re–Os ages with published models (Lamers and Carmichael, 1999; Scotchman et al., 2006) and Ar – Ar cement ages from mixed oil and aqueous fluid inclusions (Mark et al., 2005).

3: FAULT CHARGED HYDROTHERMAL-FLUID CONTAMINATION OF U.K. NORTH SEA OILS: INSIGHTS FROM RE-OS ISOTOPES.

A version of this has been accepted for publication in Geology, co–authored by David Selby (Durham University), Mark Osborne (BP) and Dan Fincune (BP).

3.1 Introduction

Rhenium-osmium (Re-Os) oil geochronology has been shown to yield the timing of oil generation and migration (Selby and Creaser, 2005; Selby et al. 2005) and information regarding the source of an oil (Selby et al. 2007). Recently, this application has also been applied to oils of the North Sea (Graham et al., 2006). North Sea oil is predominantly sourced from the Late Jurassic – Early Cretaceous shales of the Kimmeridge Clay Formation (KCF; comprising the Kimmeridge Clay, Borglum and Draupne Fms.) which started to generate oil during the Late Cretaceous (Cornford, 1998 and references therein). The KCF possesses radiogenic $^{187}Os/^{188}Os$ (Cohen et al., 1999; Selby, 2007; this study). Therefore, if generated oil inherits the $^{187}Os/^{188}Os$ of the source rock at the time of hydrocarbon maturation (Selby et al., 2007); oils of the North Sea should possess radiogenic $^{187}Os/^{188}Os$ (> 0.94 – 2.45). However, oil from the Brent Field (U.K. North Sea; Fig. 3.1) bears extremely unradiogenic $^{187}Os/^{188}Os$ compositions (~0.18; Graham et al., 2006). As a result the Os isotope data were used to suggest that a Late Jurassic shale containing an unradiogenic $^{187}Os/^{188}Os$, and therefore different from the KCF, was the source of Brent oil. This conclusion conflicts with a large body of research that indicates that the oil is sourced from the KCF (e.g. Bailey et al., 1990; Gormly et al., 1993; Cornford, 1998; Underhill, 2003).

We test the hypothesis that the oil is from an alternative source to the KCF through the analysis of oil samples from the Central Graben (CG), Moray Firth (MF), Viking Graben (VG) and East Shetland Basin (ESB) of the U.K. North Sea (Fig. 3.1). We show that oil from the CG and MF yield radiogenic $^{187}Os/^{188}Os$ as expected from being sourced from the KCF. However, oil from the VG with which the Brent field is associated, and main ESB display unradiogenic $^{187}Os/^{188}Os$. We attribute these unexpected results to contamination through interaction with an unradiogenic hydrothermal fluid either sourced from intrusive mafic igneous units or the mantle that propagate through the main fault zone of the VG and ESB. This study enhances our understanding of the Re–Os oil systematics, and agrees with current ideas regarding fault architecture, crustal thinning and associated fluid flow and interaction in the North Sea oil system.

3.2 Analytical Protocols

3.2.1 Re – Os

The Re–Os abundance and isotope compositions of the North Sea oils were established by the analysis of the asphaltene fraction, because Re and Os in oil is principally complexed within the asphaltene fraction and the Re–Os asphaltene isotope compositions approximate that of the whole oil (Selby et al., 2007). Rhenium and Os analysis was conducted at the Northern Centre for Isotopic and Elemental Tracing facility at Durham University following the analytical protocols of Selby and Creaser (2003); Selby (2007) and Selby et al. (2007). The Miller Field CO_2 abundance and $\delta^{13}C_{CO2}$ values were provided by BP having been determined using the standard ENV/E1-1003 protocol at the Laboratory of the Government Chemist, Teddington.

Asphaltene was separated from 13 oils from the UK North Sea (Fig. 3.1) using the *n*–heptane based methodology of Speight (1998) and Selby et al. (2007). In summary, in a 60 ml glass vial, 40 ml of *n*–heptane was added to 1 g of oil. The contents were thoroughly mixed and agitated for ~12 hrs. The contents of the vial were then transferred to a 50 ml centrifuge tube and centrifuged at 4000 rpm for 5 minutes to ensure complete separation of the soluble maltene and insoluble asphaltene fractions. The maltene fraction was decanted to waste and the asphaltene fraction was dried on a hot plate at ~60˚C. Using the carius tube technique (Shirey and Walker, 1995) ~0.1 – 0.2 g of asphaltene was dissolved with a known volume of ^{190}Os and ^{185}Re spike solution in 9 ml of inverse *aqua regia* (6 ml of 16 N HNO_3 and 3 ml of 12 N HCl) at 220°C for 24 hrs. Osmium was purified from the inverse *aqua regia* solution using solvent extraction ($CHCl_3$) and micro-distillation methods. After the removal of Os, the Re bearing inverse *aqua regia* solution was evaporated to dryness at 80˚C and then re-dissolved in 3 ml 0.2 N HNO_3 in preparation for Re anion exchange chromatography (e.g. Selby and Creaser 2003).

Five core samples of Kimmeridge Clay Formation (KCF) shale from the North Sea Miller oil field (well 16/8b–A01) were analysed for their Re and Os abundance and isotopic compositions. The 5 samples are from a 1.1m interval spanning 4738.4 and 4737.3 m depth. Each sample represents half of the 10 cm diameter core with a stratigraphic thickness of ~3 cm thickness and a mass of between 75 and 80 g. All samples were prepared by removing any drill core marks with a diamond polishing wheel, to avoid surface contamination, and then powdered in a ceramic mill to ensure Re and Os sample homogenisation. Applying the Carius tube technique (Shirey and

Walker, 1995) ~0.5 g of whole rock powder was dissolved with a known volume of ^{190}Os and ^{185}Re mixed tracer (spike) solution in 8 ml of 0.25 g/g CrO_3 in 4N H_2SO_4 at 220°C for 48 hrs. Osmium was purified from the CrO_3-H_2SO_4 solution using solvent extraction ($CHCl_3$) and micro–distillation methods (e.g. Selby and Creaser 2003). After the removal of Os, 1 ml of the CrO_3–H_2SO_4 was mixed with 1 ml of Milli–Q water and reduced from Cr^{6+} to Cr^{3+} by sparging with SO_2 in preparation for Re anion exchange chromatography. After chromatography the Re fraction was then further purified by single bead anion extraction.

The purified Re and Os from both asphaltene and shale samples were loaded onto a Ni and Pt filaments respectively, and analysed for their isotopic compositions using Negative Thermal Ionisation Mass Spectrometry (NTIMS; Creaser et al., 1991) on a ThermoElectron (TRITON) mass spectrometer. Re was measured using Faraday collectors and Os in peak hopping mode using a secondary electron multiplier.

Total procedural blanks for Re and Os for the inverse *aqua regia* methodology are 2.4 and <0.7 pg, respectively, with $^{187}Os/^{188}Os$ value of ~0.18 (n = 2). Total procedural blanks for Re and Os, using the CrO_3-H_2SO_4 digestion, are 12 and <0.5 pg, respectively, with an average $^{187}Os/^{188}Os$ value of ~0.4 (n = 2). Raw Re and Os oxide values were corrected for oxygen contribution and mass fractionation. The Re and Os isotopic values and elemental abundances are calculated by full propagation of uncertainties from Re and Os mass spectrometer measurements, blank abundance and isotopic composition, spike calibration and sample and spike weights. Throughout the period of this study, in house Re and Os standard solutions were repeatedly analysed to monitor instrument reproducibility. The Re standard runs produced average $^{185}Re/^{187}Re$ values of 0.5983 ± 0.0017 (1S.D. n = 35) indistinguishable from the reported values of Selby (2007; 0.5977 ± 0.0012). The NCIET Re standard is made from zone-refined Re ribbon in the same way to the in house Re standard (AB1) of the Department of Earth Sciences, University of Alberta, and the $^{185}Re/^{187}Re$ values are indistinguishable from AB1 values reported by Selby and Creaser (2003; 0.59863 ±0.00062) and Selby et al. (2005; 0.5986 ± 0.0006). The measured difference between our reported $^{185}Re/^{187}Re$ values and the accepted $^{185}Re/^{187}Re$ value (Gramlich et al., 1973) is used to correct for sample mass fractionation. The Os (AB2) standard is made from ammonium hexachloro-osmate. The average $^{187}Os/^{188}Os$ AB2 ratio, using the electron multiplier, is 0.10682 ± 0.00020 (1 S.D. n = 40), indistinguishable from AB2 values reported by Selby and Creaser (2003; 0.106838 ±0.000029), Selby et al. (2005; 0.10684 ± 0.00009) and Selby (2007; 0.10679 ± 0.00007).

3.2.2 Biostratigraphy

Biostratigraphic analysis were undertaken by BP on both palynological and micropalaeontological preparations of two KCF core samples from the 16/8b-A01 well of the Miller Field (4737.3m and 4738.4m measured core depth).The samples were processed using standard laboratory techniques to provide palynological and micropalaeontological preparations for transmitted-light and reflected light microscope analysis respectively.

3.3 Results

This study presents Re–Os data for 13 North Sea oils, Re–Os data and palynology of KCF core from well 16/8b–A1 from the Miller field and CO_2 abundance and $\delta\,^{13}C_{CO2}$ analysis of 4 Miller field oils (Fig. 3.1; Table 3.1; Table 3.2; Table 3.3).

Biostratigraphic analyses were undertaken on both palynological and micropalaeontological preparations of core samples AF01-06 and AF05-06. Key biostratigraphic events identified include the first downhole occurrence of the dinocyst *Senoniasphaera jurassica* and the common occurrence of the radiolarian *Parvicingula jonesi* at a core depth of AF05-06 (4737.3 m), which can be calibrated with the *anguiformis* boreal ammonite biozone. The core sample from AF01-06 (4738.4 m) exhibits the first downhole occurrence of *Muderongia* sp. A (Davey 1979), which is attributable to the *kerberus* biozone. This biostratigraphic interpretation places the studied section of KCF that sourced the Miller Field oils within the Tithonian between the *anguiformis* and *kerberus* Biozones (146.3 ± 4 – 147 ± 4 Ma; Gradstein et al., 2004).

The mature Miller core samples contain ~50 to 115 ppb Re and ~600 to 1700 ppt Os and the $^{187}Re/^{188}Os$ and $^{187}Os/^{188}Os$ ratios positively correlate (Table 3.2). The Os_i values calculated at 147 Ma, based on biostratigraphy (this study), range from 0.47 to 0.49. Regression of all the Re–Os data using *Isoplot* v.3 (Ludwig, 2003) and the ^{187}Re decay constant ($\lambda = 1.666 \times 10^{-11}.a^{-1}$; Smoliar et al., 1996) produce a Model 3 Re–Os age of 145 ± 17 Ma (Os_i = 0.49 ± 0.12, MSWD = 30; Fig. 3.2a). The large MSWD relates the deepest sample (AF01-06) possessing a slightly more radiogenic Os_i (~0.49) than the remaining samples (~0.47). Regression of all Re–Os data, baring AF01-06, yield a Model 3 Re–Os age of 147 ± 13 Ma (Os_i = 0.47 ± 0.01, MSWD 5.7; Fig 3.2b), which is in excellent agreement with the biostratigraphy of the Miller core. This supports previous studies that demonstrate that Re–Os systematics in shales are not disturbed by maturation (e.g. Creaser et al., 2002).

The North Sea oils contain between 0.5 and 5.5 % asphaltene, ~0.1 to 15 ppb Re and ~1 to 743 ppt Os (Table 3.1). The $^{187}Re/^{188}Os$ and $^{187}Os/^{188}Os$ values range between ~1.5 to 653, and ~0.17 to 3.34, respectively. Samples with low volumes of asphaltene generally contain low concentrations of Re and Os (e.g. G2091, 2.6 % asphaltene, 0.13 ppb Re, 1.3 ppt Os) and samples containing higher percentages of asphaltene contain higher concentrations of Re and Os (e.g. G0869, 5.4 % asphaltene; 1.99 ppb Re; 629 ppt Os). Samples G2091 and G2646 contain low Re and Os abundances and measured $^{187}Re/^{188}Os$ and $^{187}Os/^{188}Os$ have greater uncertainties. Sample G2091 possesses a significant blank correction, particularly for Os, which with complete propagation of all uncertainties yields $^{187}Re/^{188}Os$ and $^{187}Os/^{188}Os$ compositions with large uncertainties (653.3 ± 1700, 2.897 ± 7.722, respectively; Table 3.1). However, the nominal Re–Os data of sample G2091 is similar to that of oil from the next westerly quadrant (sample G0072; well 14/20- 6A). Thus, though imprecise, we interpret the Re–Os data for sample G2091 to yield a good estimate of the Re–Os isotope composition of the analyzed sample. The 4 Miller oils (wells 16/7b- 24; 16-7b- 25; 16/7b- 28B and F0501) analysed for CO_2 and $\delta^{13}C_{CO2}$ contain between 21.6 and 24.6 mol. % CO_2 and possess $\delta^{13}C_{CO2}$ values between -5.6 and -7.5 ‰ (VPDB; Table 3.3).

3.4 North Sea Re–Os Oil Systematics and Hydrothermal Fluid Contamination

The Re and Os abundances and isotopic values of asphaltene fractions from wells 3/11b- 3, 13/28a- 5RE, 14/20- 6A, 15/30- 6, 21/01- 8, 22/18- 1, 30/16- 7 and 30/24- 6 are similar to other global oil analysis (Table 3.1; Selby and Creaser, 2005; Selby et al., 2005; Selby et al. 2007). However, five asphaltene fractions from wells 3/03- 3, 16/7a- 3, and 211/18a-N4, that have similar Re–Os abundances and $^{187}Re/^{188}Os$ to other oils from the North Sea possess extremely unradiogenic $^{187}Os/^{188}Os$ values, similar to those reported from the Brent oil field (Graham et al., 2006; Table 3.1; Fig. 3.1. The Miller KCF shales analysed as part of this study have slightly enriched Re and Os abundances compared to Oxfordian/Kimmeridgian KCF shales from Skye (Selby 2007), but are similar to Kimmeridgian KCF, Kimmeridge Bay, Dorset (Cohen et al., 1999). The $^{187}Re/^{188}Os$ (~345 to 480) and $^{187}Os/^{188}Os$ (~1.42 to 1.50) for the Miller KCF shales fall within the range of the KCF of Skye and Dorset (Cohen et al., 1999; Selby 2007).

If the hypothesis is correct that oil inherits the $^{187}Os/^{188}Os$ of the source rock at the time of hydrocarbon maturation (e.g. Selby et al 2007) then given the radiogenic composition of the KCF we would expect the $^{187}Os/^{188}Os$ of the generated oil to be

radiogenic. Using the Miller KCF Re–Os data and a 65 Ma hydrocarbon maturation age the North Sea oil should possess $^{187}Os/^{188}Os$ greater than 0.94. If we also consider the Re–Os KCF data from Skye and Dorset (Cohen et al., 1999; Selby, 2007) we would again expect KCF sourced oil to have radiogenic $^{187}Os/^{188}Os$ (0.911 - 2.457). Oil from reservoirs in the CG and MF possess radiogenic $^{187}Os/^{188}Os$ values as expected (1.035 to 3.341; Table 3.1, Fig. 3.1), however, oil from reservoirs within the main ESB and VG have anomalously unradiogenic $^{187}Os/^{188}Os$ (0.166 to 0.483; Table 3.1, Fig. 3.1), which cannot have been inherited from source.

Given the likely radiogenic nature of surrounding rock units, such unradiogenic $^{187}Os/^{188}Os$ as found in the ESB and VG may require interaction with unradiogenic hydrothermal fluids associated with either the mantle or intrusive mafic volcanic units. These hydrothermal fluids typically have $^{187}Os/^{188}Os$ of between 0.12 and 0.13 (e.g. Meisel et al., 2001) and therefore provide a suitably unradiogenic mixing end member. Typical hydrothermal fluid contains ~100 fg/g Os with an $^{187}Os/^{188}Os$ of ~0.11 (Sharma et al., 2000). If we consider an average asphaltene Os_i of 1 and Os concentration of 20 ppt (Selby and Creaser, 2005; Selby et al., 2007; this study) together with the Os abundance and $^{187}Os/^{188}Os$ of a hydrothermal fluid, it is possible to estimate the approximate percentage of contamination by unradiogenic Os required to alter the asphaltene Re–Os isotope systematics using a simple two-member mixing model (Faure, 1986). This model suggests that > 70 % of the Os in the unradiogenic oils is derived from hydrothermal fluids. Osmium is organophyllic (Selby et al., 2007), and our data suggests that Os can easily be complexed with oil during interaction with an Os bearing fluid, overprinting the original radiogenic KCF ratio (>1) with an unradiogenic ratio (~0.12). Hydrothermal fluids are reported to be essentially bereft of Re (-0.92 – 5.6 pmol kg^{-1}; Miller, 2009). This may be supported by our results that show that Re abundances and $^{187}Re/^{188}Os$ are similar in oils that possess unradiogenic $^{187}Os/^{188}Os$ (0.22 – 1.4 ppb; 1.5 – 339, respectively) to oils bearing radiogenic $^{187}Os/^{188}Os$ (0.13 – 4.2 ppb; 17 – 653, respectively; Table 3.1).

An indistinguishable conclusion is drawn from CO_2 abundance, $\delta^{13}C_{CO2}$, $^{3}He/^{4}He$ and $^{21}Ne/^{22}Ne$ data of the Miller, Magnus and Sleipner oil fields (Fig. 3.1). Typically CO_2 forms ~2 mol. % of oil (Lu et al., 2009). In contrast, the concentration of CO_2 in the Miller and Sleipner oil is significantly higher than expected (Miller field, ~21– 30 mol %; Sleipner field ~10 mol. %; this study; James 1990; Baines and Worden, 2004; Lu et al., 2009). There are three main sources of CO_2 in oil systems, mantle, biogenic and inorganic, with each possessing distinct $\delta^{13}C_{CO2}$ values (Mantle sourced δ

$^{13}C_{CO2}$ ~ -5 ‰, organically derived δ $^{13}C_{CO2}$ ~ -25 ‰ and degraded limestone δ $^{13}C_{CO2}$ ~ -7 ‰; Clayton et al., 1990; Deines, 2002). Four δ $^{13}C_{CO2}$ analyses from the Miller Field give δ $^{13}C_{CO2}$ between –5.6 and –7.5 ‰ (Table 3.3), similar to δ $^{13}C_{CO2}$ values of oil from the Sleipner field (~ -5 ‰ to -12 ‰; James 1990). The δ $^{13}C_{CO2}$ data presented for Miller agrees with data from the Sleipner Field that has been used to suggest a significant mantle/mafic volcanic CO_2 contribution ($9.8*10^{-7}$g cm^{-2} yr^{-1} over 60 – 70 Ma; Lu et al., 2009) to the oil. Although it could argued that the δ $^{13}C_{CO2}$ reflect atmospheric CO_2, $^{3}He/^{4}He$ and $^{21}Ne/^{22}Ne$ data from the Magnus Oil Field, ~270 Km north of the Miller and Sleipner Fields (Ballentine et al., 1996; Fig. 3.1) suggest that 2.3 – 4.5 % of the ^{4}He (R/Ra values between 0.2 and 0.38; crustal end member ~ 0.012, mantle end member ~8) and 4.3 – 6.2 % of the ^{21}Ne (average $^{21}Ne/^{22}Ne$ are 0.0334 ± 0.0002; atmospheric end member ~0.028, mantle end member ~0.09, crustal end member 0.4; Ballentine et al., 1996; Ballantine 1997) is mantle derived. In addition, it is reported that the amount of radiogenic noble gas in the Magnus reservoir is too high to have been produced *in-situ* from radioactive decay over the lifetime of the oil system (~60 -70 Ma). Greater than 70 % of Os in the oil is hydrothermally derived, compared to ~5 % of mantle He and Ne (Ballentine et al., 1996). As Os is known to be highly organophyllic (e.g. Selby et al., 2007), we hypothesise that Os is more easily complexed into oil than He or Ne.

The Os data suggests hydrothermal fluids interacted with oil throughout the VG and main area of the ESB and not just the area around the Miller, Magnus and Sleipner fields as a result indicate that there is no need to attribute Brent field oil to a non-KCF source as proposed by Graham et al. (2006).

3.5 North Sea Structure Controlling Re–Os Oil Systematics

Oil bearing unradiogenic Os as well as mantle/mafic CO_2, Ne and He are shown only to occur in the VG and ESB, close to the Western Margin Fault Zone (WMFZ, Fig. 3.1). In contrast, oil possessing typical radiogenic $^{187}Os/^{188}Os$ occurs in the CG and MF, away from the WMFZ (Fig. 3.1). The WMFZ forms the western edge of the VG that displays >4 km of extension as a result of strain accumulation towards the rift axis during rifting throughout the early Cretaceous (Cowie et al., 2005). The CG and MF show lower levels of crustal extension (β values = 1.04 – 1.30; Barr, 1985; Roberts et al., 1993; Barr 2002) than the ESB and VG (β values = 1.1 to 1.5; Badley et al., 1988; Roberts et al., 1993; Barr, 2002; Cowie et al., 2005). During the ~27 Ma of rifting in the North Sea strain migrated towards the rift axis in the ESB and VG, with the highest

amounts of slip occurring along faults close to the axis (e.g. WMFZ / Gullfaks Fault; Fig. 3.1; Cowie et al. 2005).

Two hypothesized sources of unradiogenic hydrothermal fluid are the mantle or intrusive mafic volcanics. As normal faults play a role as fluid conduits and only oil in the ESB and VG show evidence for interaction with an unradiogenic hydrothermal fluid, it is possible that large scale basin bounding faults within the VG and ESB propagate to sufficient depth to act as a conduit for mantle sourced hydrothermal fluid. Alternatively, within the Viking Graben, magmatic processes associated with graben formation suggest that Cenozoic intrusive igneous units may be a source of unradiogenic hydrothermal fluids (e.g. Bugge et al., 1980; Holliger and Klemperer, 1989; Fjeldskaar et al., 2008). It is not possible to identify weather the source of the hydrothermal fluid is mafic volcanics or the mantle with the data in this study, however, we suggest that hydrothermal fluids associated with intrusive mafic igneous units are the more likely source. Interestingly, the enrichment of CO_2 in oil directly to the east of the WMFZ decreases with distance away from the WMFZ, suggesting that the WMFZ acts as a route for hydrothermal fluids. As the western margin of the ESB has experienced only minor thinning and is ~100 km from the main fault zone in the basin (Cowie et al., 2005) there is no evidence for interaction between oil and hydrothermal fluids. Hence, oil from well 3/11b- 3, located in the western margin of the ESB, possess radiogenic $^{187}Os/^{188}Os$.

A potential problem for this explanation is that the Brent, Thistle and Magnus reservoirs are sealed by fault traps and therefore the associated faults should be impermeable to fluid flow. However, large-scale faults have been shown to have vertical permeability, enhanced by interconnected inclusions of fractured protolith, whilst remaining impermeable to cross flow (Faulkner and Rutter, 2001). This favours fluid transport from deep sources such as the mantle, further supporting our hypothesis. The Miller oil field was charged with CO_2 bearing mantle like $\delta^{13}C_{CO2}$ values, from ~ 70 Ma that upwardly migrated along the major basin bounding fault of the VG (Lu et al 2009). The Kimmeridge Clay Formation source of the Miller oil field started to produce oil from ~65 Ma, with peak oil production occurring at ~40 Ma (Marchand et al., 2001). Secondary migration of oil occurred through fault networks (Barnard and Bastow, 1991), therefore, it is likely that the oil could have interacted with hydrothermal fluids during migration. Basin modeling indicates that this interaction would have occurred at temperatures of ~110 °C (BasinMod; Marchand et al., 2001).

3.6 Conclusions

Previous geochemical studies of separate North Sea oil fields have results attributed either to mantle contamination or inheritance from an unknown source. However, this study that covers the entire North Sea system demonstrates that unradiogenic Os isotopic values in oil are not inherited from an unknown source rock as suggested by Graham et al. (2006). Alternatively we suggest that the fault architecture in the VG and ESB enables conduits to form that permit the interaction between oil and an unradiogenic hydrothermal fluid sourced from either Cenozoic mafic volcanic units or the mantle. This model also accounts for oils within the CG and MF containing Os isotopic signatures as expected form the KCF. Within the Miller field (VG) the interaction of oil and mantle fluids occurred either during migration or within the reservoir at ~110°C. In summary, the β, CO_2, $^{187}Os/^{188}Os$, $^{3}He/^{4}He$ and $^{21}Ne/^{22}Ne$ data suggest that there has been sufficient crustal thinning (~33 %) and strain amalgamation in the ESB and VG to allow faults and deep shear zones to act as conduits for hydrothermal fluid to interact with migrating and emplaced oils. Furthermore, this study demonstrates that Os isotopes can be applied to track crustal scale fluid dynamic processes as well as acting as a tool to identify oil migration pathways in extensional basins (e.g. Békés Basin, Hungary; Clayton et al., 1990).

References.

Badley, M.E., Price, J.D., Rambech Dahl, C. and Agdestein, T. 1988 The structural evolution of the northern Viking Graben and its bearing upon extensional modes of basin formation. J. Geol. Soc. (Lon.) 145, 455-472.

Bailey, N.J.L., Burwood, R. and Harriman, G.E. 1990. Application of pyrolysate carbon isotope and biomarker technology to organofacies definition and oil correlation problems in North Sea basins. Org. Geochem. 16, 1157-1172.

Baines, S.J. and Worden, R.H. (2004). The long-term fate of CO_2 in the subsurface: natural analogues for CO_2 storage Geol. Soc. (Lon), Spec. Pub. 233, 59-85.

Ballentine, C.J. (1997) Resolving the mantle He, Ne and crustal 21Ne/22Ne in well gases Earth Planet. Sci. Lett. 152, 233 – 249.

Ballentine, C.J., O'Nions, R.K. and Coleman, M.L. (1996). A Magnus opus: Helium, neon, and argon isotopes in a North Sea oilfield. Geochim. Cosmochim. Acta 60, 831-849.

Barr, D. (1985) 3-D Palinspastic restoration of normal faults in the Inner Moray Firth: implications for extensional basin development. Earth Planet. Sci. Let. 75, 191-203.

Barr,D. (2002) Lithospheric stretching. In: Turner, J.P. & Holdsworth, R.E. (Eds) Extensional Tectonics: Regional-scale Processes. Key Issues in Earth Sciences, Geol. Soc., London p 69-71

Bugge, T., Prestvik, T. and Rokoengen, K. Lower Tertiary volcanic rocks off Kristiansund – Mid Norway. (1980) Mar. Geosci. 35, 277 – 286.

Christiansson, P., Faleide, J.I. and Berge, A.M. (2000). Crustal structure in the northern north Sea: an integrated geophysical study. In: Nottvedt, A. et al. (eds) Dynamics of the Norwegian Margin. Geol. Soc. (Lon.) Spec . Pub. 167, 397 – 410.

Clayton, J.l., Spencer, C.W., Koncz, I and Szalay, A. (1990). Origin and migration of hydrocarbon gases and carbon dioxide, Bekes basin, south-eastern Hungary. Org. Geochem. 15, 233 – 247.

Cohen, A.S., Coe, A.L., Bartlett, J.M. and Hawkesworth, C.J. (1999). Precise Re–Os ages of organic-rich mudrocks and the Os isotope composition of Jurassic seawater. Earth Planet. Sci. Lett 167, 159 – 173

Cornford, C., (1998). Source rocks and hydrocarbons of the North Sea. In Glennie, K.W. (Editor), Oil Geology of the North Sea. Blackwell Science, Oxford, p. 376-462.

Cowie, P.A., Underhill, J.R., Behn, M.D., Jian Lin and Gill, C.E. (2005) Spatio-temporal evolution of strain accumulation derived from multi-scale observations of Late Jurassic rifting in the northern North Sea: A critical test of models for lithospheric extension. Earth Planet. Sci. Lett 234, 401 – 419.

Creaser, R.A., Sannigrahi, P., Chacko, T. and Selby, D. (2002) Further evaluation of the Re–Os geochronometer in organic rich sedimentary rocks: A test of hydrocarbon maturation effects in the Exshaw Formation, Western Canada Sedimentary Basin. Geochim. Cosmochim. Acta. 66, 3441 – 3452.

Deines, D. (2002). The carbon isotope geochemistry of mantle xenoliths. Earth-Science Reviews 58, 247 – 278.

Faulkner, D.R. and Rutter, E.H. (2001) Can the maintenance of overpressured fluids in large strike-slip fault zones explain their apparent weakness? Geology, 29, 503–506.

Faure, G. (1986) Principles of isotope geology. John Wiley and sons.

Fjeldskaar, W., Helset, H.M., Johansen, H., Grunnaleite, I., and Horstad, I. (2008) Thermal modelling of magmatic intrusions in the Gjallar Ridge, Norwegian Sea: implications for vitrinite reflectance and hydrocarbon maturation. Bas. Res. 20, 143 – 159.

Gormly, J.R., Buck, S.P. & Chung, H.M. 1993. Oil-source rock correlation in the North Viking Graben. Org. Geochem. 22, 430-413.

Gradstein, et al. 2004. A Geologic Time Scale. Cambridge University Press.

Graham, S., Karlsen, D.A., Dypvik, H., Andersen, T. and Backer-Owe, K. (2006). Re–Os variations in North Sea shales and oils. Geochim. Cosmochim. Acta, 70, A211.

Holliger, K. and Klemperer, L. (1989) A comparison of the Moho interpreted from Gravity data and from deep seismic data in the northern North Sea. Geophys. J. 97, 247 – 258.

James, A.T. (1990). Correlation of reservoired gases using the carbon isotopic compositions of wet gas components. AAPG Bull. 74, 1441 – 1458.

Jiemin Lu, Wilkinson, M., Haszeldine, S and Fallick, A.E. (2009) Long-term performance of a mudrock seal in natural CO2 storage. Geology 37, 35-38

Ludwig, K.R., 2003. ISOPLOT: A Plotting and Regression Program for Radiogenic-Isotope Data, version 3.

Marchand, A.M.E., Haszeldine, R.S., Smalley, P.C., Macaulay, C.I., and Fallick, A.E., 2001, Evidence for reduced quartz cementation rates in oil-filled sandstones. Geology 29 915 – 918,

Meisel, T., Walker, R.J., Irving, A.J. and Lorand, J-P. (2001). Osmium isotopic compositions of mantle xenoliths: A global perspective. Geochim. Cosmochim. Acta 65, 1311 – 1323.

Miller, C.A. 2009. Surface-cycling of rhenium and its isotopes. Ph.D. Thesis. MIT/WHOI, 2009-13.

Roberts, A.M., Yielding, G. Kusznir, N.J., Walker, I. and Dorn_Lopez, D. (1993) Mesozoic extension in the North Sea: constraints from flextural backstripping, forward modelling and fault populations. In: Parker, J.R. (editor) Oil geology of Northwest Europe: Proceedings of the 4th Conference. Geol. Soc. (Lon.)

Selby, D. (2007). Direct Rhenium-Osmium age of the Oxfordian-Kimmeridgian boundary, Staffin bay, Isle of Skye, U.K., and the Late Jurassic time scale. Norwegian J. Geol. 87, 291-299.

Selby, D. and Creaser, R. A. (2003). Re–Os geochronology of organic rich sediments: an evaluation of organic matter analysis methods. Chem. Geol. 200, 225 – 240.

Selby, D and Creaser, R.A. (2005). Direct radiometric dating of hydrocarbon deposits using Rhenium-Osmium isotopes. Science. 308, 1293 – 1295. Selby, D., Creaser, R.A., Dewing, K. and Fowler, M. (2005). Evaluation of bitumen as a ^{187}Re–^{187}Os geochronometer for hydrocarbon maturation and migration: A test case from the Polaris MVT deposit, Canada. Earth Planet. Sci. Lett 235. 1– 15

Selby, D., Creaser. R.A. and Fowler, MG. (2007). Re–Os elemental and isotopic systematics in crude oils. Geochim. Cosmochim. Acta 71, 378 – 386.

Sharma, M., Wasserburg, G.J., Hofmann, A.W., Butterfield, D.W. (2000) Osmium isotopes in hydrothermal fluids from the Juan de Fuca Ridge Earth Planet. Sci. Lett. 179. 139-152

Smoliar, M. I., Walker, R. J., and Morgan, J. W., (1996). Re–Os ages of group IIA, IIIA, IVA, and IVB iron meteorites. Science 271, 1099 – 1102.

Underhill, J.R. 2003. The Tectonic and stratigraphic framework of the United Kingdom's oil and Gas Fields. In: Gluyas, J.G. & Hichens, H.M. (eds) United Kingdom Oil and Gas Fields, Commemorative Millennium Volume. Geol. Soc. (Lon.) Memoirs, 20, 17-59.

Table 3.1 Re-Os asphaltene results for North Sea oils

Well[a]	"G" Number	Field	Asphaltene content %	Re (ppb)	Os (ppt)	$^{187}Re/^{188}Os$	$^{187}Os/^{188}Os$	Os_g[d]
15/30- 6	G1899	Britannia	2.6[b]	1.07 ± 0.07	41.3 ± 2.6	177.7 ± 26.3	3.341 ± 0.589	3.148
13/28a- 5RE	G2091	Ross	0.8[b]	0.13 ± 0.05	1.3 ± 1.2	653.3 ± 1700.2	2.897 ± 7.722	2.187
14/20- 6A	G0072	Unnamed	2.9[b]	3.87 ± 0.08	43.5 ± 2.1	579.6 ± 69.5	2.813 ± 0.363	2.186
30/24- 6	G0228	Argyll	1[b]	0.72 ± 0.14	55.5 ± 4.1	82.1 ± 22.7	2.558 ± 0.526	2.468
22/18- 1	G1981	Arbroath	1[b]	1.76 ± 0.06	89.7 ± 5.2	119.0 ± 10.8	2.084 ± 0.425	1.956
30/16- 7	G2006	Fulmar	0.6[b]	0.90 ± 0.06	24.6 ± 1.6	219.8 ± 39.8	2.022 ± 0.365	1.784
3/11b- 3	G0941	Cheviot	1.1[b]	4.24 ± 0.05	179.2 ± 4.4	137.3 ± 6.9	1.698 ± 0.114	1.549
21/01- 8	G0869	Buchan	5.4[b]	1.99 ± 0.06	629.1 ± 12.8	17.1 ± 0.9	1.035 ± 0.060	1.017
3/03- 3	G1717	Ninian	5.5[b]	1.27 ± 0.06	18.6 ± 1.4	339.0 ± 57.6	0.475 ± 0.136	0.123
211/18a-N4	G2646	Thistle	0.8[b]	0.12 ± 0.05	11.0 ± 1.3	51.8 ± 27.6	0.266 ± 0.206	0.208
16/07a- 3	G2422	Miller	<1[c]	0.77 ± 0.01	51.8 ± 0.7	74.8 ± 2.0	0.483 ± 0.018	0.402
16/07a- 3	G2421	Miller	<1[c]	0.22 ± 0.11	742.6 ± 4.9	1.5 ± 0.7	0.301 ± 0.007	0.299
16/07a- 3	G2423	Miller	<1[c]	1.39 ± 0.03	202.4 ± 1.3	33.3 ± 0.9	0.166 ± 0.006	0.130

All uncertainties shown are 2σ.

[a] UK North Sea grid.

[b] Asphaltine content isolated at the Northern Centre for Isotopic and Elemental Tracing.

[c] Asphaltine content isolated at LGC, Teddington.

[d] Os_g = Os isotope composition at the time of petroleum generation (65 Ma).

Table 3.2 Re-Os results for Miller field core samples (well 16/8b-a01).

Sample	Well Depth (m)	Mass (g)[a]	Re (ppb)	Os (ppt)	$^{187}Re/^{188}Os$	$^{187}Os/^{188}Os$	Rho	Os_{ib}
AF05-06	4737.3	76	50.15 ± 0.16	600.4 ± 1.5	482.8 ± 1.7	1.656 ± 0.003	0.343	0.472
AF04-06	4737.7	77	115.33 ± 1.47	1697.2 ± 3.7	382.5 ± 4.9	1.417 ± 0.002	0.054	0.485
AF03-06	4738	78	94.33 ± 0.30	1285.4 ± 2.7	417.0 ± 1.4	1.501 ± 0.002	0.219	0.479
AF02-06	4738.2	78	84.71 ± 0.27	1362.1 ± 2.9	346.3 ± 1.2	1.320 ± 0.002	0.224	0.471
AF01-06	4738.4	79	58.30 ± 0.19	855.8 ± 1.9	384.2 ± 1.3	1.433 ± 0.002	0.270	0.491

All uncertainties shown are 2 σ.

[a] Mass ground to a powder.

[b] Os_i = Os isotope composition at the time of deposition (147 Ma).

Table 3.3 Miller oil field CO_2 and stable carbon isotope analysis[a]

Well	Field	$\delta^{13}C_{CO2}$ (‰)	CO_2 (Vol %)
16/07b- 24	Miller	-6.2	21.58
16/07b- 25	Miller	-6.5	22.45
16/07b- 28B	Miller	-7.5	22.77
F0501	Miller	-5.6	24.60

[a] Provided by BP

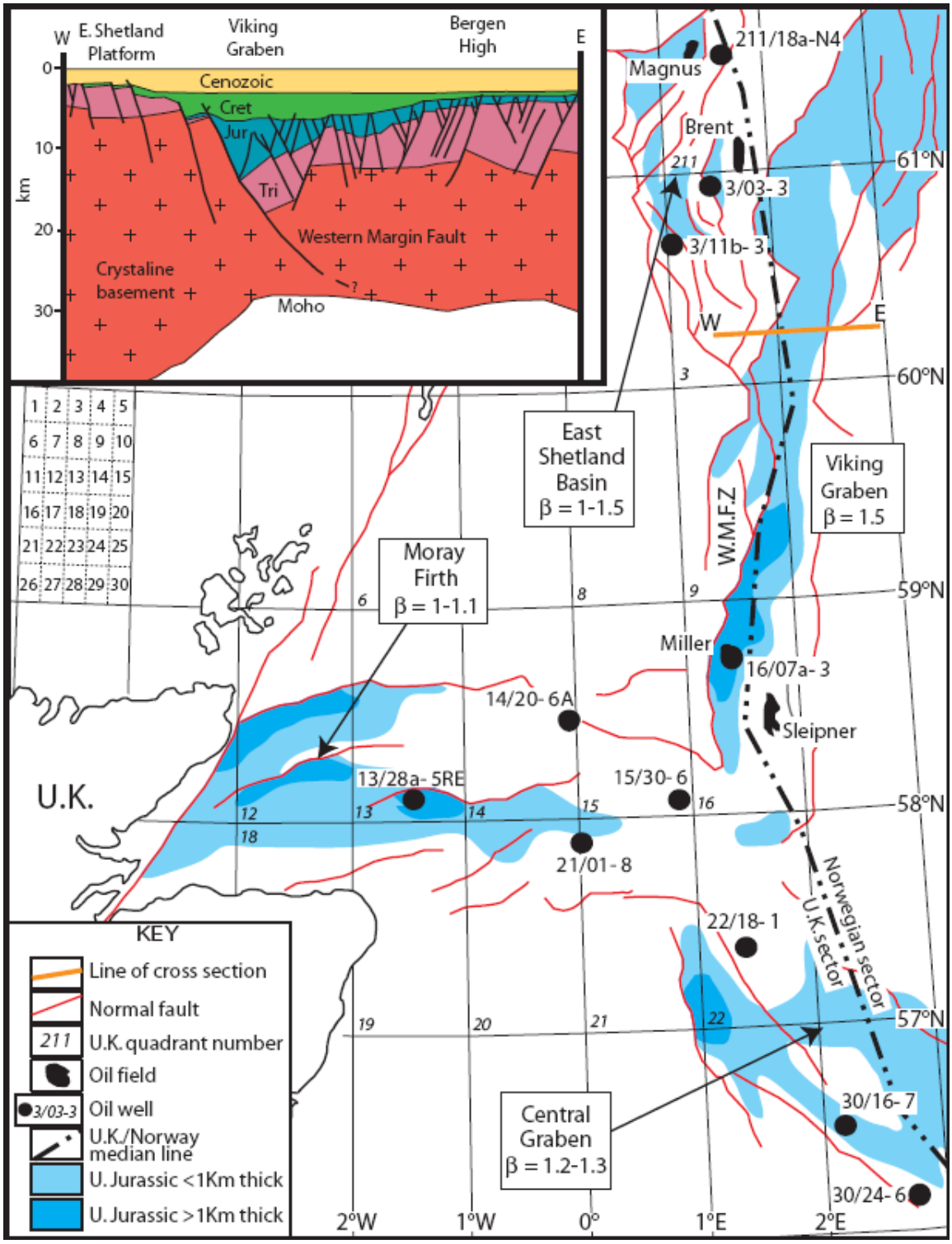

Figure 3.1 Map showing location of North Sea sample wells and oil fields used in this study. Cross section from seismic interpretation (modified from Christiansson et al., 2000). Base map, structural geology and depth of KCF modified from Cowie et al. (2005). β factors summarised from (Barr, 1985; Badley et al., 1988;Roberts et al., 1993; Barr 2002; Cowie et al., 2005).

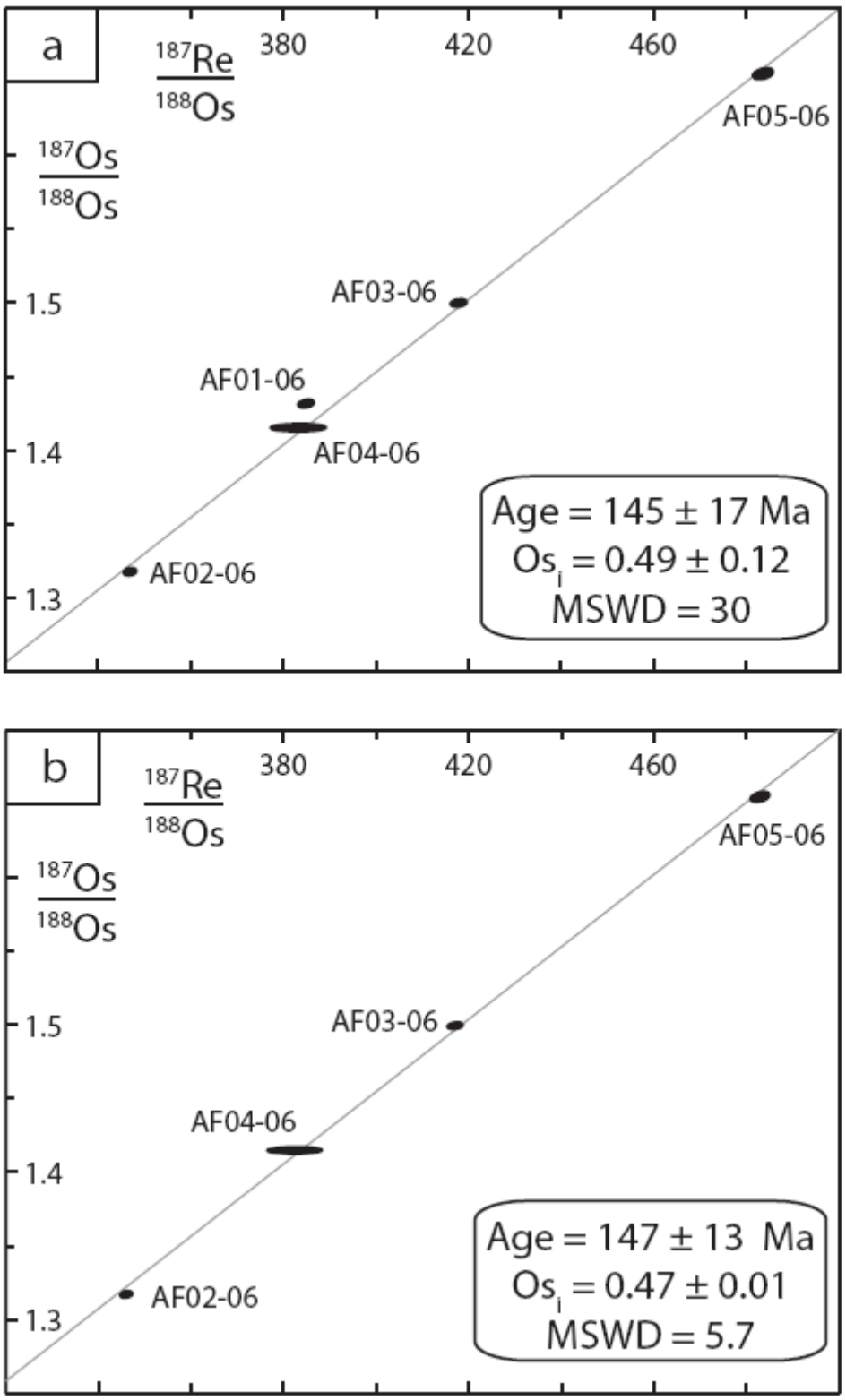

Figure 3.2 Re-Os isochrons for Miller field Core samples. Fig. 3.2a – All samples used in study, Fig. 3.2b – samples with similar Os_i. Uncertainty ellipses are at the 2σ level. See text for discussion.

4: TRACKING THE HIRNANTIAN GLACIATION USING OS ISOTOPES.

A version of this chapter has been published in Earth and Planetry Science Letters, co–authored by David Selby (Durham University) and Darren Gröcke (Durham University) and is attached as appendix 1.

4.1 Introduction

Osmium isotopes within oil provide useful information on identifying oil source (Selby and Creaser, 2005; Selby et al., 2005; Selby et al., 2007; Chapters 2 and 3). To further understand how Os isotopes can vary within a source unit this study investigates the Ordovician/Silurian "Hot" shales, a major global petroleum source unit

The Late Ordovician Hirnantian stage records the second largest mass extinction of the Phanerozoic Eon (Sheehan, 2001). This extinction eradicated 85 % of species, 61 % of genera and 12 – 24 % of families (Brenchley et al., 2001 and references therein). The extinction occurs during an abrupt change in climate (Hirnantian Glaciation) that culminated in ice-sheet growth over Gondwana and a global fall in sea-level that drained large areas of previously submerged marine shelf (Brenchley et al., 2001; Finney et al., 2007; Trotter et al., 2008).

Global Hirnantian sections (Anticosti Is. Quebec, Long, 1993a; Dob's Linn, Underwood et al., 1997; South China, Wang et al., 1997, Yan et al., 2009, Fan et al., 2009; Nevada, Finney et al., 1999; Estonia/Latvia, Brenchley et al., 2003; Arctic Canada, Melchin and Holmden, 2006; North America and China, Young, 2008; Fig. 4.1) record positive inorganic and organic carbon-isotope excursions at the onset of the glaciation (Fig. 4.2), which have been attributed to increased weathering of ^{13}C-enriched carbonates exposed during the glacio-eustatic lowstand (e.g. Kump et al., 1999; Melchin and Holmden, 2006; LaPorte et al., 2009). The major positive $\delta^{13}C_{org}$ excursion during the Late Ordovician is referred to as the Hirnantian Isotopic Carbon Excursion (HICE; Bergstrom et al., 2008), which broadly coincides with the phases of the Hirnantian extinction.

During the Cenozoic, osmium isotope ($^{187}Os/^{188}Os$) values of organic-rich marine sediments have been used to reconstruct changes in seawater $^{187}Os/^{188}Os$ (Pegram et al., 1992; Ravizza et al., 2001; Ravizza and Peucker-Ehrenbrink 2003; Oxburgh et al., 2007; Dalai et al., 2006). During the Pleistocene interglacial, seawater $^{187}Os/^{188}Os$ ratios are more radiogenic (~1.04) than during the glacial period (~0.94; Oxburgh et al., 2007). This has been interpreted to reflect the reduction in weathering of radiogenic continental crust in response to burial beneath ice sheets and decreased rates

of chemical weathering. However, following deglaciation increased chemical weathering combined with exposure of easily leached glacial deposits releases more radiogenic $^{187}Os/^{188}Os$ into the oceans (Peucker-Ehrenbrink and Blum 1998), thus causing a rise in seawater $^{187}Os/^{188}Os$. In contrast to the Cenozoic glaciations, the $^{187}Os/^{188}Os$ profile of the Hirnantian glaciation (recorded in the Dob's Linn section) reflects a much more dramatic change (~0.4; this study).

Herein, we document similar climatically driven shifts in silicate weathering through the application of initial $^{187}Os/^{188}Os$ (Os_i) from ocean basin sediments preserved at Dob's Linn (Point Linn Branch section) in the Southern Uplands of Scotland — the Global Stratotype Section and Point (GSSP) for the basal Silurian. We discuss how Os isotopes track events prior to, during and after the Hirnantian glaciation and the associated implications for Earth processes during this time. In addition to the Os_i data, we present a new $\delta\ ^{13}C_{org}$ profile for the GSSP. The two complementary proxies track changes in climatic conditions and continental weathering to the Iapetus Ocean throughout the Hirnantian glaciation. During the Hirnantian the Iapetus Ocean was connected to the Rheic Ocean (Cocks and Torsvik, 2006). The climatic events that drive silicate weathering have a global rather than local influence (c.f. Sheehan, 2001). Therefore, as the Iapetus and Rheic Oceans were interconnected (Fig. 4.1), it is feasible that the general trend in Os isotope compositions during the Late Hirnantian presented here may reflect that of a global oceanic signature. This study also demonstrates the application of Os isotopes for understanding palaeoceanographic and geological processes. Furthermore, we present the first use of Os_i stratigraphy for a Paleozoic sedimentary succession.

4.2 Geological Setting

The base Silurian GSSP is found in the Linn Branch section, Dob's Linn, which is located in the Central Zone of the Southern Uplands Terrane, Scotland (Williams, 1983; Cocks, 1985; Fig. 4.1; location, 55º25'47.56"N 003º16'72.91"W (OSGB-36), UK National Grid NT 1962, 1584). The Linn Branch section is comprised of two geological formations of the Moffat Shale Group: the stratigraphically lower Upper Hartfell Shale, which is overlain by the Lower Birkhill Shale (Fig. 4.2). The Upper Hartfell Shale is comprised of two lithologies (Fig. 4.2). The major lithology is an organic-poor (~0.1 - 0.4 % Total Organic Carbon [TOC]) grey shale, with no preserved graptolites or sedimentary structure and minor amounts of disseminated pyrite. In the studied area this unit is interbedded with six, ~5 to 20 cm thick bands of organic-rich

(~1 – 2 % TOC) black to dark grey shale. These bands are laminated and contain abundant graptolites and disseminated pyrite (Armstrong and Coe, 1997).

The Lower Birkhill Shale is and organic-rich (TOC = 0.63 to 1.69 %), laminated, graptolite-rich black shale. Disseminated pyrite is abundant throughout the unit and pyrite also forms regular sub mm layers parallel to lamination (Armstrong and Coe, 1997). Both units are interbedded with numerous <1 cm to ~5 cm scale bentonite horizons. This study also observed a poorly developed low angle cleavage through the section.

The stratigraphy of the GSSP section represents a distal micro-turbidite that was deposited on the eastern continental margin of Laurentia during the closure of the Iapetus Ocean (Armstrong and Coe, 1997; Armstrong and Owen, 2002). The Hirnantian, specifically the *extraordinarius* and *persculptus* Biozones (Figs. 4.1 – 4.3) records the glaciation that covered Gondwana up to ~30ºS (Cocks and Torsvik, 2006). The end of this glacial period is marked by the global deposition of black anoxic shales as the climate returned to greenhouse conditions (Armstrong and Coe, 1997).

The black shale units of the Hartfell and Birkhill Shale Formations are rich in numerous species of graptolites that are used as the main criteria for defining the biostratigraphy of the Ordovician and Silurian (cf. Lapworth, 1878; Williams, 1983; Cocks, 1985; Fan et al., 2009; Fig. 4.1 – 4.3). Graptolites within these bands define the *Dicellograptus anceps* Biozone (Lapworth, 1878), that have been further subdivided into the *Dicellograptus complexus* and *Paraorthograptus pacificus* Subzones, and the younger *Normalograptus extraordinarius* Biozone (Melchin et al., 2003; Fig. 4.1 and 4.2). The graptolites *Climacograptus hastus* and *Glyptograptus posterus* within the *anceps* Biozone of the Hartfell Shale are correlated with Australian and Chinese Ordovician/Silurian sections (Williams, 1988). The first occurrence of *Akidograptus ascensus* within the Birkhill Shale, which is used to define the base of the Silurian, occurs 1.6 m above the base of the Lower Birkhill Shale units (Melchin et al., 2003; Rong et al., 2006). The base Silurian is not marked by any major lithological change.

It is important to note that there is a small fault, not discussed in detail in the published literature, ~50 cm below the GSSP (Fig. 4.1). The displacement from this fault is masked by two bentonite horizons, smeared into each other. The exact loss of stratigraphy is unknown, but is likely to be ~15 cm from field observations (this study). This is likely to account for the different measured distances between the GSSP and Upper Hartfell / Lower Birkhill Shale formation contact of 1.72 m (Verniers and Vandenbroucke, 2006) and 1.6 m (Cocks, 1985; this study).

There are numerous bentonites within the Upper Hartfell Shale and the Lower Birkhill Shale at Dob's Linn, however they are rare in the *extraordinarius* to mid-*persculptus* Biozone, which span the glacial maximum (Fig. 4.1 – 4.3). The rarity of bentonite horizons may be related to the suppression of eruptions in response to the ice cover of the Hirnantian glaciation. The numerous bentonite units within the Linn Branch section are suggested to be the product of subduction-related, explosively erupted ashes of intermediate to acid composition (Cameron and Anderson, 1980; Batchelor and Weir, 1988; Huff et al., 1988, 1991; Merriman and Roberts, 1990). Multi-grain U-Pb zircon geochronology of bentonites ~4.5 m below and ~6 m above the Ordovician / Silurian boundary yield dates of 445.7 ± 2.4 and 438.7 ± 2 Ma, respectively (Tucker et al., 1990). Mathematical fitting of these dates gives an age of 443 ± 1.5 Ma for the Ordovician / Silurian boundary (Geologic Time Scale 2008, Ogg et al, 2008).

The bentonite units are dominated by illite and smectite with minor chlorite that formed during anchizone (prehnite-pumpellyite / low greenschist facies) metamorphism (Huff et al., 1991). Peak metamorphism occurred at ~340ºC during the Wenlock (428 – 422 Ma; Oliver and Leggett, 1980), which coincides with the Scandian orogeny (435 – 425 Ma; Trewin and Rollin, 2002). However, determining the absolute timing of metamorphism at Dob's Linn is challenging because of the low blocking temperature of the K-Ar systematics in illite / smectite (I/S; ~200˚C; Huff et al., 1991). The < 0.5 µm I/S fraction from nine bentonites in the lower Llandovery at Dob's Linn and correlated sections in County Down, Ireland, yield a mean age of 390 ± 10 Ma. The K-Ar dates from Dob's Linn are 406 ± 10 Ma and 383 ± 10 Ma, suggesting that metamorphism and cooling to ~200˚C occurred by the early-mid Devonian (Huff et al., 1991).

4.3 Samples and Analytical Protocols

Samples (n = 23) were collected from within the Linn Branch Stratotype Section, Dobs Linn, for $\delta\ ^{13}C_{org}$ and $^{187}Os/^{188}Os$ analysis during the summers of 2007 and 2008. The samples were approximately 10 cm x 10 cm x 3 cm (stratigraphic height) in size, weighing ~50 – 80 g, and were collected from both black and grey shale horizons, 0.9 m above to 7.1 m below the GSSP.

Carbon isotope analysis was conducted on decalcified bulk sediment powders by mixing 3M HCl with ~1 g powder in 50 ml centrifuge tubes for 24 hrs, after which they were thoroughly washed using ultra pure water (Milli-Q) until neutralised. The samples were dried in an oven at 60°C for 48 hrs. The residue was then reground to homogenise

the sample and loaded into tin capsules. Stable isotope measurements were performed at Saskatchewan and Durham using a Costech EA coupled to a ThermoFinnigan DeltaPlus XL and a Costech EA coupled to a ThermoFinnigan Delta V Advantage, respectively. Carbon-isotope ratios are corrected for ^{17}O contribution (Craig, 1957) and reported in standard delta (δ) notation in per mil (‰) relative to the VPDB scale. Carbon-isotope data is calibrated against international standards, L-SVEC ($\delta^{13}C$ = –46.6 ‰ VPDB) and IAEA-CH6 ($\delta^{13}C$ = –10.45 ‰ VPDB; Coplen et al., 2006). An intermediate international standard (IAEA-CH7) yielded a $\delta^{13}C$ value of –32.14 ± 0.03 ‰ VPDB (n = 12), which is within uncertainty of the accepted value ($\delta^{13}C$ = –32.15 ± 0.10 ‰ VPDB; Coplen 2006). Data accuracy is monitored through routine analyses of in-house standards, which are stringently calibrated against the international standards noted above. Analytical uncertainty for $\delta^{13}C_{org}$ measurements is typically better than ± 0.1 ‰. Total organic carbon (TOC) data was obtained as part of this method.

Prior to crushing, all samples were polished to remove cutting and drilling marks to eliminate any contamination. The samples were dried at 60 °C for ~12 hrs and then crushed to a fine powder ~30 μm. The samples of ~50 – 80 g represent ~3 cm of stratigraphy and were broken into chips with no metal contact and powdered in a ceramic mill. Rhenium-Osmium isotope analysis was carried out at Durham University's TOTAL laboratory for source rock geochronology and geochemistry at the Northern Centre for Isotopic and Elemental Tracing (NCIET) using Cr^{VI}-H_2SO_4 digestion and solvent extraction ($CHCl_3$), micro-distillation and anion chromatography methods and negative ionisation mass spectrometry (cf. Selby and Creaser, 2003; Selby 2007).

Rhenium-Os analysis of organic-rich rocks involves whole-rock digestion. Previous research has shown that the Re and Os abundances and isotopic compositions for organic-rich sediments predominantly reflect the hydrogenous uptake of Re and Os from seawater (Ravizza and Turekian, 1989; Cohen et al., 1999; Selby and Creaser, 2003). Further, the Re and Os are complexed by organic matter (Ravizza and Turekian, 1989; Cohen et al, 1999; Selby and Creaser, 2003). The detrital fraction of the sediment may also contain a minor abundance of Re and Os (~0.2 to 2 ppb Re and ~50 ppt Os; Esser and Turekian, 2003; Peucker-Ehrenbrink and Jahn, 2001). However, the CrO_3-H_2SO_4 digestion method employed here principally dissolves the organic fraction of a shale, thus principally liberates the hydrogenous Re–Os load of the sediment (Selby and Creaser, 2003; Kendall et al., 2004).

Total procedural blanks for Re and Os are 12 and < 0.5 pg, respectively, with an

average $^{187}Os/^{188}Os$ value of ~0.4 (n = 2). Raw Re and Os oxide values were corrected for oxygen contribution and mass fractionation. The Re and Os isotopic values and elemental abundances are calculated by full propagation of uncertainties from Re and Os mass spectrometer measurements, blank abundance and isotopic composition, spike calibration, and sample and spike weights. Throughout the period of this study, in-house Re and Os standard solutions were repeatedly analysed to monitor instrument reproducibility. The NCIET Re standard is made from 99.999 % zone-refined Re ribbon and is considered to be indistinguishable from the AB1 Re standard of the Department of Earth Sciences, University of Alberta. The Re standard runs produced average $^{185}Re/^{187}Re$ values of 0.5980 ± 0.0019 (1S.D. n = 20) indistinguishable from 0.5977 ± 0.0012 (Selby, 2007 and references therein). The measured difference between the $^{185}Re/^{187}Re$ values and the accepted $^{185}Re/^{187}Re$ value of Gramlich et al. (1973) is used to correct for sample mass fractionation. The Os (AB2) standard is made from ammonium hexachloro-osmate. The average $^{187}Os/^{188}Os$ AB2 ratio, using an electron multiplier, is 0.10681 ± 0.00022 (1 S.D. n = 24), indistinguishable from reported AB2 values (0.10679 ± 0.00007, Selby, 2007 and references therein).

Initial $^{187}Os/^{188}Os$ compositions (Os_i) are calculated for the time of deposition using the age of the basal Silurian (443 ± 1.5 Ma; Ogg et al, 2008) and the ^{187}Re decay constant of $\lambda = 1.666 \times 10^{-11} a^{-1}$ (Smoliar et al., 1996). The calculated initial is taken to represent the Iapetus oceanic $^{187}Os/^{188}Os$ composition at the time of sediment deposition.

4.4 Results

A $\delta^{13}C_{org}$ profile of the Dob's Linn section was determined by Underwood et al. (1997) for chemostratigraphic correlation of Late Ordovician successions. However, no explanation of the excursion was given and no TOC data was reported. The TOC contents for our samples range between 0.03 and 2.18 %, which reflect lithological variations of the Upper Hartfell Shale and Lower Birkhill Shale (Table 4.1; Fig. 4.3). For example, the Upper Hartfell Shale black shale bands have TOC values between 1.06 and 2.18 %, whereas grey shale units of the Upper Hartfell Shale are between 0.03 to 0.17 % (Table 4.1). From the base of the Lower Birkhill Shale at 1.6 m below the GSSP within the *persculptus* Biozone TOC values increase from ~0.6 % to a maximum of ~1.7 %, 0.05 m below the GSSP. Above the GSSP the TOC values are similar (~1.6 %).

Our $\delta^{13}C_{org}$ data range between –29.15 and –32.86 ‰ and fit the observed trend reported by Underwood et al. (1997; Figs. 4.2, 4.3; Table 4.1). Throughout the Katian

(*complanatus* to top of the *anceps* Biozone; 7.1 to 3.69 m below the GSSP) $\delta^{13}C_{org}$ values display a relative stable profile, with a minor (~0.5 ‰) shift to more positive $\delta^{13}C_{org}$ values. Throughout this interval the mean $\delta^{13}C_{org}$ value is –30.9 ‰ (S.D. = 0.95, n = 14; Fig. 4.3). From the base of the Hirnantian (*extraordinarius* Biozone), $\delta^{13}C_{org}$ values become less negative, peaking at –28.2 ‰ at 1.72 m below the GSSP (mid-*persculptus* Biozone). From here to 0.75 m below the GSSP (upper-*persculptus* Biozone) $\delta^{13}C_{org}$ values shift to more negative values after which they become relatively constant at ~ –32.5 ‰ (S.D. = 0.2, n = 14). This profile is similar to other global HICE excursions (Fig. 4.2) suggesting minimal disturbance from metamorphism.

The Re and Os abundances and $^{187}Re/^{188}Os$ and $^{187}Os/^{188}Os$ ratios are variable throughout the studied section (Re = 0.14 to 81 ppb; Os = 29 to 6393 ppt [common Os = 28 to 5335 ppt]; $^{187}Re/^{188}Os$ = 14.23 to 832.54 and $^{187}Os/^{188}Os$ = 0.551 to 6.972, Table 4.1). The uncertainty in Re and Os abundance varies from varies from 0.12 – 6.92 %, 0.22 – 1.98 % and $^{187}Re/^{188}Os$ and $^{187}Os/^{188}Os$ varies from 0.34 – 6.80 % and 0.12 – 5.99 % respectively. The Os_i values range from 0.28 – 1.08 and have uncertainties of 0.41 – 1.08 % (Fig. 4.3; Table 4.1).

From 7.1 to 4.85 m below the GSSP, within the *complanatus* and *anceps* Biozones, the Os_i increases from 0.37 to 1.08. From 4.85 to 3.10 m below the GSSP within the late *anceps* to early *extraordinarius* Biozones Os_i becomes less radiogenic (~0.4) and then remains constant at ~0.6 to 1.7 m below the GSSP within the *persculptus* Biozone. Between 1.7 and 1.5 m below the GSSP there is an abrupt increase to more radiogenic Os_i compositions (0.6 to 1.1; Fig. 4.3). From 1.6 m below to 0.9 m above the GSSP within the *persculptus* and *ascensus* Biozones Os_i values decrease to 0.60 (Fig. 4.3).

4.5 Discussion

4.5.1 Updated Dob's Linn $\delta^{13}C_{org}$ profile throughout the Hirnantian Glaciation

The new $\delta^{13}C_{org}$ profile for Dob's Linn shows the same general trend as other global late Ordovician / early Silurian profiles (Quebec, Long, 1993a; South China, Wang et al., 1997; Yan et al., 2009; Fan et al., 2009; Nevada, Finney et al., 1999; Estonia / Latvia, Brenchley et al., 2003; Kaljo et al., 2004; Arctic Canada, Melchin and Holmden, 2006; North America and China, Young, 2008; Fig. 4.2 and 4.3). During this interval the $\delta^{13}C_{org}$ values change from being very similar throughout the Katian to becoming less negative values from the base of the Hirnantian until the mid-late

Hirnantian *persculptus* Biozone. At this point the $\delta^{13}C_{org}$ becomes abruptly more negative and return to values similar to those prior to the excursion over ~1 m. This $\delta^{13}C_{org}$ profile is known as Hirnantian Isotopic Carbon Excursion (HICE; Bergstrom et al., 2008).

The HICE is proposed to have been triggered by the increased weathering of silicate terrains during the Caledonian Orogeny, which resulted in the draw down of atmospheric CO_2 (Kump et al., 1999). This reduction in greenhouse gas drove global cooling that resulted in a glaciation and marine regression during the Hirnantian. The marine regression caused significant areas of shallow marine carbonate (enriched in ^{13}C) to be exposed to weathering, increasing the flux of ^{13}C into the oceans (e.g. Kump et al., 1999; Melchin and Holmden, 2006). At Dob's Linn this event occurs in the *extraordinarius* and early - mid *persculptus* Biozones, 3.69 to 1.72 m below the GSSP, where $\delta^{13}C_{org}$ values become less negative peaking at –28.2 ‰. As global temperatures fell the chemical weathering rates decreased reducing silicate weathering and associated atmospheric CO_2 drawdown. In response atmospheric CO_2 levels increased back to pre glaciation greenhouse levels. This drove rapid deglaciation and a marine transgression, which flooded previously exposed carbonates, thus limiting the flux of ^{13}C to the oceans.

4.5.2 Re – Os systematics in the Dob's Linn section

Although not collected specifically for Re-Os geochronology, samples spanning the GSSP (DS03-04, DS01-04, DS05-04, AF03-07, DS02-04 and AF04-07) possess similar Os_i (0.71 – 0.81; Table 4.1; Fig. 4.3) when calculated at the age of the Ordovician / Silurian boundary (443 Ma; Ogg et al., 2008). These samples, similar to the majority of samples from organic-rich black shale horizons from the Dobs Linn stratigraphy, are enriched in Re and Os (6.71 to 81.01 ppb Re, 317.96 to 6393.04 ppt Os; Table 4.1). The Re-Os data for samples DS03-04, DS01-04, DS05-04, AF03-07, DS02-04 and AF04-07 yield a Re-Os age (449 ± 22 Ma, MSWD = 15, *Isoplot* v.3 Model 3, Ludwig, 2003, Fig. 4.4a). This Re-Os age is within uncertainty of the determined GSSP age given by U-Pb zircon geochronology (443 ± 1.5 Ma; Ogg et al., 2008). Given the positive correlation of $^{187}Re/^{188}Os$ with $^{187}Os/^{188}Os$ and the agreement of the determined Re-Os age with the known age of the stratigraphic interval, we are confident that our Re-Os analyses reflect the hydrogenous Re–Os load and that the Re-Os systematics have not been significantly affected by weathering or Silurian lower greenschist metamorphism (Oliver and Leggett, 1980). This conclusion is consistent

with previous studies (e.g. Peucker-Ehrenbrink and Hannigan, 2000; Jaffe et al., 2002; Kendall et al., 2004; Kendall et al., 2009). As a result we infer the Os_i values to record that of Iapetus Ocean contemporaneous with sediment deposition.

In contrast to the organic-rich black shales of the Dobs Linn stratigraphy, grey shales from the Upper Hartfell Shale are less enriched in Re and Os (0.14 to 0.89 ppb Re; 29.58 to 102.64 ppt Os; Table 4.1). These samples have similar Re and Os abundances to the average upper continental crust (Esser and Turekian, 1993; Peucker-Ehrenbrink and Jahn, 2001; Sun et al., 2003). As a result, a minor contribution of detritus with average upper continental radiogenic $^{187}Os/^{188}Os$ composition (~1.4) during the whole rock digestion process could modify the hydrogenous $^{187}Os/^{188}Os$ composition of the grey shale. However, we consider our Os_i grey shale data to record the hydrogenous $^{187}Os/^{188}Os$ composition as explained below.

Firstly, four grey shale samples (AF23-07, AF24-07, AF25-07 and AF26-07) with similar Os_i (0.6 – 0.64; Table 4.1) show a positive correlation of $^{187}Re/^{188}Os$ and $^{187}Os/^{188}Os$ values. The Re-Os age derived from the Re-Os data is imprecise (394 ± 200 Ma) because of the limited spread in the Re-Os data (~15 $^{187}Re/^{188}Os$ units; ~0.11 $^{187}Os/^{188}Os$ units; Table 4.1; Fig. 4.4b). However, the nominal agreement of the Re-Os age to the known age of the Dobs Linn section, may possibly suggest that the grey shale Re-Os data predominantly reflect the hydrogenous Re-Os load.

It is beyond the scope of this research to identify every source of sediment shedding into the Iapetus Ocean during the Late Ordovician. However, we suggest that the majority of the detritus entering into the Iapetus Ocean was predominantly from radiogenic continental crust from the Laurentian, Avalonia-Baltican and Siberian cratons, with only minor mafic inputs (Wilde et al., 1986; McKaffrey and Kneller 1996; Oliver et al., 2000; Cocks and Torsvik, 2006). Thus, any detrital Re and Os contribution to the grey shales should result in radiogenic Os_i compositions. In contrast, we observe significantly less radiogenic Os_i compositions (0.4 to 0.64; Fig. 4.3; Table 4.1). To generate non hydrogenous Os_i compositions of 0.4 and 0.6 would require detrital input from less radiogenic material (e.g., ultramafic/mafic or cosmic components), however there is no evidence for a major increase in sourcing of unradiogenic material during the Hirnantian (Wilde et al., 1986; Oliver et al., 2000; Shields et al., 2003). Therefore it is unlikely that a detrital input to the analysis is the cause of the trend to unradiogenic values across the grey shales of the glacial maximum.

The Os_i of samples AF23-07 and AF32-07 (1.7 and 1.6 m below the GSSP), which border the stratigraphic interval between the Upper Hartfell shale and Lower

Birkhill are similar (0.6 and 0.7, respectively). Despite similar Os_i for samples AF23-07 and AF32-07 they contain significantly different Re and Os abundances (0.31 and 11.71 ppb Re; 89.81 and 317.96 ppt Os; Table 4.1). This suggests that the Re-Os grey shale data reflects predominantly the hydrogenous Re and Os load and by inference the Os_i is that of Iapetus Ocean at the time of sediment deposition.

In addition, oxic organic-poor sediments (TOC not given; DSDP site 522; Angola basin; Ravizza and Peucker-Ehrenbrink 2003) are shown to yield the same hydrogenous Os_i trends as sub-oxic organic-rich (TOC = ~0.5 to 4 %) sediments from the same correlative stratigraphic interval (ODP site 959; eastern equatorial Atlantic; Ravizza and Paquay, 2008), across the Eocene – Oligocene transition (including the first Oilgocene glaciation), therefore displaying no evidence that Osi is controlled by TOC and oxia/anoxia. Furthermore, the organic-poor sediments contain similar Re and Os abundances to the grey shales of Dob's Linn (6 to 256 ppt; Ravizza and Peucker-Ehrenbrink, 2003; Oxburgh et al., 2007; Dalai et al., 2006). Also, similar to the Dob's Linn grey shales, the Cenozoic sediments predominantly comprise a matrix that does not host hydrogenous Re and Os (e.g. carbonates and silicates). The hydrogenous Re and Os is complexed by organic matter (Selby and Creaser, 2003). From this we can suggest that the Re and Os contents for both Dob's Linn and the Cenozoic sediments are similar and do not reflect detrital contamination. Given the above discussion we consider the Os_i data for the grey shales at Dobs Linn to record the hydrogenous Os_i signal of the contemporaneous Iapetus Ocean.

4.5.3 Tracking the Hirnantian Glaciation using initial $^{187}Os/^{188}Os$ (Os_i)

Throughout the *complanatus* and *anceps* Biozones, from 7.1 to 4.85 m below the GSSP, Os_i compositions become more radiogenic increasing from ~0.37 to 1.08. The Os_i abruptly increase (0.48 to 1.08) over a short time interval (< 40 cms of the *anceps* Biozone, 5.22 to 4.85 m below the GSSP; Fig. 4.3). The most radiogenic Os_i (1.08) is typically more radiogenic than the $^{187}Os/^{188}Os$ for seawater for the entire Phanerozoic, until the last 2 Myrs, and is comparable to present day sea water (~1.06; Peucker-Ehrenbrink and Ravizza, 2000 and references there in; Selby and Creaser, 2003; Ravizza and Peucker-Ehrenbrink, 2003; Widom et al., 2004; Williams and Turekian, 2004; Dalai et al., 2005; Dalai et al., 2006; Poirier, 2006; Burton, 2006; Turgeon et al., 2007; Ravizza, 2007; Selby, 2007; Oxburgh et al., 2007; Turgeon and Creaser, 2008; Selby et al., 2009). Within the same stratigraphic interval (7.1 to 4.85 m below the GSSP) the $\delta\,^{13}C_{org}$ shows only a minor (~0.5 ‰ increase to heavier values; Fig. 4.3).

The increasingly radiogenic Os_i across the late Katian suggest that the Os influx to the Iapetus Ocean became dominated by a radiogenic crustal component. This is supported by observed concordant increasingly radiogenic $^{87}Sr/^{86}Sr$ compositions (Shields et al., 2003). Throughout the Early and Middle Ordovician seawater $^{87}Sr/^{86}Sr$ decreased (0.7090 to 0.7088) with a sudden decrease across the Middle to Late Ordovician (Late Darwillian, Sandbian and Early Katian) to 0.7078. From this point to near the End Ordovician $^{87}Sr/^{86}Sr$ remains stable at ~0.7078 before becoming more radiogenic throughout the Silurian (Shields et al., 2003). The Ordovician unradiogenic $^{87}Sr/^{86}Sr$ values are attributed to low continental erosion rates and an increased submarine hydrothermal exchange rate (Shields, 2003). The change to radiogenic $^{87}Sr/^{86}Sr$ is coincident with the increasingly radiogenic Os_i values (~0.3 to ~0.6). The source of Sr to the global ocean is similar (e.g. Shields, 2003) to Os, suggesting that the Iapetus Ocean became increasingly dominated by a radiogenic crustal component from the Katian. Thus, we consider the predominant detritus shed into the Iapetus Ocean to be from the radiogenic Laurentian, Avalonia-Baltican and Siberian cratons, with only minor mafic inputs (Wilde et al., 1986; McKaffrey and Kneller 1996; Oliver et al., 2000; Cocks and Torsvik, 2006). We suggest that the significant increase in Os_i relates to increased silicate weathering of the Caledonian Orogen.

From the peak of Os_i (1.08) at 4.85 m below the GSSP, Os_i compositions become abruptly less radiogenic within the *extraordinarius* Biozone (0.85; 3.69 m below the GSSP and 0.4, 3.1 m below the GSSP), and then remain stable (~0.6) until 1.70 m below the GSSP in the *persculptus* Biozone. This stratigraphic interval coincides with the positive, glacial, limb of the $\delta^{13}C_{org}$ excursion ($\delta^{13}C_{org}$ = –31.3 to –28.2 ‰; Fig. 4.3). Between 1.7 and 1.51 m below the GSSP there is a very abrupt increase to more radiogenic Os_i compositions (0.6 to 1.05), which coincides with the negative, deglacial limb of the $\delta\ ^{13}C_{org}$ excursion. From 1.6 m below the GSSP to the top of the studied section within the *persculptus* and *ascensus* Biozones Os_i values decrease to ~0.6.

Given the radiogenic $^{187}Os/^{188}Os$ input into the Iapetus Ocean from the Laurentian, Avalonia-Baltican and Siberian Cratons, unradiogenic Os_i (0.4 to 0.64) would not be expected during the *persculptus* Biozone, as observed here (Fig. 4.3). To generate Os_i compositions of 0.4 and 0.6 would require detrital input from less radiogenic material (e.g., ultramafic / mafic or cosmic components), however there is no evidence for a major increase in sourcing of unradiogenic material during the Hirnantian (Wilde et al., 1986; Oliver et al., 2000; Shields et al., 2003).

The decrease in Os_i coincides with the ~4 ‰ increase to heavier $\delta^{13}C_{org}$ values

during the same interval that globally marks the onset of the Hirnantian glaciation. This shift in $\delta\ ^{13}C_{org}$ is attributed to the flux of ^{13}C into the oceans from the weathering of exposed marine carbonates as a result of sea level fall (Kump et al., 1999; Melchin and Holmden, 2003; LaPorte et al., 2009). The less radiogenic Os_i compositions recorded during the glacial period are likely to have been caused by a decrease in chemical weathering rates, caused by a reduction in global temperatures coupled with glacial ice cover that diminished the flux of radiogenic $^{187}Os/^{188}Os$ material into both the Iapetus and global oceans (Trotter et al., 2008). Intriguingly the Os_i during the glacial maximum (~0.6) are higher than at the start of the section (~0.3). We attribute this to the weathering of radiogenic marine sediments exposed during glacial low stand.

The observed Os_i trend at Dobs Linn is similar to that associated with Cenozoic glacial periods and appears to be related to a marine regression causing the exposure and weathering of young, unradiogenic, continental shelf material (Williams and Turekian, 2004). An increased flux of unradiogenic $^{187}Os/^{188}Os$ will cause the seawater $^{187}Os/^{188}Os$ to decrease during glacial periods, as observed at Dob's Linn (Fig. 4.3). Given the short residence time of Os in the ocean (5 – 50 kyrs; Oxburgh et al., 2007), we interpret the change in the Os_i at Dob's Linn to capture the time when the Hirnantian glaciation and deglaciation caused drastic changes in continental weathering. Global cooling and the onset of the Hirnantian Glaciation are proposed to be caused by the drawdown of atmospheric CO_2 driven by a period of high silicate weathering (Kump et al., 1999). This hypothesis is supported by the trend towards more radiogenic Os_i (0.37 to 1.08) during the Katian (7.1 to 4.85 m below the GSSP; Fig. 4.3), suggesting that increased silicate weathering was the driving process for the onset of the Hirnantian glaciation.

The rapid increase to radiogenic Os_i (0.6 to 1.05 over 19 cm) during the mid *persculptus* Biozone occurs at the correlative stratigraphic interval, in addition to the $\delta\ ^{13}C_{org}$ deglacial limb, as field evidence for deglaciation in North Africa (LeHeron et al., 2008). Post-glacial erosion of glacial deposits provides an easily leachable source of radiogenic Os into the oceans (Peucker-Ehrenbrink and Blum, 1998). Consequently, erosion of glacial deposits, combined with an increase in chemical weathering rates, rapidly increases the flux of radiogenic Os into the Iapetus and Rheic Oceans as reflected in the rapid shift to radiogenic Os_i compositions seen at Dob's Linn. The Hirnantian spans 1.9 Ma and covers ~3.75 m of stratigraphy at Dob's Linn. If a constant rate of sedimentation across the Hirnantian is assumed the compacted sedimentation rate is 2 m/Ma. Therefore, the rapid increase in $^{187}Os/^{188}Os$ (over 19 cms)

spans 95 ka across the deglacial period. However, the sedimentation rate across the Hirnantian was not constant, minor deposition occurred during the glacial maximum and maximum deposition occurring with the deglaciation. Therefore the 19 cm of stratigraphy which covers the deglacial period likely has a duration <95 ka.

4.5.4 Comparing the Hirnantian glacial Os_i profile with Cenozoic glaciations

Osmium isotope analysis of global Eocene/Oligocene and Pleistocene sediments show a correlation between $^{187}Os/^{188}Os$ compositions and glacial/interglacial climatic conditions (Ravizza et al., 2001; Ravizza and Peucker-Ehrenbrink, 2003; Williams and Turekian, 2004; Dalai et al., 2006; Oxburgh et al, 2007). These correlations highlight radiogenic values occurring during interglacial periods and less radiogenic values occurring during glacial periods. The changes seen in the Os_i compositions during the Hirnantian glaciation (~0.6 to 1.1) are greater than that observed in the Pleistocene glacial / interglacial periods (~0.94 to 1.04; Williams and Turekian, 2004). This difference relates to the climatic and geographic conditions of the glacial and interglacial cycles of the Hirnantian and Pleistocene.

Although the Hirnantian glaciation was smaller in area than the Pleistocene (30,000,000 km^2 as opposed to 44,000,000 km^2; Sheehan, 2001) it was centred near the South Pole and thus covered a large proportion of the Gondwanan craton and little of the global ocean (LeHeron et al., 2008). In contrast, the Pleistocene glacial maximums covered large areas of open ocean as well as the Canadian and Fennoscandinavian craton. However, significant areas of Archean cratons with highly evolved radiogenic signatures remained exposed e.g. Australasian, South American, African and Indian (Mercer, 1983; Clark and Mix, 2002; Pearson and Wittig, 2008). From this tectonic setting / scenario the extensive cratonic glacial cover during the Hirnantian would have reduced the radiogenic $^{187}Os/^{188}Os$ flux into the oceans. Furthermore, sea level fall resulting from the Hirnantian glaciation is estimated to be <100 m compared to 100 – 150 m for the Pleistocene glacial maximum (Sheehan, 2001; Brenchley et al., 2003; Williams and Turekian, 2004). Thus, Hirnantian glaciation lead to less exposure and reworking of radiogenic anoxic deep marine ORS (e.g. black shales) than the Pleistocene.

Finally, CO_2 levels at ~440 Ma were ~14 times higher than present (Berner, 2006). This indicates, with oxygen isotopes (Trotter et al., 2008), that global temperatures and therefore chemical weathering rates were higher during the late Ordovician than in the Pleistocene. Therefore, the reduction in chemical weathering

rates as a result of the Hirnantian icehouse would have been greater than during the Pleistocene, further decreasing the input of radiogenic Os to the Iapetus Ocean. This has been observed during the Toarcian OAE where a similar magnitude Os_i shift of ~0.6 is attributed to an increase in chemical weathering rates caused by a rise in temperature of ~10°C (Cohen et al., 2004; Waltham and Gröcke, 2006). This temperature rise is indistinguishable from that determined during the Hirnantian glaciation (Trotter et al., 2008).

4.6 Conclusions

Through the integration of Os_i and $\delta\,^{13}C_{org}$ profiles at Dob's Linn it has proved possible to track the onset and cessation of the Hirnantian glaciation (Fig. 4.3). We interpret the Os_i stratigraphy at Dob's Linn to record the evolution in seawater Os isotopic composition of the Iapetus Ocean. However, given that this seaway was connected to the global ocean it may also reflect that of global seawater. The changes in climate that force the trends in the profile described for Dob's Linn are global and therefore will have the same effect on both Iapetus and the global oceans. Thus, we hypothesise that although absolute data may vary between Iapetus and other global Ordovician/Silurian oceans (e.g. Rheic) the trends in the profile will be similar.

Throughout the Katian, Os_i becomes increasingly radiogenic, as a result of increased silicate weathering of radiogenic orogenic material associated with the Caledonian Orogen. As a result of atmospheric CO_2 drawdown, global cooling ensued, causing the onset of the Hirnantian Glaciation. Reduced chemical weathering rates and growth of continental ice cover significantly reduced the input of radiogenic Os into the oceans. Increased ice volume resulted in falling sea levels, thus exposing marine carbonates and unradiogenic shelf to weathering. These new weathering regimes lead to an increased flux of ^{13}C and unradiogenic Os into the oceans. As a direct result of the decrease in silicate weathering during the Hirnantian, atmospheric CO_2 returned to greenhouse levels, causing rapid deglaciation during the Late Hirnantian mid *persculptus* Biozone. This de-glacial period is recorded by a dramatic rise in Os_i (0.6 – 1.05) over 19 cm of stratigraphy at Dob's Linn. We interpret this dramatic rise to be a consequence of the leaching of radiogenic $^{187}Os/^{188}Os$ from glacial deposits and increased weathering of radiogenic $^{187}Os/^{188}Os$ silicate terrane.

The results of this study further highlight the use of Os_i as a powerful tool for understanding the Earth climate system and, in particular, aid in monitoring changes in weathering and its affect on palaeoceanography (e.g. Cohen et al., 1999; 2004; Ravizza

and Peucker-Ehrenbrink, 2003; Oxburgh et al., 2007; Ravizza and Paquay, 2008). In addition, the short residence time of Os (5 – 50 kyrs) in comparison to Sr (1 – 4 Ma) allows for a greater resolution for enhancing our understanding of palaeoenvironmental processes (cf. Cohen et al., 1999; Peucker-Ehrenbrink and Ravizza, 2000; Turgeon and Creaser, 2008; Selby et al., 2009; this study). For example, diachronous Neoproterozoic Sturtian deglacial sediments have been shown to have highly radiogenic Os_i (0.82 – 1.00; Kendall et al., 2006; Kendall et al., 2009). These values are remarkably similar to that reported here for the Hirnantian deglaciation. Thus, suggesting an increased continental weathering rate associated with deglaciation. However, we have no known values of seawater Os_i for pre/syn Neoproterozoic Sturtian glaciation. Therefore, Os_i data could provide increased understanding of weathering rates associated with Neoproterozoic global glaciations.

References

Armstrong, H.A., Coe, A.L., 1997. Deep-sea sediments record the geophysiology of the late Ordovician glaciation. J. Geol. Soc. (Lond.) 154, 929–934.

Armstrong, H.A., Owen, A.W., 2002. Euconodont paleobiogeography and the closure of the Iapetus Ocean. Geology 30, 1091–1094.

Batchelor, R.A., Weir, J.A., 1988. Metabentonite geochemistry: magmatic cycles and graptolite extinctions at Dob's Linn, southern Scotland. Trans. R. Soc. Edinburgh 79, 19–41.

Bergstrom, S.M., Chen, X., Gutierrez-Marco, J.C., Dronov, A., 2008. The new Chronostratigraphic classification of the Ordovician System and its relations to major regional series and stages and to δ13C chemostratigraphy. Lethaia 42, 97–107.

Berner, R.A., 2006. GEOCARBSULF: a combined model for Phanerozoic atmospheric O2 and CO2. Geochim. Cosmochim. Acta 70, 5653–5664.

Brenchley, P.J., Marshall, J.D., Underwood, C.J., 2001. Do all mass extinctions represent an ecological crisis? Evidence from the Late Ordovician. Geol. J. 36, 329–340.

Brenchley, P.J., Carden, G.A., Hints, L., Kaljo, D., Marshall, J.D., Martma, T., Meidla, T.,Nolvak, J., 2003. High-resolution stable isotope stratigraphy of Upper Ordovician sequences: constraints on the timing of bioevents and environmental changes associated with mass extinction and glaciation. Geol. Soc. Am. Bull. 115, 89–104.

Burton, K.W., 2006. Global weathering variations inferred from marine radiogenic isotope records. J. Geochem. Explor. 88, 262–265.

Cameron, T.D.J., Anderson, T.B., 2007. Silurian metabentonites in County Down, Northern Ireland. Geol. J. 15, 59–75.

Clark, P.U., Mix, A.C., 2002. Ice sheets and sea level of the last glacial maximum. Quat.Sci. Rev. 21, 1–7.

Cocks, L.R.M., 1985. The Ordovician–Silurian boundary. Episodes 8, 98–100.

Cocks, L.R.M., Torsvik, T.H., 2006. European geography in a global context from the Vendian to the end of the Palaeozoic. Geol. Soc. (Lon) Mem. 32, 83–95.

Cohen, A.S., Coe, A.L., Bartlett, J.M., Hawkesworth, C.J., 1999. Precise Re–Os ages of organic-rich mudrocks and the Os isotope composition of Jurassic seawater. Earth Planet. Sci. Lett. 167, 159–173.

Cohen, A.S., Coe, A.L., Harding, S.M., Schwark, L., 2004. Osmium isotope evidence for the regulation of atmospheric CO_2 by continental weathering. Geology 32, 157–160.

Coplen, T.B., Brand, W.A., Gehre, M., Groning, M., Meijer, H.A.J., Toman, B., Verkouteren, R.M., 2006. New guidelines for $\delta^{13}C$ measurements. Anal. Chem. 78, 2439–2441.

Craig, H., 1957. Isotopic standards for carbon and oxygen and correction factors for massspectrometric analysis of carbon dioxide. Geochim. Cosmochim. Acta 12, 133–149.

Creaser, R.A., Papanastassiou, D.A., Wasserburg, G.J., 1991. Negative thermal ion massspectrometry of osmium, rhenium, and iridium. Geochim. Cosmochim. Acta 55, 397–401.

Dalai, T.K., Suzuki, K., Minagawa, M., Nozaki, Y., 2005. Variations in seawater osmium isotope composition since the last glacial maximum: a case study from the Japan Sea. Chem. Geol. 220, 303–314.

Dalai, T.K., Ravizza, G.E., Peucker-Ehrenbrink, B., 2006. The Late Eocene $^{187}Os/^{188}Os$ excursion: chemostratigraphy, cosmic dust flux and the Early Oligocene glaciation. Earth Planet. Sci. Lett. 241, 477–492.

Esser, B.K., Turekian, K.K., 1993. Anthropogenic osmium in coastal deposits. Environ. Sci. Technol. 27, 2719–2724.

Fan, J., Peng, P., Melchin, M.J., 2009. Carbon isotopes and event stratigraphy near the Ordovician–Silurian boundary, Yichang, South China. Palaeogeogr. alaeoclimatol. Palaeoecol. 276, 160–169.

Finney, S.C., Berry, W.B.N., Cooper, J.D., Ripperdan, R.L., Sweet, W.C., Jacobson, S.R., Soufiane, A., Achab, A., Noble, P.J., 1999. Late Ordovician mass extinction: a new perspective from stratigraphic sections in central Nevada. Geology 27, 215–218.

Finney, S.C., Berry, W.B.N., Cooper, J.D., 2007. The influence of denitrifying seawater on graptolite extinction and diversification during the Hirnantian (latest Ordovician) mass extinction event. Lethaia 40, 281–291.

Gramlich, J.W., Murphy, T.J., Garner, E.L., Shields, W.R., 1973. Absolute isotopic abundance ratio and atomic weight of a reference sample of rhenium. J. Res. Nat. Bur. Stand. 77, 691–698.

Huff, W.D., Whiteman, J.A., Curtis, C.D., 1988. Investigation of a K-bentonite by X-ray powder diffraction and analytical transmission electron microscopy. Clays Clay Miner. 36, 83–93.

Huff, W.D., Anderson, T.B., Rundle, C.C., Odin, G.S., 1991. Chemostratigraphy, K–Ar ages and illitization of Silurian K-bentonites from the Central Belt of the Southern Uplands-Down-Longford Terrane, British Isles. J. Geol. Soc. (Lond) 148, 861–868.

Jaffe, L.A., Peucker-Ehrenbrink, B., Petsch, S.T., 2002. Mobility of rhenium, platinum group elements and organic carbon during black shale weathering. Earth Planet. Sci. Lett. 198, 339–353.

Kaljo, D., Hints, L., Martma, T., Nolvak, J., Oraspold, A., 2004. Late Ordovician carbon isotope trend in Estonia, its significance in stratigraphy and environmental analysis. Palaeogeogr. Palaeoclimatol. Palaeoecol. 210, 165–185.

Kendall, B.S., Creaser, R.A., Ross, G.M., Selby, D.S., 2004. Constraints on the timing of Marinoan "Snowball Earth" glaciation by ^{187}Re–^{187}Os dating of a Neoproterozoic, post-glacial black shale in Western Canada. Earth Planet. Sci. Lett. 222, 729–740.

Kendall, B.S., Creaser, R.A., Selby, D.S., 2006. Re–Os geochronology of postglacial black shales in Australia: constraints on the timing of "Sturtian" glaciation. Geology 34, 729–732.

Kendall, B.S., Creaser, R.A., Calver, C.R., Raub, T.D., Evans, A.D., 2009a. Correlation of Sturtian diamictite successions in southern Australia and northwestern Tasmania by Re–Os black shale geochronology and the ambiguity of "Sturtian"-type diamictite-cap carbonate pairs as chronostratigraphic marker horizons. Precambrian Res. 172, 301–310.

Kendall, B.S., Creaser, R.A., Selby, D., 2009b. ^{187}Re–^{187}Os geochronology of Precambrian organic-rich sedimentary rocks. Geol. Soc. (Lond). Spec. Publ. 326, 85–107.

Kump, L.R., Arthur, M.A., Patzkowsky, M.E., Gibbs, M.T., Pinkus, D.S., Sheehan, P.M., 1999. A weathering hypothesis for glaciation at high atmospheric pCO_2 during the Late-Ordovician. Palaeogeogr. Palaeoclimatol. Palaeoecol. 152, 173–187.

LaPorte, D.F., Holmden, C., Patterson, W.P., Loxton, J.D., Melchin, M.J., Mitchell, C.E., Finney, S.C., Sheets, H.D., 2009. Local and global perspectives on carbon and nitrogen

cycling during the Hirnantian glaciation. Palaeogeogr. Palaeoclimatol. Palaeoecol. 276. 1–4, 182–195.
Lapworth, C., 1878. The Moffat series. Q. J. Geol. Soc. 34, 240–346.
Le Heron, D.P., Khoukhi, Y., Paris, F., Ghienne, J.F., Le Herisse, A., 2008. Black shale, grey shale, fossils and glaciers: Anatomy of the Upper Ordovician–Silurian succession in the Tazzeka Massif of eastern Morocco. Gondwana Res. 14, 483–496.
Long, D.G.F., 1993. Oxygen and carbon isotopes and event stratigraphy near the Ordovician–Silurian boundary, Anticosti Island Quebec. Palaeogeogr. Palaeoclimatol. Palaeoecol. 104, 49–59.
Ludwig, K.R., 2003. ISOPLOT: A Plotting and Regression Program for Radiogenic-Isotope Data, version 3.
McCaffrey, W.D., Kneller, B.C., 1996. Silurian turbidite provenance on the north Avalonian margin. J. Geol. Soc. (Lond) 153, 437–450.
Melchin, M.J., Holmden, C., 2006. Carbon isotope chemostratigraphy in Arctic Canada: sea-level forcing of carbonate platform weathering and implications for Hirnantian global correlation. Palaeogeogr. Palaeoclimatol. Palaeoecol. 234, 186–200.
Melchin, M.J., Holmden, C., Williams, S.H., 2003. In: Albanesi, G.L., Beresi, M.S., Peralta, S. H. (Eds.), Ordovician from the Andes – Proceedings of the 9th International Symposium on the Ordovician System: INSUGEO, Serie Correlación Geológica, 17, pp. 101–104.
Mercer, J.H., 1983. Cenozoic glaciation in the southern hemisphere. Annu. Rev. Earth Planet Sci. 11, 99–132.
Merriman, R.J., Roberts, B., 1990. Metabentonites in the Moffat Shale Group, Southern Uplands of Scotland — geochemical evidence of ensialic marginal basin volcanism. Geol. Mag. 127, 259–271.
Ogg, J.G., Ogg, G., Gradstein, F.M., 2008. The Concise Geologic Time Scale. Cambridge University Press.
Oliver, G.J.H., Leggett, J.K., 1980. Metamorphism in an accretionary prism: prehnite–pumpellyite facies metamorphism of the Southern Uplands of Scotland. Trans. R. Soc. Edinburgh Earth Sci. 71, 235–246.
Oliver, G.J.H., Chen, F., Buchwaldt, R., Hegner, E., 2000. Fast tectonometamorphism and exhumation in the type area of the Barrovian and Buchan zones. Geology 28, 459–462.
Oxburgh, R., Pierson-Wickmann, A.C., Reisberg, L., Hemming, S., 2007. Climatecorrelated variations in seawater 187Os/188Os over the past 200,000 yr: evidence from the Cariaco Basin, Venezuela. Earth Planet. Sci. Lett. 263, 246–258.
Pearson, D.G., Wittig, N., 2008. Formation of Archaean continental lithosphere and its diamonds: the root of the problem. J. Geol. Soc. (Lond) 165, 895–914.
Pegram, W.J., Krishnaswami, S., Ravizza, G.E., Turekian, K.K., 1992. The record of sea water 187Os/186Os variation through the Cenozoic. Earth Planet. Sci. Lett. 113, 569–576.
Peucker-Ehrenbrink, B., Blum, J.D., 1998. Re – Os isotope systematics and weathering of Precambrian crustal rocks: implications for the marine osmium record. Geochim. Cosmochim. Acta 62, 3193–3203.
Peucker-Ehrenbrink, B., Hannigan, R.E., 2000. Effects of black shale weathering on the mobility of rhenium and platinum group elements. Geology 28, 475–478.
Peucker-Ehrenbrink, B., Jahn, B., 2001. Rhenium–osmium isotope systematics and platinum group element concentrations: loess and the upper continental crust. Geochem. Geophys. Geosyst. 2, 1061.
Peucker-Ehrenbrink, B., Ravizza, G., 2000. The marine osmium isotope record. Terra Nova 12, 205–219.
Poirier, A., 2006. Re–Os and Pb isotope systematics in reduced fjord sediments from Saanich Inlet (Western Canada). Earth Planet. Sci. Lett. 249, 119–131.
Ravizza, G., 2007. Reconstructing the 187Os/188Os record and the particulate flux of meteoric osmium during the late Cretaceous. Geochim. Cosmochim. Acta 71, 1355–1369.
Ravizza, G., Paquay, F., 2008. Os_i isotope chemostratigraphy applied to organic-rich marine sediments from the Eocene–Oligocene transition on the West African margin (ODP Site 959). Paleoceanography 23, PA2204.

Ravizza, G., Peucker-Ehrenbrink, B., 2003. The marine ^{187} Os/^{188}Os record of the Eocene–Oligocene transition: the interplay of weathering and glaciation. Earth Planet. Sci. Lett. 210, 151–165.

Ravizza, G., Turekian, K.K., 1989. Application of the ^{187}Re–^{187}Os system to black shale geochronometry. Geochim. Cosmochim. Acta 53, 3257–3262.

Ravizza, G., Norris, R.N., Blusztajn, J., Aubry, M.-P., 2001. An osmium isotope excursion associated with the late Paleocene thermal maximum: evidence of intensified chemical weathering. Paleoceanography 16, 155–163.

Rong, Jia-yu, Boucot, A.J., Harper, D.A.T., Ren-bin, Zhan, Neuman, R.B., 2006. Global analyses of brachiopod faunas through the Ordovician and Silurian transition: reducing the role of the Lazarus effect. Can. J. Earth Sci. 43, 23–39.

Selby, D., 2007. Direct Rhenium–Osmium age of the Oxfordian–Kimmeridgian boundary, Staffin bay, Isle of Skye, U.K., and the Late Jurassic time scale. Norw. J. Geol. 87, 291–299.

Selby, D., Creaser, R.A., 2003. Re–Os geochronology of organic rich sediments: an evaluation of organic matter analysis methods. Chem. Geol. 200, 225–240.

Selby, D., Creaser, R.A. 2005. Direct radiometric dating of hydrocarbon deposits using Rhenium-Osmium isotopes. Science. 308, 1293 – 1295.

Selby, D., Mutterlose, J., Condon, D.J., 2009. U–Pb and Re–Os geochronology of the Aptian/Albian and Cenomanian/Turonian stage boundaries: implications for timescale calibration, osmium isotope seawater composition and Re–Os systematics in organic-rich sediments. Chem. Geol. 265, 394–409.

Sheehan, P.M., 2001. The Late Ordovician mass extinction. Annu. Rev. Earth Planet. Sci. 29, 331–364.

Shields, G.A., Carden, G.A.F., Veizer, J., Meidla, T., Rong, J.Y., Li, R.Y., 2003. Sr, C, and O isotope geochemistry of Ordovician brachiopods: a major isotopic event around the Middle-Late Ordovician transition. Geochim. Cosmochim. Acta 67, 2005–2025.

Smoliar, M.I., Walker, R.J., Morgan, J.W., 1996. Re–Os ages of group IIA, IIIA, IVA, and IVB iron meteorites. Science 23, 1099–1102.

Sun,W., Bennett, V.C., Eggins, S.M., Kamenetsky, V.S., Arculus, R.J., 2003. Enhanced mantleto-crust rhenium transfer in undegassed arc magmas. Nature 422, 294–297.

Trewin, N.H., Rollin, K.E., 2002. Geological history and structure of Scotland. In: Trewin, N.H. (Ed.), The Geology of Scotland. The Geological Society, London, pp. 1–25.

Trotter, J.A., Williams, I.S., Barnes, C.R., Lecuyer, C., Nicoll, R.S., 2008. Did cooling oceans trigger Ordovician biodiversification? Evidence from conodont thermometry. Science 321, 550–554.

Tucker, R.D., Krogh, T.E., Ross Jr., R.J., Williams, S.H., 1990. Time-scale calibration by high-precision U–Pb zircon dating of interstratified volcanic ashes in the Ordovician and Lower Silurian stratotypes of Britain. Earth Planet. Sci. Lett. 100, 51–58.

Turgeon, S.C., Creaser, R.A., 2008. Cretaceous oceanic anoxic event 2 triggered by a massive magmatic episode. Nature 454, 323–326.

Turgeon, S.C., Creaser, R.A., Algeo, T.J., 2007. Re–Os depositional ages and seawater Os estimates for the Frasnian–Famennian boundary: implications for weathering rates, land plant evolution, and extinction mechanisms. Earth Planet. Sci. Lett. 261, 649–661.

Underwood, C.J., Crowley, S.F., Marshall, J.D., Brenchley, P.J., 1997. High-resolution carbon isotope stratigraphy of the basal Silurian stratotype (Dob's Linn, Scotland) and its global correlation. J. Geol. Soc. (Lond) 154, 709–718.

Verniers, J., Vandenbroucke, T.R.A., 2006. Chitinozoan biostratigraphy in the Dob's Linn Ordovician–Silurian GSSP, Southern Uplands, Scotland. GFF 128, 195–202.

Waltham, D., Gröcke, D.R., 2006. Non-uniqueness and interpretation of the seawater ^{87}Sr/^{86}Sr curve. Geochim. Cosmochim. Acta 70, 384–394.

Wang, K., Chatterton, B.D.E., Wang, Y., 1997. An organic carbon isotope record of Late Ordovician to Early Silurian marine sedimentary rocks, Yangtze Sea, South China: implications for CO2 changes during the Hirnantian glaciation. Palaeogeogr. Palaeoclimatol. Palaeoecol. 132, 147–158.

Widom, E., Gaddis, S.J., Wells Jr., N.E., 2004. Re–Os isotope systematics in carbonates from Serpent Mound, Ohio: implications for Re–Os dating of crustal rocks and the osmium isotopic composition of Ordovician seawater. Geochem. Geophys. Geosyst. 5, Q03006.

Wilde, P., Berry, W.B.N., Quinbyhunt, M.S., Orth, C.J., Quintana, L.R., Gilmore, J.S., 1986. Iridium abundances across the Ordovician –Silurian Stratotype. Science 233, 339–341.

Williams, S.H., 1983. The Ordovician–Silurian boundary graptolite fauna of Dob's Linn, southern Scotland. Palaeontology 26, 605–639.

Williams, S.H., 1986. Top Ordovician and lowest Silurian of Dob's Linn. Geol. Soc. (Lond.) Spec. Publ. 20, 165–171.

Williams, S.H., 1988. Dob's Linn—the Ordovician–Silurian boundary stratotype. In: Cocks, L.R.M., Rickards, R.B. (Eds.), A Global Analysis of the Ordovician–Silurian Boundary: Bull. Brit. Mus. (Nat. Hist.) Geol., 43, pp. 17–30.

Williams, G.A., Turekian, K.K., 2004. The glacial–interglacial variation of seawater osmium isotopes as recorded in Santa Barbara Basin. Earth Planet. Sci. Lett. 228, 379–389.

Yan, D., Chen, D., Wang, Q., Wang, J., Wang, Z., 2009. Carbon and sulphur isotopic anomalies across the Ordovician–Silurian boundary on the Yangtze Platform, South China. Palaeogeogr. Palaeoclimatol. Palaeoecol. 274, 32–39.

Young, S.A., Saltzman, M.R., Bergström, S.M., Leslie, S.A., Chen, Ru, 2008. Paired $\delta^{13}C_{carb}$ and $\delta^{13}C_{org}$ records of Upper Ordovician (Sandbian–Katian) carbonates in North America and China: implications for paleoceanographic change. Palaeogeogr. Palaeoclimatol. Palaeoecol. 270, 166–178.

Table 4.1 Total organic carbon, $d^{13}C_{org}$ and Re – Os data for the Dob's Linn Basal Silurian GSSP

Sample	Distance from O/S GSSP (m)	TOCa (wt. %)	$d^{13}C_{org}$ (‰, V-PDB)	Re (ppb)	Os (ppt)	$^{187}Re/^{188}Os$	$^{187}Os/^{188}Os$	Os_i[b]	[Os]*[c]
AF20-07	0.9	1.57	-32.7	59.33 ± 0.2	692.9 ± 2.8	728.4 ± 2.8	5.995 ± 0.013	0.598 ± 0.003	392
DS03-04	0.07	1.57	-32.82	58.15 ± 0.19	671.4 ± 2.8	753 ± 2.9	6.291 ± 0.014	0.713 ± 0.003	371
DS01-04	0.03	1.41	-32.17	63.2 ± 0.21	835.9 ± 3.1	607.5 ± 2.2	5.243 ± 0.009	0.744 ± 0.003	500
DS05-04	0.03	1.41	-32.17	50.05 ± 0.17	571.1 ± 2.6	769.8 ± 3.1	6.437 ± 0.016	0.73 ± 0.003	313
AF03-07	0	1.66	-32.6	66.27 ± 0.22	726.9 ± 3.2	831.5 ± 3.2	6.972 ± 0.016	0.812 ± 0.004	383
DS02-04	-0.03	1.66	-32.86	64.03 ± 0.21	701.7 ± 3.1	832.3 ± 3.2	6.972 ± 0.016	0.806 ± 0.026	370
AF04-07	-0.05	1.69	-32.6	66.44 ± 0.22	1043 ± 6	472.2 ± 2.1	4.259 ± 0.02	0.761 ± 0.004	676
AF07-07	-1.1	0.54	-30.77	19.94 ± 0.07	505.1 ± 1.8	260.1 ± 1	2.944 ± 0.007	1.018 ± 0.005	368
AF08-07	-1.51	0.91	-30.17	29.03 ± 0.1	465.3 ± 2	474.8 ± 1.9	4.567 ± 0.012	1.05 ± 0.005	294
AF32-07	-1.6	0.63	-30.08	11.71 ± 0.04	318 ± 1.1	230.3 ± 0.9	2.407 ± 0.006	0.702 ± 0.009	244
AF23-07	-1.7	0.14	-29.26	0.31 ± 0.01	89.8 ± 1.8	17.8 ± 0.8	0.729 ± 0.042	0.6 ± 0.042	83.2
AF24-07	-2.2	0.11	-29.15	0.16 ± 0.01	57.1 ± 1.1	14.2 ± 0.8	0.71 ± 0.041	0.604 ± 0.048	53.0
AF25-07	-2.4	0.15	-29.45	0.15 ± 0.01	48.1 ± 1	15.8 ± 0.9	0.758 ± 0.044	0.641 ± 0.052	44.4
AF26-07	-2.7	0.13	-29.92	0.27 ± 0.01	47.5 ± 0.9	29.5 ± 1.4	0.823 ± 0.048	0.605 ± 0.045	43.5
AF27-07	-3.1	0.12	-29.49	0.28 ± 0.01	37.4 ± 0.7	37.4 ± 1.8	0.685 ± 0.04	0.404 ± 0.03	34.8
AF11-07	-3.69	1.06	-31.02	6.71 ± 0.03	1349 ± 9	26.9 ± 0.2	1.047 ± 0.016	0.85 ± 0.014	1202
AF13-07	-4.85	1.25	-30.99	81.01 ± 0.27	6393 ± 14	73 ± 0.3	1.625 ± 0.002	1.084 ± 0.005	5335
AF29-07	-5	0.17	-29.87	8.1 ± 0.01	102.6 ± 1.2	46.8 ± 1	1.069 ± 0.031	0.726 ± 0.026	91.2
AF14-07	-5.22	2.18	-31.26	16.45 ± 0.06	578 ± 1.7	165.4 ± 0.6	1.702 ± 0.004	0.477 ± 0.002	478
AF15-07	-5.88	2.11	-31.59	20.25 ± 0.29	914 ± 5	126.1 ± 1.9	1.517 ± 0.01	0.583 ± 0.009	772
AF30-07	-5.9	0.03	-29.53	0.8 ± 0.01	44.5 ± 0.4	96.7 ± 2.1	0.983 ± 0.017	0.279 ± 0.007	40.0
AF30 rpt	-	-	-	0.8 ± 0.01	44.5 ± 0.4	96.7 ± 2.1	0.983 ± 0.017	0.28 ± 0.006	40.0
AF31-07	-7.1	0.08	-31.88	0.14 ± 0.01	29.6 ± 0.6	24.9 ± 1.7	0.551 ± 0.033	0.381 ± 0.033	28.0

Note: Uncertainties are given as 2s. Samples are held by Alexander Finlay.

[a]Total organic carbon.

[b] Os_i - initial $^{187}Os/^{188}Os$ composition calculated at time of deposition (443 Ma). Os_i uncertainties are calculated through full propagation of calculated $^{187}Re/^{188}Os$ and $^{187}Os/^{188}Os$ uncertainties

[c][Os]* - calculated common Os.

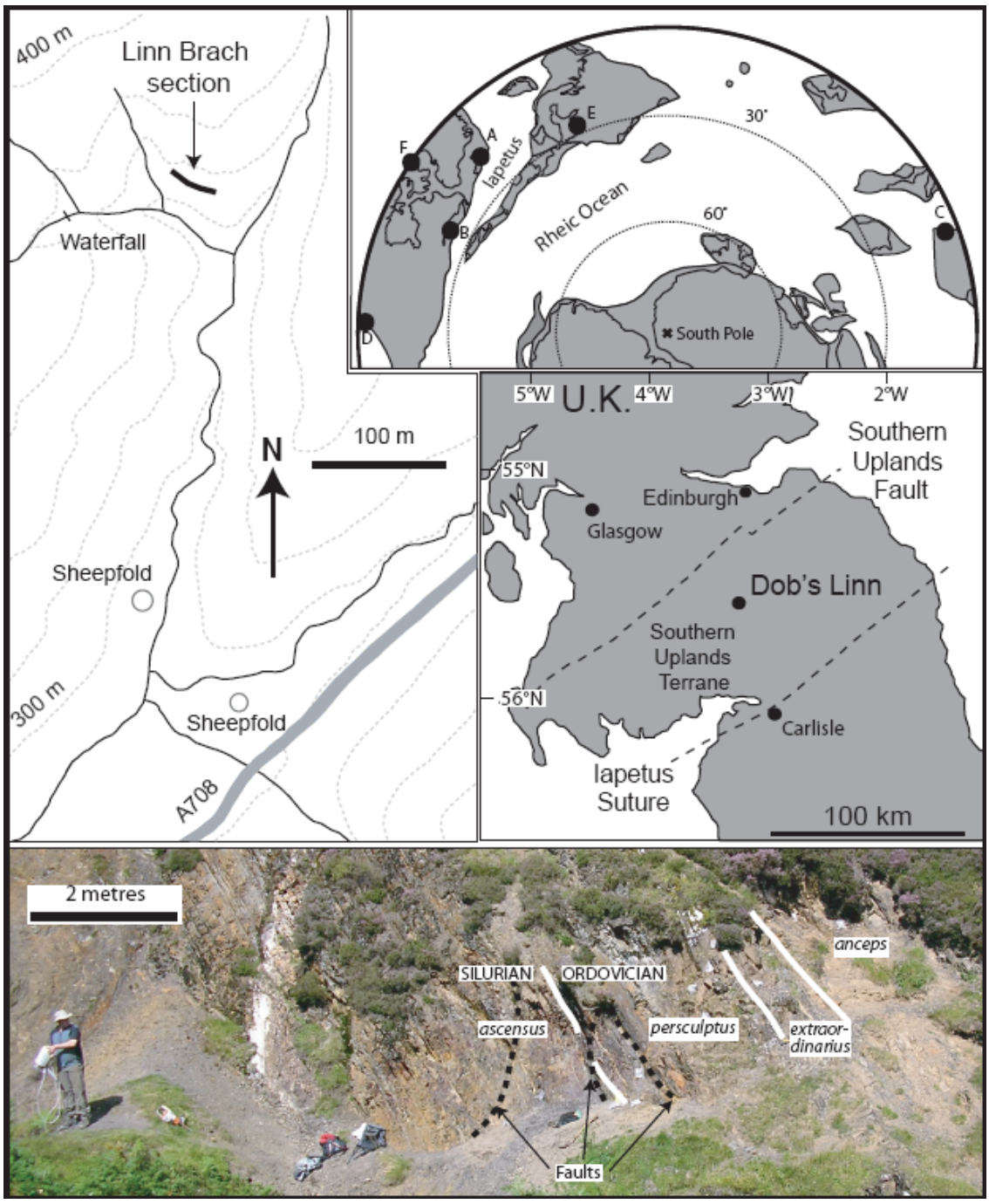

Figure 4.1 Location maps for the study area, Dob's Linn, Scotland. Palaeogeographic map for 440 Ma (modified from Cocks and Torsvik, 2006) showing locations discussed in text; A – Dob's Linn, Scotland; B – Anticosti Island, Quebec; C – South China; D – Nevada, USA; E, Estonia/Latvia; and F – Arctic Canada. Linn Branch Section at Dob's Linn location; 55º25'47.56"N 003º16'72.91"W (OSGB-36), UK National Grid NT 1962, 1584. Contour lines represent 25 m elevation. Photograph of Linn Branch section taken facing North East.

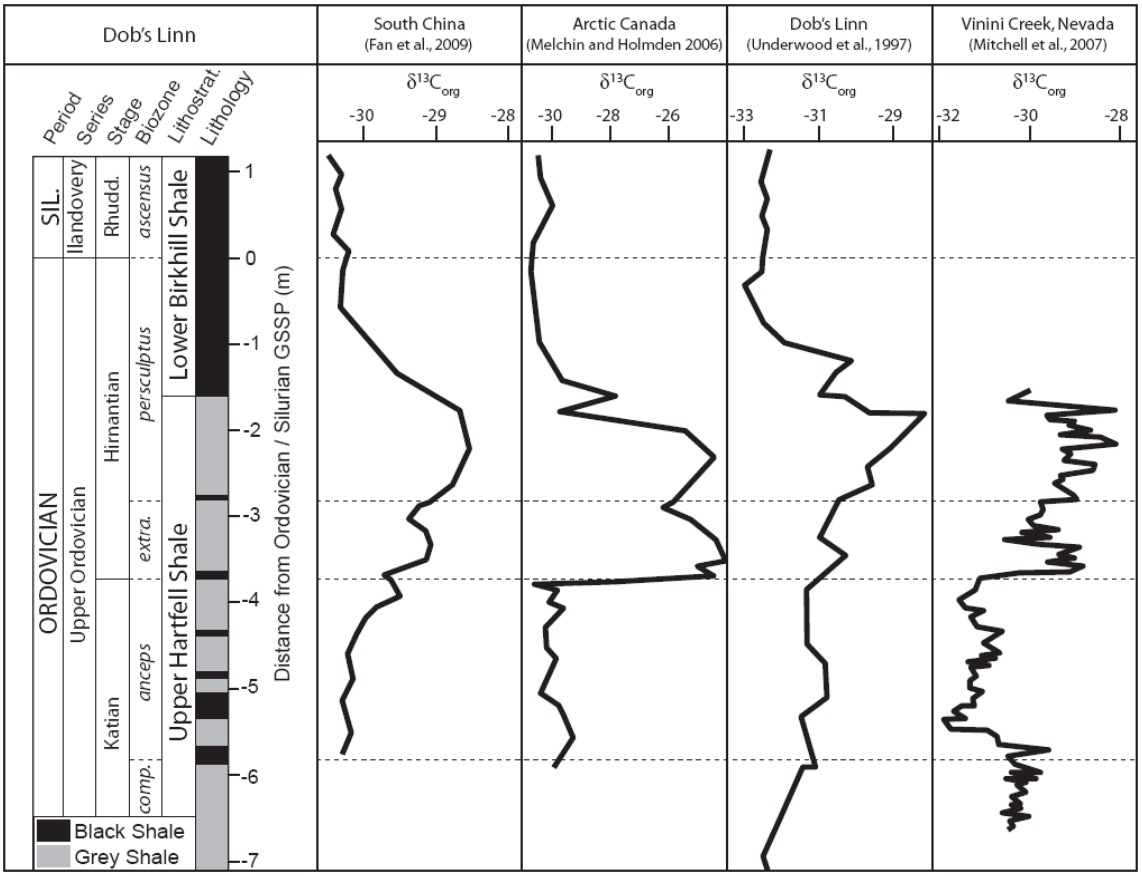

Figure 4.2 Stratigraphic column for the Linn Branch Section at Dob's Linn. Periods, series and stages from Ogg et al. (2008). Biozones taken from Melchin et al. (2003). Lithostratigraphy and broad lithological changes taken from Williams (1986); Melchin et al. (2003); and field observations (this study). The $\delta^{13}C_{org}$ profiles modified from Fan et al. (2009) to fit Dob's Linn biostratigraphy. Abbreviations; Sil. – Silurian; Rhudd. – Rhuddanian; *comp. – complanatus*; *extra. – extraordinarius*

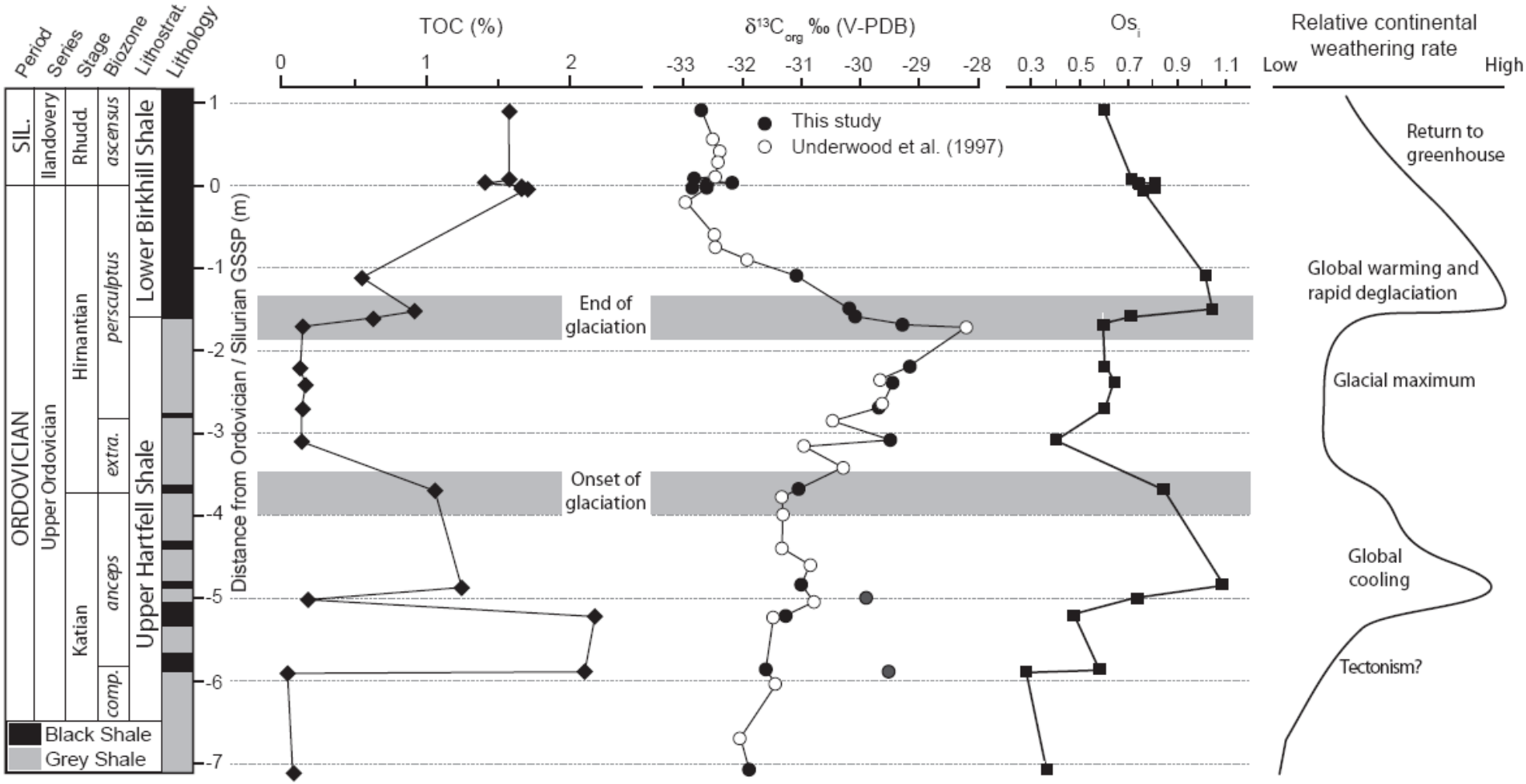

Figure 4.3 Stratigraphic column as in Fig. 4.2. The onset and end of glaciation placed as given for the Hirnantian (Brenchley et al., 2003). The $\delta^{13}C_{org}$ profile comprise data from this study and Underwood et al. (1997). The Os_i (calculated at 443 Ma) profile from the Dob's Linn is used to produce a relative weathering rate. Note $\delta^{13}C_{org}$ and Os_i symbol sizes are greater than uncertainty for each point. See text for discussion.

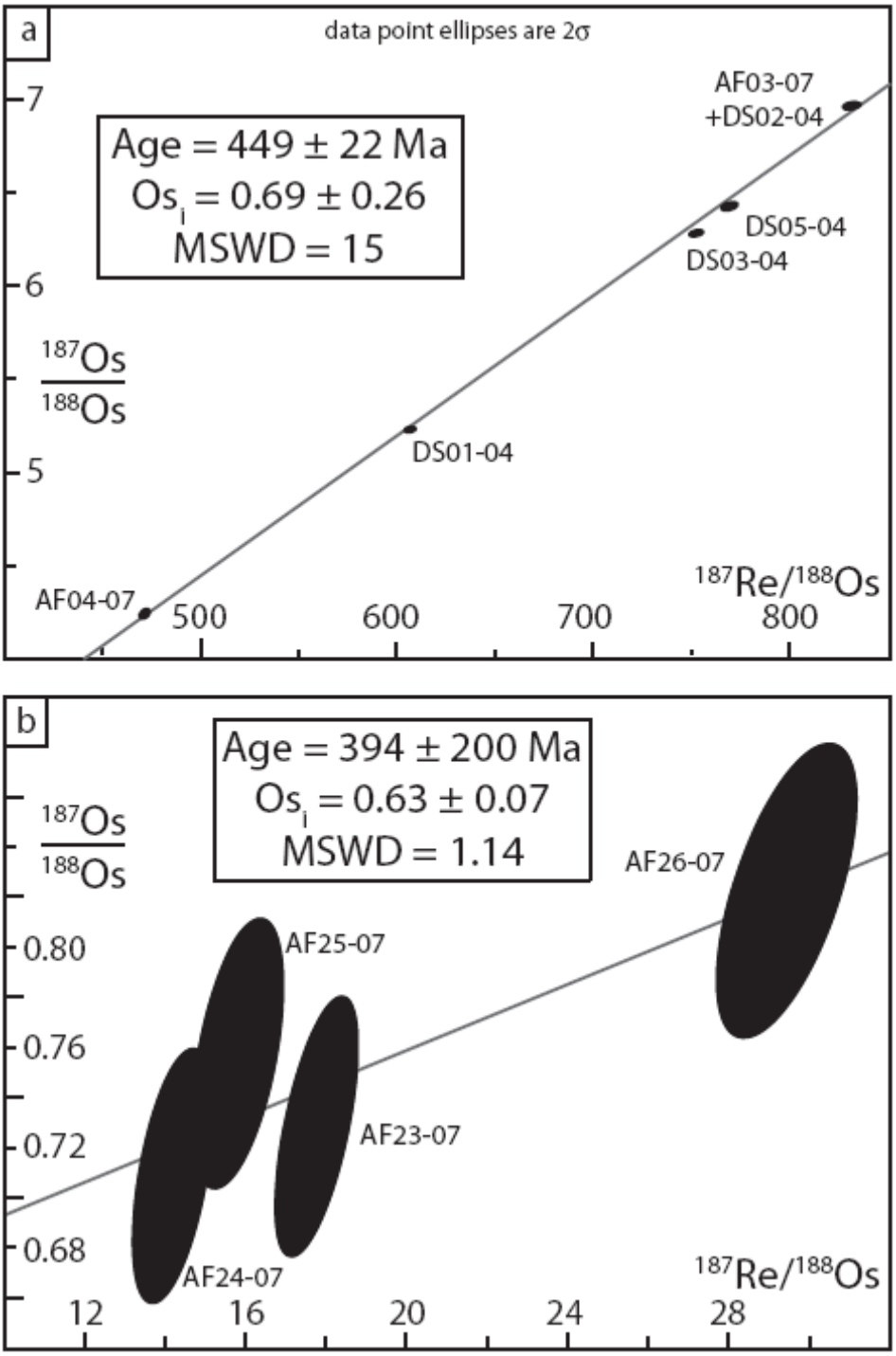

Figure 4.4 Re-Os isochrons for the Linn Branch section. Fig. 4.4a – area surrounding the GSSP, Fig 4.4b – area spanning Hirnantian glaciation. Uncertainty ellipses are at the 2σ level. See text for discussion.

5: PGE FINGERPRINTING OF OILS TO SOURCE

5.1 Introduction

To date, Platinum Group Element (PGE; Os, Ir, Ru, Rh Pt and Pd) studies of organic-rich sedimentary rocks have dealt with metalliferous black shales (i.e., hydrothermally enriched; cf. Xu et al., 2007), units related to extraterrestrial impacts (i.e., Ir anomalies: cf. Schmimitz et al., 2006) and weathered shales (disturbed PGE systematics: cf. Jaffe et al., 2002). There are also two studies that have investigated the PGEs abundance in petroleum which focus on new analytical methods, and, demonstrate that oil can be enriched in PGEs (Woodland et al., 2000; Fedorov et al., 2007). Although these studies demonstrate that the PGEs are enriched in oils and organic-rich sediments there is only a limited understanding of the behaviour of PGEs in "standard" organic-rich shales and oils.

The Re – Os system has been demonstrated to be an effective tool for providing spatial and temporal constraints for petroleum systems (this thesis; Selby and Creaser 2005a; Selby et al., 2007). However, in some source units, (e.g. Ordovician/Silurian "Hot" shales) the Os isotopic composition at the time of deposition, and therefore generation, varied greatly (Os_i ~0.3 – ~1.1; Finlay et al., 2010; Chapter 4), reducing their effectiveness at constraining oil source. Rhenium and the PGEs are all organophyllic (e.g. Coloder et al., 1992; Woodland et al., 2000; Fedorov et al., 2007), therefore, the presence of PGEs in petroleum and petroleum source rocks means that, with better understanding of their behaviour and combined with the Re – Os system, the PGEs may provide a tool to fingerprint oil sources.

To be effective as an oil source fingerprinting tool the PGEs must be: Unaffected by hydrocarbon maturation; similar within discrete source units; distinct between different source units within a petroleum system; and be similar between oils and their source. These factors will be evaluated in this study using a new method of analysing PGEs, specifically Pt and Pd ratios, in organic-rich shales and oils from the United Kingdom Atlantic Margin (UKAM), and the West Canadian Tar Sands (WCTS) of the West Canadian Sedimentary Basin (WCSB).

The UKAM is a well-constrained petroleum system with one predominant source unit, the Kimmeridge Clay Fm. (KCF; e.g. Chapter 2; Scotchman et al., 2006). This study demonstrates that Re and PGE values within UKAM oil reflect those of the KCF. Therefore, we can be confident that Re and PGEs of petroleum have been inherited from the source unit.

The Western Canadian Tar Sands (WCTS; Fig. 5.1) contains approximately 1.75 trillion barrels of crude oil making it one of the largest global petroleum deposits (Creaney and Allan, 1990), however, the WCTS are heavily biodegraded. Biodegradation preferentially removes light hydrocarbons (Peters et al., 1999). Even for moderately biodegraded oils, traditional oil to source fingerprinting techniques are challenged (e.g. Biomarkers and Carbon isotopes, Peters et al., 1999). A biomarker biodegradation scale (BBS) ranks the effects of biodegradation in oil from 1 - 10 (Peters et al., 2005). For example, *n*-alkanes are destroyed under low levels of biodegradation (BBS = 1-3), the isoprenoids are destroyed under moderate levels of biodegradation (BBS = 2 - 4) and the aromatic steroids are destroyed under high levels of biodegradation (BBS = 8 - 10; Peters et al., 2005). Biodegradation varies in the WCTS from a BBS level of ~4 in the Peace River deposit to 8 in the Athabasca deposit (Zhou et al., 2008; Fig. 1). As a result, the source(s) of the WCTS are highly debated (Brooks et al., 1988; Riediger, 1990; Creaney and Allan, 1990; 1992; Allan and Creaney 1991; Barson et al., 2000; Riediger et al., 2000; Fowler et al., 2001; Zhou et al., 2008; Higley et al., 2009).

There are currently two main theories for the source of the WCTS. The first proposes that mass balance calculations rule out a single source unit, and, as a result up to four units from the Western Canadian Sedimentary Basin (WCSB) could have formed / contributed to the WCTS. These are, in order of importance, the Lower Jurassic Gordondale Fm. (previously the Nordegg; Asgar-Deen et al., 2004), the Devonian-Mississippian Exshaw Fm., and the Middle Triassic Doig and Upper Devonian Duvernay Fms. (e.g., Creaney and Allan, 1990; 1992; Allan and Creaney 1991; Higley et al., 2009). The second theory argues that, when the effects of biodegradation are removed, there is sufficient geochemical evidence available to suggest a single source (e.g., Brooks et al., 1988). Biomarker preservation is thought to have been sufficient to show that, after the effects of biodegradation are removed, the Exshaw Fm. is the principal source of the WCTS (Barson et al., 2000; Riediger et al., 2000; Fowler et al., 2001; Zhou et al., 2008). Furthermore, it is suggested that the Gordondale Fm. cannot be the source of the WCTS as, except for a region in the east of the WCSB, generated oil would be trapped by the overlying impermeable Lower-Jurassic Poker Chip Fm. and oil production from the exposed Gordondale Fm. would only be sufficient to fill the Peace River deposit (Riediger, 1990). However, Higley et al. (2009) demonstrate that the area of Gordondale Fm. that is hydrocarbon mature is 17.3 times greater than that of Riediger (1990), and that that Poker Chip trapping

mechanisms are limited. Therefore, long distance petroleum migration of up to 500 km, the same scale as the Phosphoria petroleum system (Claypool et al., 1978), could have occurred during the formation of the WCTS (Higley et al., 2009).

Rhenium and Os are concentrated in the asphaltene fraction of oil (Selby et al., 2005; Selby et al., 2007). As a result of heavy biodegradation, both Re and Os are enriched in the WCTS (Selby and Creaser, 2005). Petroleum Re – Os geochronology demonstrate that hydrocarbon generation occurred at 111.6 ± 5.3 Ma within the WCSB (Selby and Creaser, 2005). As Re and the PGEs share the same organophyllic behaviour, it is likely that PGEs are enriched in the WCTS, potentially making them suitable for PGE analysis. Consequently this study uses PGE analysis to attempt to identify the source of the WCTS. It demonstrates that maturation does not affect Pt/Pd values in source rocks; that Pt/Pd values within the same source unit are similar; and that Pt/Pd values between differing source units are distinct. Furthermore, by combining Pt/Pd with the $^{187}Os/^{188}Os$ composition at the time of hydrocarbon generation (Os_g) within the WCTS and WCSB, this study confirms that the Gordondale Fm. is the main source of the WCTS with a minor input from the Exshaw Fm., as previously hypothesised (Creaney and Allan, 1990; 1992; Allan and Creaney, 1991; Higley et al., 2009).

5.2 Samples and Geological Setting.

5.2.1 U.K. Atlantic margin

The geological history of the United Kingdom Atlantic Margin (UKAM) is presented in Chapter 2 (section 2.2; Fig. 2.2). Briefly, the UKAM petroleum system comprises of a belt of Devonian to Miocene rift basins situated between the Shetland platform and Faroe Islands (e.g., Spencer et al., 1999; Carruth 2003; Fig. 2.1). Two main phases of rifting occurred during the Early Cretaceous and Late Cretaceous/Palaeocene forming local depocentres. Reservoirs are found in Devonian/Carboniferous sediments and fractured and weathered basement (e.g. structural trapped Clair field (e.g. Carruth 2003) and Jurassic and Palaeogene sediments (e.g. stratigraphically trapped Foinaven and Schiehallion fields; Spencer et al., 1999). A large body of geochemical and basin modelling research indicate a major Upper Jurassic marine source unit (equivalent to the North Sea KCF; e.g. Scotchman et al., 2006).

Three asphaltene samples analysed for Re – Os in chapter 2 were analysed for PGE abundances (Clair oil field, sample G0123, well 206/8-3A; Foinaven oil field, samples G2075 and G2763, well 204/24A-1; Fig. 2.1). Five samples of KCF from the

North Sea Miller field (well 16/8b-a01; analysed for Re-Os in Chapter 3; Fig. 3.2) and three samples of UKAM KCF equivalent shale (Clair oil field, well 205/22-1A; Fig. 2.1) were analysed for PGE abundances. The UKAM organic-rich sedimentary samples were also analysed for Re – Os abundances and isotopic compositions (Table 5.1).

5.2.2 West Canadian Tar Sands petroleum system

The West Canadian Sedimentary Basin (WCSB; Fig 5.1) covers an area of ~1,400,000 km^2 and contains ~1.75 trillion barrels of crude oil (cf. Creaney and Allan, 1990). The sedimentary units within the basin were deposited in two distinct tectonic settings and range in age from the Early Palaeozoic to the Early Tertiary. Palaeozoic to Jurassic sedimentary units, dominated by carbonates, were unconformably deposited on the Laurention craton under passive margin conditions. Middle Jurassic to Palaeocene, dominantly clastic, units formed in a foreland basin succession in response to the Cretaceous Laramide orogeny (e.g., Creaney and Allan, 1990; Zhou et al., 2008).

Petroleum generation in the WCSB was modelled to either have occurred as a result of sediment burial at ~110 Ma (e.g. Barson et al., 2000; Riediger et al., 2000; Zhou et al., 2008) or due to crustal down warping associated with the Laramide orogeny at ~ 60 - 65 Ma (e.g. Creaney and Allan, 1990; Higley et al., 2009). Direct Re – Os dating of oils from the WCTS demonstrated that oil generation occurred at 111.6 ± 5.3 Ma (Selby and Creaser 2005a), which is supported by K-Ar geochronology of diagenetic illite from K-bentonites within the Exshaw Fm. (which forms at the same temperatures as hydrocarbon maturation; Meyer et al., 2008). Although the source of the WCTS is highly debated it is accepted that their present bituminous state is a result of the biodegradation of conventional oil during migration and emplacement (cf. Zhou et al., 2008 and references therein).

Despite there being no consensus on the proportion of oil sourced from the different units within the WCSB, the Upper Devonian Duvernay, Devonian/Mississippian Exshaw and Lower Jurassic Gordondale Fms. have all been proposed as possible source units (e.g., Higley et al., 2009 and references therein). Therefore, fifteen samples of these units were analysed as part of this study (Table 5.2; 5.3).

Two core samples of Upper Devonian Duvernay Fm were analysed for PGE and Re abundances as well as Re – Os isotopic composition (Table 5.2; Fig. 5.1). The Duvernay Fm. is comprised of two interbedded lithofacies controlled by bottom water oxia/anoxia: bioturbated, nodular, lime mudstones, deposited under oxic conditions and

unbioturbated bituminous mudstones, deposited under deep water anoxic conditions. The bituminous mudstones form the oil source intervals and vary from being mature to the south west to immature in the north east (c.f. Creaney and Allan, 1990; Cioppa et al., 2002).

The PGE abundances of seven samples of regional Exshaw Fm. were determined (Table 5.2; Fig. 5.1). The Exshaw Fm. formed during a Devonian/Mississippian marine transgression and is continuous across the WCSB, varying in thickness from 2 – 16 m (Creaney and Allan, 1990; Creaser et al., 2002). The Exshaw Fm. comprises two lithofacies, a stratigraphically lower Devonian/Mississippian organic-rich member (TOC < 20%) and a stratigraphically higher Mississippian siltstone. The samples analysed in this study are all sourced from the lower organic-rich member, deposited in low energy anoxic conditions around 361.3 ± 2.4 Ma (Creaney and Allan, 1990; Selby and Creaser, 2005b). The Exshaw Fm. varies in maturity from being overmature in the south west to immature in the north east of the WCSB (Tmax 421 – 485 °C; Piggot and Lines, 1992; Creaser et al., 2002).

Six samples of regional Gordondale Fm. (formally "Nordegg" member; Asgar-Deen et al., 2004) were analysed for PGE and Re abundances as well as Re – Os isotopic composition (Table 5.2; Fig. 5.1). The Lower Jurassic (Sinemurian) Gordondale Fm. was deposited during a major marine transgression and varies from 19 – 50m of stratigraphical thickness across the WCSB. It comprises dark brown, finely laminated, radioactive, calc-mudstones, containing up to 27 % TOC. The Gordondale Fm. is predominantly mature, only being overmature in the far south west and immature in the north east of the WCSB (Tmax 415 – 566°C; Creaney and Allan, 1990; Riediger et al., 1990; Asgar-Deen et al., 2004)

The PGE abundances of Twenty four asphaltenes from the WCTS were determined. Three oils were sourced from the Athabasca deposit (wells 15-12-93-13W4, 6-93-10W4, 95-9W4), five from Cold Lake (wells 1-14-65-2W4, 28-61-4W4), three from Grossmont (well 14-5-88-19W4), three from Lloydminster (wells 03-14-49-27W3, A12-19-50-24-W3, A13-35-49-24W3), three from Peace River (well 4-21-85-18W5), three from Provost (well 5-20-37-1W4) and four from Wabasca (wells 2-24-84-22W4, 14-28-81-22W4; Table 5.3; Fig 5.1).

5.3 Analytical methodology

5.3.1 Re – Os Analysis

Previous Re – Os data from Miller oil field KCF (Chapter 3), UKAM oils (Chapter 2) WCSB Exshaw Fm. (Creaser et al., 2002) and WCTS (Selby and Creaser, 2005) are reproduced in Tables 5.1, 5.2 and 5.3. Core samples from the Gordondale (n = 6) and Duvernay (n = 2) Fms. were analysed for Re – Os abundance and isotopic composition (Table 5.2). Prior to crushing, the samples were polished, on a diamond polishing wheel, to remove cutting and drilling marks to eliminate any contamination. The ~50 – 80 g samples (represent ~3 cm of stratigraphy) were dried at 60 °C for ~12 hrs, broken into chips with no metal contact and powdered in a ceramic mill. Rhenium-Osmium isotope analysis was carried out at Durham University's TOTAL laboratory for source rock geochronology and geochemistry at the Northern Centre for Isotopic and Elemental Tracing (NCIET) using Cr^{VI}-H_2SO_4 digestion. Osmium was purified from the CrO_3-H_2SO_4 solution using solvent extraction ($CHCl_3$) and micro–distillation methods. After the removal of Os, 1 ml of the CrO_3–H_2SO_4 was mixed with 1 ml of Milli–Q water and reduced from Cr^{6+} to Cr^{3+} by sparging with SO_2 in preparation for Re anion exchange chromatography. After chromatography the Re fraction was then further purified by single bead anion extraction (c.f. Selby and Creaser, 2003).

The purified Re and Os were loaded onto Ni and Pt filaments respectively, and analysed for their isotopic compositions using Negative Thermal Ionisation Mass Spectrometry (NTIMS; Creaser et al., 1991) on a ThermoElectron (TRITON) mass spectrometer. Re was measured using Faraday collectors and Os in peak hopping mode using a secondary electron multiplier.

Total procedural blanks for Re and Os are < 12 and < 0.5 pg, respectively, with an average $^{187}Os/^{188}Os$ value of ~0.4 (n = 2). Raw Re and Os oxide values were corrected for oxygen contribution and mass fractionation. The Re and Os isotopic values and elemental abundances are calculated by full propagation of uncertainties from Re and Os mass spectrometer measurements, blank abundance and isotopic composition, spike calibration, and sample and spike weights. Throughout the period of this study, in-house Re and Os (DROsS) standard solutions were repeatedly analysed to monitor instrument reproducibility. The NCIET Re standard is made from 99.999 % zone-refined Re ribbon and is considered to be indistinguishable from the AB1 Re standard of the Department of Earth Sciences, University of Alberta. The Re standard runs produced average $^{185}Re/^{187}Re$ values of 0.5966 ± 0.0017 (1S.D. n = 1) indistinguishable within uncertainty to 0.5977 ± 0.0012 (Selby, 2007 and references

therein). The measured difference between the $^{185}Re/^{187}Re$ values and the accepted $^{185}Re/^{187}Re$ value of Gramlich et al. (1973) is used to correct for sample mass fractionation. The average DROsS $^{187}Os/^{188}Os$ ratio, using an electron multiplier, is 0.160797 ± 0.000214 (1 S.D. n = 3), indistinguishable from reported DROsS values (0.160924 ± 0.000003 (2 SD, n=21; Nowell et al., 2008; 0.160965 ± 0.000337, Rooney et al., 2010)

Source unit and oil $^{187}Os/^{188}Os$ compositions at the time of oil generation (Os_g) are calculated using the Re – Os age of generation (UK Atlantic Margin, 68 Ma, see chapter 2; WCTS, 112 Ma , Selby and Creaser 2005a) and the ^{187}Re decay constant of $\lambda = 1.666 \times 10^{-11} a^{-1}$ (Smoliar et al., 1996).

5.3.2 PGE Analysis

Biodegraded oil samples from the WCTS (n = 24) and asphaltene separated from UK Atlantic margin oils (n = 3) were analysed for their PGE abundances using the following method. Asphaltene was separated from three UK Atlantic margin oils using the *n*–heptane based methodology of Speight (1998) and Selby et al. (2007). Forty millilitres of *n*–heptane was added to 1 g of oil in a 60 ml glass vial, thoroughly mixed and agitated for ~12 hrs. The contents of the vial were then transferred to a 50 ml centrifuge tube and centrifuged at 4000 rpm for 5 minutes to ensure complete separation of the soluble maltene and insoluble asphaltene fractions. The maltene fraction was decanted to waste and the asphaltene fraction was dried on a hot plate at ~60˚C.

Oil was removed from the WCTS using a method modified from Selby et al., (2005). Approximately 1 g of WCTS was washed in ~1/2 ml of $CHCl_3$ which was then decanted into a 15 ml centrifuge tube. This process was repeated until the $CHCl_3$ remained clear. The $CHCl_3$ + oil solution was then repeatedly centrifuged to separate any suspended sediment from the solution. The $CHCl_3$ + oil solution was then transferred to a 22 ml glass vial and the $CHCl_3$ evaporated at ~ 60 C. The WCTS are heavily biodegraded and so are naturally enriched in asphaltene, rendering separation of asphaltene for analysis unnecessary.

Shale and oil were digested for PGE analysis using a method modified from Dale et al. (2009 and references therein). One gram of powdered shale or ~ 0.1 g of asphaltene were loaded into quartz high-pressure asher (HPA) vessel with a mixed ^{191}Ir, ^{196}Pt and ^{106}Pd tracer (spike) solution and inverse aqua-regia (shale - 2.5 ml 11 N HCl and 5 ml 16 N HNO_3; oil – 1.5 ml 11 N HCl and 3 ml 16 N HNO_3). The vessels were placed into an Anton Paar HPA (housed at NCIET) and heated to 220 °C for 13 hours at

~110 bars. After digestion the inverse aqua regia solution was dried, converted to the chloride species and re-dissolved in 4 ml of 0.2 N HCl for purification of Pd and Ir and Pt using anion exchange chromatography. Briefly this chromatography involved loading 1 cm^3 of AG 1x8 (100 – 200 mesh) anion resin onto the column and washing with 6 ml of 6 N HCl. The column was then rinsed with 10 ml of Milli Q and preconditioned with 5 ml of 0.5 N HCl. The sample in a HNO_3 solution was centrifuged and added to the column. The column was then washed with 10 ml of 1N HCl/HF to remove high field strength elements and conditioned with 10 ml of 0.8 N HNO_3. The Ir and Pt were eluted in 12 ml of 13.5 N HNO_3. The column was rinsed in 5 ml of Milli Q, washed with 10 ml of 1N HCl/HF and rinsed with 5 ml of Milli Q. Finally the purified Pd was eluted in 20 ml of 9 N HCl.

Due to the low abundance of some PGE samples, Ir, Pt and Pd were measured by inductively coupled plasma mass spectrometry (ICPMS) on the highly sensitive ThermoFinnigan Element 2 at Durham University. Solutions were introduced using a MicroMist micro-concentric nebuliser and ESI stable sample introduction system (dual-cyclonic quartz spray chamber). Mixed solutions of natural PGEs and solutions of Hf, Zr, Y and Mo (all 1ppb) were used to quantify the degree of mass fractionation and the production rates of HfO+, ZrO+, YO+, and MoO+ (which possess oxides of equivalent mass to isotopes of Ir, Pt, and Pd) before, during and after the analysis.

During the course of this study PGE standard solutions and the USGS Devonian Ohio Shale standard (SDO-1 ; Kane et al., 1990) was repeatedly analysed for PGE abundances (n = 5; Table 5.4). The standard PGE solutions produced results within uncertainty of the known value. The SDO1 standard produced Ir values ranging from 0.054 to 0.051 ppb, Pt values ranging from 1.39 to 1.50 ppb and Pd values ranging from 2.22 to 3.41. The individual measured analysis of SDO-1 yield uncertainties of ~17 %, ~3.4 % and ~13 % (at the 2 S.D. level) for Ir, Pt and Pd, respectively (Table 5.4). Repeat analysis of SDO-1 yield a 2 S.D. uncertainty of 18.4%, 5.9% and 35.7% for Ir, Pt and Pd abundances, respectively (Table 5.4). Therefore, so as to not underestimate the uncertainty in our PGE data, the 2 S.D. reproducibility uncertainties for SDO-1 are applied as the uncertainty for the Ir, Pt and Pd for shale and petroleum samples. A previous study that analysed the SDO-1 standard for PGEs present data that just lie within uncertainty of our values (Ir = 0.077 ± 112% ppb, Pt = 2.15 ± 28% ppb, Pd = 2.42 ± 32% ppb (Meisel and Moser, 2004). However, not only are these values imprecise, but the presented Re and Os values are significantly different to those produced at NCIET (93 ± 140% ppb Re and 1.159 ± 38% ppb Os, Meisel and Moser,

2004; 76.6 ± 0.9 ppb Re, 0.638 ± 0.019 ppt Os (n=6), NCIET, Du Vivier, 2010). Meisel and Moser (2004) only utilised a three hour digestion, therefore, it is likely that these differences are caused by either incomplete sample digestion or incomplete sample/spike equilibrium.

Eight full procedural blanks were undertaken throughout the period of this study. Iridium blank values ranged from 0.1 to 0.7 pg (mean = 0.3, S.D = 0.2), Pt blanks ranged from 0.3 to 22.7 pg (mean = 5.5, S.D. = 8.2) and Pd blanks ranged from 72 to 547 pg (mean = 217, S.D. 172). The highest PGE blank values (90.7, 22.7 and 547 pg for Ir, Pt and Pd respectivly) were all from the same batch, contaminated by a N-benzoyl-N-phenylhydroxylamine – Chloroform solution. This solution was applied, after anion exchange chromatography, to remove high field strength elements that have PGE isotope interferences ($^{89}Y^{16}O = {}^{105}Pd$; $^{92}Zr^{16}O = {}^{108}Pd$; $^{177}Hf^{16}O = {}^{193}Ir$; $^{179}Hf^{16}O = {}^{195}Pt$; $^{180}Hf^{16}O = {}^{196}Pt$; Shinotsuka and Suzuki, 2007). Because of the ability to introduce contamination, this stage was not repeated during subsequent analysis.

5.4 Results

5.4.1 Re – Os.

In UKAM source units (n = 3), Re – Os abundances range from 110.5 to 242.1 ppb and 0.754 to 1.383 ppt, respectively. $^{187}Rhenium/^{188}Os$ and $^{187}Os/^{188}Os$ values positively correlate and range from 958.6 to 1216.5 and 3.048 to 3.463, respectively. The $^{187}Os/^{188}Os$ values calculated at the time of petroleum generation (Os_g; 68 Ma, see chapter 2) range from 1.414 to 1.575. Os_g values are calculated from data presented in Chapter 3 (Table 3.2) for the Miller field and range from 0.943 – 1.129 (Table 5.1).

The regional Gordondale Fm. samples (n = 6) contain Re – Os abundances ranging from 7195.3 to 574.9 and 1.12 to 6.34 ppb, respectively. $^{187}Rhenium/^{188}Os$ and $^{187}Os/^{188}Os$ values positively correlate and range from 178.6 to 933.2 and 1.372 to 5.900, respectively. The $^{187}Os/^{188}Os$ values calculated for the time of petroleum generation (Os_g; 112 Ma, Selby and Creaser 2005a) range from 1.041 to 2.796. The regional Duvernay Fm. samples (n = 2) contain Re – Os abundances ranging from 7.41 to 11.55 and 0.327 to 0.569 ppb, respectively. $^{187}Rhenium/^{188}Os$ and $^{187}Os/^{188}Os$ values positively correlate and range from 104.4 to 109.5 and 1.037 to 1.036, respectively. The $^{187}Os/^{188}Os$ values calculated at the time of petroleum generation (Os_g; 112 Ma, Selby and Creaser 2005a) range from 0.830 to 0.841. Rhenium – Os data for regional Exshaw Fm. shales have been published by Creaser et al., 2002 and Selby and Creaser (2005). Os_g values calculated from this data range from 1.239 – 4.163 (Table 5.2).

5.4.2 PGEs

The Ir, Pt and Pd abundances of samples from the KCF from the North Sea Miller oil field (n = 5; Table 5.1) range from 0.020 to 0.047, 2.20 to 4.66 and 3.7 to 11.5 ppb, respectively. The Pt/Pd values vary between 0.40 and 0.54. The Ir, Pt and Pd abundances of samples from the KCF from the UKAM (n = 3; Table 5.1) range from 0.040 to 0.098, 4.28 to 4.64 and 7.3 to 13.9 ppb, respectively, similar to those from the North Sea. The Pt/Pd values vary between 0.33 and 0.63, indistinguishable within uncertainty to those from the Miller Field. The Ir, Pt and Pd abundances of samples from regional Exshaw Fm. shales (n = 7; Table 5.2) range from 0.025 to 0.099, 1.07 to 3.33 and 0.78 to 2.49 ppb, respectively. The Pt/Pd values range from 1.15 to 2.0. The Regional Gordondale Fm. samples (n=6; Table 5.2) contain 0.022 to 0.143 ppb Ir, 1.27 to 6.45 ppb Pt and 1.40 – 8.1 ppb Pd. The Pt/Pd values range between 0.25 and 0.65. Regional Duvernay Fm. samples (n = 2; Table 5.2) contain 0.016 and 0.036 ppb Ir, 0.75 and 0.85 ppb Pt and 0.77 and 0.79 ppb Pd. The Pt/Pd values for the two samples are 0.73 and 0.76.

Two whole oil samples from the UKAM (G2749, G2851; Table 2.1) were analysed for PGE abundances. However, the low abundance, hence the ICP-MS low signal intensity meant that the data produced was extremely imprecise (G2749 measured Pt uncertainty 24 %, Pd uncertainty 167 %; G2851 measured Pt uncertainty 39 %, Pd uncertainty 218 %). Therefore as PGEs are likely to be enriched within asphaltene, the asphaltene fraction of oil was analysed. Asphaltenes separated from UKAM oils contain between 0.019 and 0.157 ppb Ir, 0.23 and 10.98 ppb Pt and 2.8 to 16.8 ppb Pd (measured Pt uncertainty = 3 – 6 %, measured Pd uncertainty = 19 – 60 %; n=3; Table 5.1). The Pt/Pd values range between 0.05 and 0.44. Oils from the WCTS (n=24, Table 5.3) contain between 0.001 and 0.134 ppb Ir, 0.07 and 8.03 ppb Pt and 0.11 and 8.4 ppb Pd. The Pt/Pd values range from 0.03 to 10.8.

5.5 Discussion

5.5.1 Re-Os

Rhenium – Os data from the Miller oil field KCF has been discussed in detail in Chapter 3. In brief, the UKAM KCF samples (n = 3) contain similar amounts of Os to the Miller KCF, but are enriched in Re. Therefore, the UKAM $^{187}Re/^{188}Os$ (976.7 – 1217) and $^{187}Os/^{188}Os$ (3.057 – 2.463) values are higher in UKAM KCF than in Miller KCF. The limited spread in UKAM $^{187}Re/^{188}Os$ data means that they produce extremely imprecise geochronological data (106 ± 520 Ma; MSWD = 379). The UKAM Os_g

(Calculated at 68 Ma; Chapter 2) are more radiogenic (1.41 – 4.57) than Miller (0.943 – 1.129; Table 5.1). The UKAM and Miller KCF display a range of $^{187}Re/^{188}Os$ and $^{187}Os/^{188}Os$ (346.3 – 1217 and 1.320 – 3.463, respectively) similar to those of KCF from Kimmeridge Bay, Dorset (Cohen et al., 1999), and Staffin, Skye (Selby, 2007). Therefore, it is likely that the Os_g data, from the UKAM and Miller oil field, are representative of regional KCF.

Six regional samples of Gordondale Fm. core are highly enriched in both Re (195.3 – 574.9 ppb) and Os (1.12 – 6.34 ppb; Table 5.2) and have a large spread in $^{187}Re/^{188}Os$ and $^{187}Os/^{188}Os$ (550.4 – 1674 and 1.372 – 5.900, respectively). Despite this large spread in isotopic data the Re – Os regression analysis gives an age that is imprecise (184 ± 29 Ma; MSWD 2153). To obtain a reliable Re–Os age, as well as having a large spread in $^{187}Re/^{188}Os$, the Re–Os isotopic systematics must remain undisturbed and the $^{187}Os/^{188}Os$ at the time of deposition (Os_i) must be similar (Cohen et al., 1999). Hydrocarbon maturation has been shown to not disturb the Re – Os black shale geochronometer (Creaser et al., 2002) and there was no evidence for disturbance to the core samples (e.g. calcite veining). The Gordondale Fm. samples were collected to represent the regional variations within the Fm rather than for geochronology, therefore, due to stratigraphic variation, they have a large spread in Os_i (0.34 – 0.80) which is responsible for the imprecision in the age. The Gordondale encompasses Hettangian (~199 Ma) to Toarcian (~175 Ma) age shales (Asgar-Deen et al., 2004) and so, although imprecise, the Re – Os age is agreement with the biostratigraphic constraints. The two regional Duvernay Fm. samples analysed contain lower Re and Os abundances than the Gordondale Fm (0.383 – 0.569 and 7.41 – 11.55 ppb, respectively; Table 5.2). The $^{187}Re/^{188}Os$ (104.4, 109.5) and $^{187}Os/^{188}Os$ (1.036, 1.037) values are too similar for Re – Os geochronology.

The majority of the WCTS oils produce a generation age of 111.6 ± 5.3 Ma and a range in Os_g of 1.30 – 1.76 (Selby and Creaser, 2005a). Applying this 111.6 Ma hydrocarbon generation age to the Gordondale, Exshaw and Duvernay Fm. Re – Os results produces a range in Os_g from 1.041 – 2.796, 1.24 – 4.16 and 0.830 – 0.841 respectively. The Os_g of oil is inherited from the source unit (Selby and Creaser, 2005a; Selby et al., 2005; Selby et al., 2007; Chapter 2), therefore, due to similarities in Os_g the WCTS could have been sourced from either the Gordondale and/or Exshaw Fms., but not the Duvernay Fm (Table 5.3, 5.4).

5.5.2 PGE variations within oils and Source Rocks

Reported PGE values in black shale units range from 0.003 – 3.00 ppb Ir (mean = 0.262, 1 S.D. = 0.458, n = 138), 0.2 – 180 ppb Pt (mean = 8.26, 1 S.D. = 21, n = 138) and 0.27 – 106 ppb Pd (mean = 7.80, 1 S.D. = 16.5, n = 90), however the majority of these studies deal with either metalliferous (i.e. enriched), impact related (i.e. Ir anomaly) or weathered (disturbed PGE values) shales (Coveney et al., 1992; Coloder et al., 1992; Sawlowicz, 1993; Over et al., 1997; Woodland et al 2000; Peucker-Ehrenbrink and Hannibal, 2000; Jaffe et al., 2002; Meisel and Moser 2004; Siebert et al., 2005; Schmimitz et al., 2006; Ru et al., 2007; Jaing et al., 2007; Brookfield et al., 2010). Therefore direct comparison with this data must be treated with caution; however, the data presented in this study do lie within the range of published values (Table 5.1, 5.2). The majority of published PGE data are presented normalised to chondrite therefore, to aid with comparison , when the data in this study is normalised to chondrite (Siebert et al., 2005) Ir is the most depleted PGE, Pt is less depleted and Pd is the least depleted (Fig. 5.2a, c). This is the same trend as observed in the published literature (Coveney et al., 1992; Siebert et al., 2005; Peucker-Ehrenbrink and Hannibal, 2000; Peucker-Ehrenbrink and Jahn 2001; Brookfield et al., 2010). Hydrogenous Pt and Ir can be scavenged into organic-rich sediments and the lower Ir abundances, compared to Pt, reflect concentrations in sea water (Coloder et al., 1992). This hypothesis is in direct agreement with Os enrichment in organic-rich shales (e.g. Ravizza and Thracian, 1989; Cohen et al., 1999; Selby and Creaser, 2003; Finlay et al., 2010). Therefore, it is likely that the PGE values reported in this study are hydrogenous and are complexed into the organic fraction of organic-rich sediments.

Reported PGE values in oils range from 0.002 – 0.37 ppb Ir (mean = 0.098, 1 S.D. = 0.144, n=14), 0.05 – 320 ppb Pt (mean = 19.7, 1 S.D. = 75 n=18) and .003 – 16.4 ppb Pd (mean = 3.00, 1 S.D. = 4.78, n=15; Woodland et al, 2000; Fedorov et al., 2007). The data presented in this study lie within this range of data (0.006 – 0.157 ppb Ir, 0.07 – 10.98 ppb Pt and 0.11 – 16.8 ppb Pd; Table 5.1, 5.3). Furthermore, the chondrite normalised oil PGE plots (Figure 5.2b, d) display the same trend as those of shales, (Fig. 5.2a, c), suggesting that they are inherited from source units, therefore further supporting the hypothesis that PGEs are complexed in the organic fraction of source units (Woodland et al, 2000; Coloder et al., 1992).

Figure 5.2a and 5.2c show that the KCF, Exshaw, Gordondale and Duvernay Fms have Pt and Pd abundances that are similar, but are enriched compared to Ir (Table 5.1, 2). However, the gradients between Pt and Pd values, and therefore Pt/Pd ratio,

differ between the contrasting source units. Consequently, the Pt/Pd value is tested as a tool for fingerprinting an oil to its source

5.5.3 Testing the effect of hydrocarbon maturation on Pt/Pd and applying Pt/Pd as an oil source fingerprinting tool

To be effective as an oil source fingerprinting tool Pt/Pd values in source units must be; undisturbed by maturation; similar within a source unit; distinct between different source units within a petroleum system; and similar between oils and their source units. Hydrocarbon maturation has been shown to have minimal effect on Re – Os shale systematics (Creaser et al., 2002; Selby and Creaser, 2005b). Therefore, as the PGEs share the same chemical characteristics as Re-Os, it is unlikely that Pt/Pd values will be affected by maturation. If maturation disturbs Pt/Pd ratios it would be observed by either a trend to higher or lower Pt/Pd values in immature, mature and overmature shales of the same source unit. This is not observed in samples of different maturity from within the Gordondale and Exshaw Fms. (Fig. 5.3a), so, it is unlikely that hydrocarbon maturation significantly disturbs the Pt/Pd ratio.

Regional KCF (North Sea Miller field and UKAM Clair field samples) possess Pt/Pd values that are indistinguishable within uncertainty (Miller, 0.40 to 0.54; Clair, 0.33 to 0.63; Table 5.1; Fig. 5.3b). Platinum/Pd values are also similar within source formations of the WCSB (Duvernay, 1.03 – 1.07; Gordondale, 0.36 – 0.91; Exshaw, 1.15 – 2.0; Table 5.2, 3; Fig. 5.3b). Furthermore, despite some overlap within uncertainty, the main Pt/Pd data clusters for the Duvernay, Gordondale and Exshaw Fms are distinct. This demonstrates that, Pt/Pd values are similar within distinct source unit formations, but differ between the proposed source units within the WCTS petroleum system.

Asphaltenes separated from UKAM oils contain Pt/Pd values that range from 0.32 ± 0.21 to 0.65 ± 0.30, indistinguishable from the range observed in KCF (Table 5.1; Fig. 5.3b). The KCF has been demonstrated to be the dominant source unit in the UKAM (Chapter 2; e.g. Scotchman et al., 2006). Therefore, it is likely that the Pt/Pd value of the oil has been inherited from the source unit.

It is possible to further test this hypothesis through comparison of Pt/Pd with Os_g. Platinum and Pd share the same chemical characteristics and organophyllic affinity as Re and Os (e.g. Woodland et al., 2000) and the Os_g of oil has been demonstrated to be inherited from source (Selby and Creaser, 2005a; Selby et al., 2005; Selby et al., 2007; Chapter 2). Therefore if the Os_g values of oil and source correlate

with Pt/Pd, it is highly likely that Pt/Pd value of the oil has been inherited from the source unit.

KCF equivalent core samples utilised for PGE analysis from the UKAM yield an Os_g (at 68 Ma; Chapter 2) between 1.41 and 1.57 (Table 5.1), and KCF samples from the North Sea Miller oil field have a calculated Os_g between 0.943 and 1.13 (Table 5.1), as a result, the regional variance in KCF Os_g is 0.943 – 1.57. The Os_g of the UKAM asphaltene samples utilised in this study varies from 0.92 – 1.25 (Table 5.1), a variation similar to the KCF Os_g. When Pt/Pd is compared to Os_g, the UKAM oil data field overlap with the KCF data field (Fig 5.4a, b), suggesting that, in addition to the Os_g (Chapter 2, Chapter 3, Selby et al., 2007), the Pt/Pd value of oil is inherited from the source unit. Therefore, as Pt/Pd is; not disturbed by hydrocarbon maturation; is similar within a source unit; distinct between different potential source units within a petroleum system; and similar within oils and their source it suggests that Pt/Pd can be used to fingerprint an oil to its source.

5.5.4 Rhenium and PGE Fingerprinting of oils to source in the WCSB

Oils from the WCTS contain Pt/Pd values ranging from 0.15 to 10.8, however, 21 of the 24 data are very similar (0.15 – 1.26; Table 5.3). The main WCTS data set contains Pt/Pd values that are almost indistinguishable from those observed in the Gordondale Fm, except for two Provost samples that have lower Pt/Pd values (Fig 5.3b). The higher main WCTS Pt/Pd oil values (n = 5) overlap, within uncertainty, with those observed in the Duvernay and Exshaw Fms. This suggests that the majority of the WCTS have been sourced from the Gordondale Fm. with a limited input from the Exshaw and Duvernay Fms.

The WCTS Os_g range from 0.52 ± 0.04 – 1.76 ± 0.04 (Selby and Creaser, 2005; Table 5.3), lower than the majority of the Exshaw Fm. and higher than the Duvernay Fm. The WCTS Os_g are, however, similar to those of the Gordondale Fm (Fig. 5.4c). By comparing the Pt/Pd and Os_g of the WCTS to the source unit samples it is apparent that, with the exception of the Provost deposit, the majority of WCTS data are similar to the Gordondale Fm. (Fig. 5.4d). Accordingly, this study hypothesises that the Gordondale Fm is the predominant source unit for the WCTS with minor inputs from the Exshaw Fm. This further suggests that the Lower-Jurassic Poker Chip Fm. does not seal the Gordondale Fm. as suggested by Riediger (1990) and, therefore, supports the mass balance calculations of Creaney and Allan (1990); (1992); Allan and Creaney (1991) and the 4D modelling of Higley et al. (2009).

The three oil samples, separate from the main WCTS data, are from separate deposits and lie outside of two standard deviation of the mean of the main data set (mean = 0.56; 2 S.D. = 0.742 ; Athabasca, 2.5; Lloydminster, 6.0; Peace River, 11; Table 5.3). Their Pt/Pd values are greater than any observed Pt/Pd value presented in this study. Possible explanations for these data are that they have been sourced from a unit, not analysed as part of this study, that is extremely enriched in Pt compared to Pd, that the Pt/Pd values have been disturbed, or that source to oil Pt/Pd fractionation has effected these samples. Woodland et al. (2000) reported extreme Pt enrichment in an oil sample from the Dauntless oil field (UK North Sea) and suggested that it was due to Pt contamination. Therefore the Pt enriched data must be treated with caution.

Oils from the Provost deposit have significantly lower Os_g values than the other WCTS (Provost = 0.52 – 0.60; WCTS = 1.42 – 1.76). The Provost oils also display Pt/Pd values lower than the majority of the WCTS and the source samples analysed in this study (Fig. 5.4c, d). Therefore, it is likely that they have been sourced from a unit not analysed in this study. A potential separate source for the Provost deposit is the Lower Cretaceous Mannville Group Ostracode bed (e.g. biomarkers, Karavas et al., 1998; 4D modelling, Higley et al., 2009). As the Ostracode bed is younger than the other proposed source units of the WCSB, it is therefore less radiogenic as shown by the Os_g. Additional PGE analysis may prove in identifying the Ostracode bed as the source of the Provost oil field.

5.6 Conclusions

This study has presented Re and PGE data from the well constrained U.K. Atlantic Margin (UKAM) petroleum system and the poorly constrained West Canadian Tar Sands (WCTS) petroleum system. This study demonstrates that the PGEs, specifically Pt/Pd and Os, can be a useful oil to source correlation tool.

To be applied as an oil source correlation tool Pt/Pd must not only be similar between oils and their source units but also be undisturbed by hydrocarbon maturation, similar within a source unit and distinct between different source units within a petroleum system. Within the U.K. Atlantic margin petroleum system, Pt and Pd have been demonstrated to be enriched in the asphaltene fraction of oil. Furthermore, asphaltene separated from UKAM oil display Pt/Pd values that are indistinguishable from those of the Kimmeridge Clay Fm., the known source unit of the UKAM (e.g. Scotchman et al., 2006).

The West Canadian Tar Sands are highly biodegraded, reducing the effectiveness of traditional oil source correlation methods, as a result the source of the WCTS is highly debated (e.g. Riediger, 1990; Higley et al., 2009). Three possible WCTS source units, the Gordondale, Exshaw and Duvernay Fms, have been analysed for Pt/Pd to attempt to solve this debate. Analysis of immature, mature and overmature samples from the Gordondale and Exshaw Fms. demonstrates that hydrocarbon maturation does not disturb the Pt/Pd values. Furthermore within the Gordondale, Exshaw and Duvernay Fms. Pt/Pd values are similar, however, the Pt/Pd values differ between the three formations. The majority of Pt/Pd values from WCTS deposits contain Pt/Pd values that are similar to the Gordondale Fm., there is also some overlap between samples from the WCTS and the Exshaw and Duvernay Fms.

As the Os_g of oil is inherited from source (Chapters 2 and 3; e.g. Selby and Creaser 2005a), to further constrain the source of the WCTS, the Pt/Pd data are compared to oil and source rock Os_g. Within the UKAM, asphaltene Pt/Pd and Os_g is extremely similar to that of the Kimmeridge Clay Fm, justifying this approach. When this is applied to the WCTS, the Duvernay Fm. samples contain Osg values (0.830-0.841) that are significantly lower than those of the majority of the WCTS (1.42 – 1.76), disqualifying it as a potential source. The majority of the WCTS oils contain Pt/Pd and Os_g values that correlate well with the Lower Jurassic Gordondale Fm., however, three WCTS samples contain Pt/Pd and Osg values that are similar to those of the Exshaw Fm. Therefore it is likely that the Gordondale Fm. is the predominant source for the WCTS with a minor input from the Exshaw Fm. Oils from the Provost deposit have Pt/Pd and Os_g values that are significantly lower than the other WCTS deposits and the three source units analysed in this study, meaning their source remains ambiguous.

References

Allan, J., Creaney, S. 1991. Oil families of the Western Canada Basin. Bull. Can. Pet. Geol. 39, 107–122.

Asgar-Deen, M, Riediger, C., Hall, R. 2004. The Gordondale Member: designation of a new member in the Fernie Formation to replace the informal "Nordegg Member" nomenclature of the subsurface of west-central Alberta. Bull Can. Pet. Geol. 52, 201-214.

Barson, D., Bartlett, R., Hein, F., Fowler, M., Grasby, S., Riediiger, C., Underschultz, J. 2000, Hydrogeology of heavy oil and tar sand deposits: Water flow and supply, migration and degradation, Field Trip Notes (Geological Survey of Canada, 2000), Open File Report 3946.

Brookfield, M.E., Shellnutt, J.G., Liang, O., Hannihan, R. Bhad, G.M., Wignall, P.B. 2010. Platinum element group variations at the Permo–Triassic boundary in Kashmir and British Columbia and their significance. Chem. Geol. 272, 12–19

Brooks, P. W., Fowler, M.G., Macqueen, R.W. 1988, Biological marker and conventional geochemistry of oil sands/heavy oils, Western Canada Basin. Org. Geochem. 12. 519–538.

Carruth, A.G.. 2000. The Foinaven field, Blocks 204/19 and 204/24a, UK North Sea. In: Gluyas, J.G. & Hichens, H.M. (eds) United Kingdom Oil and Gas Fields, Commemorative Millennium Volume. (Geological Society, London, Memoir 20, 121-130).

Cioppa, M.T., Symons, D.T.A., Al-Aasm, I.S., Gillen, K.P. 2002, Evaluating the timing of hydrocarbon generation in the Devonian Duvernay Formation: paleomagnetic, rock magnetic and geochemical evidence. Mar. Pet. Geol. 19, 275 – 287.

Claypool, G. E., Love, A. H. Maughan, E. K. 1978. Organic geochemistry, incipient metamorphism, and oil generation in black shale members of Phosphoria Formation, Western Interior, United States. AAPG Bull. 62, 98–120.

Cohen, A.S., Coe, A.L., Bartlett, J.M., Hawkesworth, C.J. 1999. Precise Re–Os ages of organic-rich mudrocks and the Os isotope composition of Jurassic seawater. Earth Planet. Sci. Lett 167, 159 – 173.

Colodner, D.C., Boyle, E.A., Edmond, J.M., Thomson, J. 1992. Post-depositional mobility of Platinum, iridium and rhenium in marine sediments. Nature, 358, 402 – 404.

Coveney, R.M., Murowchick, J.B., Grauch, R.I., Glascock, M.D., Denison, J.R., 1992. Gold and platinum in shales with evidence against extraterrestrial sources of metals. Chem. Geol. 99. 101-114

Creaney, S., Allan, J., 1990. Hydrocarbon generation and migration in the Western Canada sedimentary basin. In: Brooks, J. (ed.), Classic Petroleum Provinces, Geological Society Special Publication 50, 189-202.

Creaney, S., Allan, J. 1992. Petroleum systems in the foreland basin of western Canada. In:Macqueen, R.W. Leckie, D.A. (eds.) Foreland basins and fold belts: AAPG Memoir 55, 279–308.

Creaser, R.A., Sannigrahi, P., Chacko, T. and Selby, D. 2002. Further evaluation of the Re–Os geochronometer in organic rich sedimentary rocks: A test of hydrocarbon maturation effects in the Exshaw Formation, Western Canada Sedimentary Basin. Geochim. Cosmochim. Acta. 66, 3441 – 3452.

Dale, C.W., Burton, K.W., Pearson, D.G., Gannoun, A., Alard, O., Argles, T.W., Parkinson, I.J. 2009. Highly siderophile element behaviour accompanying subduction of oceanic crust: Whole rock and mineral-scale insights from a high-pressure terrain. Geochim.Cosmochim. Acta 73, 1394–1416

Du Vivier, A.D.C., 2010 Progression of seawater 187Os/188Os throughout the Oceanic Anoxic Event (OAE) 2: Implications for mechanisms driving global ocean anoxia and ocean palaeocirculation. Unpublished MSci thesis(Department of Earth Sciences, Durham University).

Fedorov, Y.N., Ivanov,K.S. Erokhin, Y.V., Ronkin, Y.L. 2007. Inorganic Geochemistry of the Oil of West Siberia: First ICP-MS Data Doklady Akademii Nauk, 414, 385–388.

Finlay, A.J., Selby, D., Groke, D.R., 2010, Tracking the Hirnantian Glaciation using Os isotopes. Earth. Planet. Sci. Lett. 293, 339-348

Fowler, M. G., Stasiuk, L.D., Hearn, M., Obermajer, M. 2001. Devonian hydrocarbon source rocks and their derived oils in Western Canada sedimentary basin. Bull. Can. Pet. Geol. 49, 117–148.

Gramlich, J.W., Murphy, T.J., Garner, E.L. & Shields, W.R. 1973. Absolute isotopic abundance ratio and atomic weight of a reference sample of rhenium. J. res. Nat. Bur. Stand. 77, 691– 698.

Higley, D.K., Lewan, M.D., Roberts, L.N.R., Henry, M. 2009, Timing and petroleum sources for the Lower Cretaceous Mannville Group oil sands of northern Alberta based on 4-D modelling. AAPG Bull.

Jaffe, L.A., Peucker-Ehrenbrink, B. and Petsch, S.T. 2002 Mobility of rhenium, platinum group elements and organic carbon during black shale weathering. Earth Planet. Sci. Lett. 198, 339-353.

Jiang, S-Y., Yang, J-H., Ling, H-F., Chen, Y_Q., Feng, H_Z., Zhao, K-D., Ni, P., 2007. Extreme enrichment of polymetallic Ni–Mo–PGE–Au in lower Cambrian black shales

of South China: An Os isotope and PGE geochemical investigation. Palaeogeog., Palaeoclim., Palaeoecol., 254, 217–228.
Kane, J.S., Arbogast, B.F., Leventhal, J.S., 1990. Characterization of Devonian Ohio Shale SDO-1 as a USGS geochemical reference sample: Geostandards Newsletter 14, 169-196.
Karavas, F.A., Riediger, C.L., Fowler, M.G., Snowdon, L.R. 1998. Oil families in Mannville Group reservoirs of southwestern Alberta, Western Canada sedimentary basin. Org. Geochem. 29, 769-784.
Meisel, T., Moser, J., 2004. Platinum-Group Element and Rhenium Concentrations in Low Abundance Reference Materials. Geostandards and geoanalytical research. 28, 233 - 250
Meyer, E.E., Nadeau, P.H., Aronson, J.L. Riediger, C.L., Hillier, S. Richards, B. 2008. Dating the Tectonic Burial and Maturation of the Principal Source Rocks of the Alberta Tar Sands in the Western Canada Sedimentary Basin. 2008 Joint Meeting of The Geological Society of America
Nowell, G.M., Luguet, A., Pearson, D.G., Horstwood, M.S.A., 2008. Precise and accurate 186Os/188Os and 187Os/188Os measurements by multi-collector plasma ionisation mass spectrometry (MC-ICP-MS) part I: Solution analyses. Chem. Geol. 248, 363–393.
Over, D.J., Conaway, C.A., Katz, D.J., Goodfellow, W.D., Gregoire, D.C. 1997 Platinum group element enrichments and possible chondritic Ru:Ir across the Fransnian-Famennian boundary, western New York State. Palaeogeog. Palaeoclimate. Palaeoecol. 132 399-410.
Peters, K.E., Fraser, T.H., Amris, W. Rustanto, B. & Hermanto, E. 1999. Geochemistry of Crude Oils from Eastern Indonesia. AAPG Bull. 83, 1927-1924.
Peters, K. E., Walters, C.C., Moldowan, J. M. 2005. The Biomarker Guide Volume 1: Biomarkers and Isotopes in the Environment and Human History (Cambridge University Press. 2005).
Peucker-Ehrenbrink, B., Hannigan, R.E. 2000 Effects of black shale weathering on the mobility of rhenium and platinum group elements. Geology, 28, 475-478.
Peucker-Ehrenbrink, B., Jahn, B. 2001. Rhenium-osmium isotope systematics and platinum group element concentrations: Loess and the upper continental crust Geochem. Geophys. Geosyst. 2. 1061.
Piggott N., Lines M. D. 1992. A case study of migration from the West Canada Basin. In Petroleum Migration (eds. W. A. England and A. J. Fleet). Geol. Soc. Spec. Pub. 59, 207–225.
Ravizza, G. & Thracian, K.K. 1989. Application of the 187Re-187Os system to black shale geochronometry. Geochim. Cosmochim. Acta, 53, 3257–3262.
Riediger, C.L. 1990. Migration of "Nordegg" oil in the Western Canadian Basin. How much and how far? Bull. Can. Pet. Geol. 42, 63-73.
Riediger, C. L., Bloch, J.D. 1995. Depositional and diagenetic controls on source rock characteristics of the Lower Jurassic "Nordegg member", Western Canada. J. Sed. Res. 65. 112 – 126.
Riediger, C.L., Fowler, M.G., Snowdon, L.R., Goodarzi, F., Brooks, P.W. 1990. Source rock analysis of the Lower Jurassic "Nordegg Member" and oil – source rock correlations, northwestern Alberta and northeastern British Columbia. Bull. Can. Pet. Geol. 38, 236 – 249.
Riediger, C., Ness, S., Fowler, M., Akpulat, T. GeoCanada 2000 CD Archive.
Rooney, A.D., Selby, D., Houzay, J_P., Renne, P.R. 2010, Re–Os geochronology of a Mesoproterozoic sedimentary succession, Taoudeni basin, Mauritania: Implications for basin-wide correlations and Re–Os organic-rich sediments systematics. Earth. Planet. Sci. Lett. 289, 486–496.
Sawlowicz, Z. 1993. Iridium and other platinum-group elements as geochemical markers in sedimentary environments. Palaeogeog. Palaeoclim. Palaeoecol. 104, 253 – 270.
Schmitz, B., Ellwood, B.B., Peucker-Ehrinbrink, B., El Hassani, A., Bultynek, P. 2006. Platinum group elements and 187Os/188Os in a purported impact ejecta layer near the Eifelian-Givetian stage boundary, Middle Devonian. Earth Planet. Sci. Lett. 249 162 – 172.

Scotchman, I.C., Carr, A.D., Parnell, J. 2006. Hydrocarbon generation modelling in a multiple rifted and volcanic basin: a case study in the Foinaven Sub-basin, Faroe-Shetland Basin, UK Atlantic margin. Scot. J. Geol. 42, 1-19.

Selby, D. 2007. Direct Rhenium-Osmium age of the Oxfordian-Kimmeridgian boundary, Staffin bay, Isle of Skye, U.K., and the Late Jurassic time scale. Norwegian J. Geol. 87, 291-299.

Selby, D., Creaser, R.A., 2003 Re–Os geochronology of organic rich sediments: an evaluation of organic matter analysis methods Re–Os geochronology of organic rich sediments. Chem. Geol. 200, 225– 240.

Selby, D., Creaser, R.A. 2005a. Direct radiometric dating of hydrocarbon deposits using Rhenium-Osmium isotopes. Science. 308, 1293 – 1295.

Selby, D., Creaser, R.A. 2005b. Direct radiometric dating of the Devonian-Mississippian time-scale boundary using the Re-Os black shale geochronometer. Geology. 33, 545 – 548.

Selby, D., Creaser, R.A., Dewing, K. & Fowler, M. 2005. Evaluation of bitumen as a 187Re–187Os geochronometer for hydrocarbon maturation and migration: A test case from the Polaris MVT deposit, Canada. Earth Planet. Sci. Lett 235. 1– 15.

Selby, D., Creaser. R.A. & Fowler, 2007. MG. Re-Os elemental and isotopic systematics in crude oils. Geochim. Cosmochim. Acta 71, 378 – 386.

Shinotsuka, K., Suzuki, K. 2007. Simultaneous determination of platinum group elements and rhenium in rock samples using isotope dilution inductively coupled plasma mass spectrometry after cation exchange separation followed by solvent extraction. Anal. Chim. Acta. 603, 129 – 139.

Siebert, C., Kramers, J.D., Meisel, T., Morel, Ph., Nagler, T.F., 2005. PGE, Re-Os and Mo isotope systematics in Archean and early Proterozoic sedimentary systems as proxies for redox conditions of the early earth. Geochim. Cosmochim. Acta, 69, 1787 - 1801.

Smoliar, M. I., Walker, R. J., Morgan, J. W. 1996. Re-Os ages of group IIA, IIIA, IVA, and IVB iron meteorites. Science 271, 1099 – 1102.

Speight, J.G. 1998. The chemistry and Technology of petroleum. Marcel Dekker, Inc., New York.

Spencer, A.M., Birkeland, Ø., Knag, G.Ø., Fredsted, R. 1999. Petroleum systems of the Atlantic margin of northwest Europe. In: Fleet, A.J. & Boldy, S.A.R. (eds) Petroleum Geology of Northwest Europe: Proceedings of the 5th Conference, 231-246. (Geol. Soc. Lon. 1999).

Woodland, S.J., Ottley, C.J., Pearson, D.G., Swarbrick, R.E. 2000. Microwave digestion od oils for analysis of platinum group and rare earth elements by ICP-MS. in Holland and Tanner (eds) Plasma source mass spectrometry: the new millennium, Volume.

Xu, L., Lin, Y., Shen, W., Qi, L., Xie, l., Ouyang, Z. 2007. Platinum-group elements of the Meishan Permian–Triassic boundary section: Evidence for flood basaltic volcanism. Chem. Geol. 246, 55–64

Zhou, S., Huang, H., Liu, Y., 2008. Biodegradation and origin of oil sands in the Western Canada Sedimentary Basin. Pet. Sci. 5, 87 – 94

Table 5.1 United Kingdom Atlantic Margin Re and PGE results.

Sample	Well	Depth (m)	Os (ppb)	±	Ir (ppb)	±	Pt (ppb)	±	Pd (ppb)	±	Re (ppb)	±	Pt/Pd	±	$^{187}Re/^{188}Os$	±	$^{187}Os/^{188}Os$	±	Os_g [c]	±
Clair Oil Field KCF																				
3178	205/22-1A	3178.0	1.383	0.003	0.057	0.010	4.64	0.27	13.9	4.9	219.8	1.3	0.33	0.12	1059	6	3.057	0.003	1.41	0.01
3178.5	205/22-1A	3178.5	1.376	0.004	0.040	0.007	4.28	0.25	7.30	2.56	242.1	1.4	0.59	0.21	1217	7	3.463	0.004	1.57	0.01
3179	205/22-1A	3179.0	0.754	0.002	0.098	0.018	4.60	0.27	7.31	2.56	110.5	0.7	0.63	0.22	976.7	5.9	3.068	0.004	1.55	0.01
Miller Oil Field KCF[a]																				
AF01-06	16/8b-a01	4738.4	0.856	0.002	0.039	0.007	2.41	0.14	4.65	1.63	58.30	0.19	0.52	0.18	384.2	1.3	1.433	0.002	1.015	0.004
AF02-06	16/8b-a01	4738.2	1.362	0.003	0.045	0.008	4.66	0.27	11.5	4.0	84.71	0.27	0.40	0.14	346.3	1.2	1.320	0.002	0.943	0.004
AF03-06	16/8b-a01	4738.0	1.285	0.003	0.042	0.008	3.91	0.23	8.01	2.80	94.33	0.30	0.49	0.17	417.0	1.4	1.501	0.002	1.050	0.004
AF04-06	16/8b-a01	4737.7	1.697	0.004	0.047	0.009	4.48	0.26	10.3	3.6	115.3	1.5	0.44	0.16	382.5	4.9	1.417	0.002	1.01	0.01
AF05-06	16/8b-a01	4737.3	0.600	0.002	0.020	0.004	2.02	0.12	3.73	1.30	50.15	0.16	0.54	0.19	482.8	1.7	1.656	0.003	1.129	0.004
Clair Oil Field Asphaltene[b]																				
G0123	206/8-3A	-	0.227	0.003	0.019	0.003	11.0	0.6	16.8	6.3	1.47	0.04	0.65	0.25	35.12	1.18	1.055	0.032	1.02	0.05
Foinaven Oil Field Asphaltene[b]																				
G2075	204/24A-1	-	0.062	0.001	0.157	0.029	2.12	0.13	3.69	1.38	1.63	0.04	0.57	0.22	142.0	6.5	1.084	0.050	0.92	0.06
G2763	204/24A-1	-	0.055	0.002	0.016	0.003	4.23	0.25	13.0	4.9	0.74	0.04	0.32	0.12	75.63	6.28	1.340	0.100	1.25	0.14

[a] Re - Os data from chapter 3 (Table 3.2)

[b] Re - Os data from chapter 2 (Table 2.2)

[c] Os_g - $^{187}Os/^{188}Os$ calculated at the time of oil generation (68Ma; see chapter 2)

Table 5.2. West Canadian Sedimentary Basin Re and PGE results.

Sample	Well	Depth (m)	Maturity	Os	±	Ir	±	Pt	±	Pd	±	Re	±	Pt/Pd	±	$^{187}Re/^{188}Os$	±	$^{187}Os/^{188}Os$	±	Os_g[c]	±
				(ppb)		(ppb)		(ppb)		(ppb)		(ppb)								(112 Ma)	
Gordondale Fm.[a]																					
DS09-03	07-31-79-10w6	1557	M	6.34	0.02	0.14	0.03	6.45	0.38	7.27	2.54	574.9	1.9	0.89	0.31	550.4	1.9	2.116	0.003	1.096	0.004
DS10-03	14-24-80-7w6	1183.5	M	1.86	0.01	0.022	0.004	2.90	0.17	7.01	2.45	369.2	1.2	0.41	0.15	1674	6	5.900	0.010	2.796	0.011
DS11-03	14-24-80-7w6	1190.4	M	1.83	0.01	0.061	0.011	3.44	0.20	5.16	1.81	229.9	0.8	0.67	0.24	885.8	3.2	3.655	0.007	2.013	0.008
DS12-03	8-26-69-7w6	2271.4	O	6.13	0.03	0.072	0.013	2.89	0.17	8.06	2.82	195.3	0.7	0.36	0.13	178.6	1.0	1.372	0.009	1.041	0.009
DS14-03	10-17-84-22w5	2361	I	1.12	0.00	0.038	0.007	1.27	0.08	1.40	0.49	196.2	0.7	0.91	0.32	1352	5	4.748	0.012	2.243	0.011
DS26-03	6-29-85-11w5	1148.68	M	3.05	0.01	0.14	0.03	5.96	0.35	6.95	2.43	402.6	1.4	0.86	0.30	933.2	3.3	3.716	0.005	1.986	0.008
Exshaw Fm.[b]																					
PEX10	3-19-80-23W5	1756.5	I	0.495	-	0.099	0.018	1.07	0.06	0.84	0.29	32.25	-	1.3	0.4	435.70	-	3.167	0.011	2.32	-
PEX11	13-18-80-23W5	1748.8	I	0.644	-	0.034	0.006	1.14	0.07	0.81	0.28	49.10	-	1.4	0.5	535.30	-	3.685	0.002	2.64	-
PEX12	13-18-80-23W5	1750.9	I	1.15	-	0.048	0.009	2.18	0.13	1.27	0.44	71.18	-	1.7	0.6	408.50	-	3.009	0.001	2.19	-
PEX13	4-23-72-10W6	3570.4	O	0.290	-	0.025	0.005	1.53	0.09	0.78	0.27	31.28	-	2.0	0.7	904.60	-	5.955	0.004	4.16	-
PEX14	4-23-72-10W6	3567.7	O	0.811	-	0.029	0.005	2.00	0.12	1.34	0.47	42.26	-	1.5	0.5	326.90	-	2.467	0.003	1.76	-
PEX20	8-29-78-01W6	2099.1	M	1.38	-	0.060	0.011	3.33	0.20	2.49	0.87	92.53	-	1.3	0.5	409.43	-	3.038	0.001	2.71	-
PEX21	8-29-78-01W6	2099.2	M	0.698	-	0.050	0.009	1.44	0.08	1.25	0.44	19.98	-	1.2	0.4	163.20	-	1.561	0.001	1.24	-
Duvernay Fm.																					
DS44-03	2-12-50-26W4	1751.6	-	0.383	0.002	0.036	0.007	0.79	0.05	0.77	0.27	7.41	0.03	1.0	0.4	104.4	0.6	1.037	0.006	0.841	0.007
DS69-03	8-35-31-25W4	2340.9	-	0.569	0.002	0.016	0.003	0.85	0.05	0.79	0.28	11.55	0.04	1.1	0.4	109.5	0.5	1.036	0.004	0.830	0.006

[a] Maturity from Riediger and Bloch (1995)

[b] Maturity and Re - Os data from Creaser et al. (2002)

[c] Os_g - $^{187}Os/^{188}Os$ calculated at the time of oil generation (112 Ma; Selby and Creaser, 2005)

- Undisclosed value

Table 5.3 West Canadian Tar Sands Re and PGE results.

Sample[a]	Well/Core	Os (ppb)	±	Ir (ppb)	±	Pt (ppb)	±	Pd (ppb)	±	Re (ppb)	±	Pt/Pd	±	$^{187}Re/^{188}Os$	±	$^{187}Os/^{188}Os$	±	Os_g[b] (112 Ma)	±
Athabasca																			
DS49-00	15-12-93-13W4	0.074	0.001	0.081	0.015	3.49	0.21	1.40	0.52	12.9	0.1	2.5	0.95	1231	28	3.680	0.093	1.42	0.05
6403^	6-93-10W4	0.144	0.002	0.018	0.003	0.48	0.03	0.63	0.24	26.2	0.1	0.77	0.29	1331	23	4.138	0.085	1.69	0.05
6438^	95-9W4	0.062	0.001	0.011	0.002	0.40	0.02	1.02	0.38	11.2	0.1	0.39	0.15	1291	33	3.800	0.11	1.43	0.05
Cold Lake																			
DS39-00	1-14-65-2W4	0.169	0.002	0.090	0.017	5.78	0.34	5.16	1.93	25.8	0.1	1.1	0.4	1072	20	3.624	0.076	1.65	0.05
655^	28-61-4W4	0.288	0.006	0.007	0.001	1.54	0.09	4.26	1.60	50.1	0.2	0.36	0.14	1233	40	3.735	0.17	1.47	0.08
667^	-	0.230	0.002	0.020	0.004	1.34	0.08	1.88	0.71	42.7	0.1	0.71	0.27	1369	17	4.210	0.006	1.69	0.02
6400^	-	0.235	0.003	0.018	0.003	0.77	0.05	0.61	0.23	40.7	0.1	1.3	0.5	1227	17	3.738	0.067	1.49	0.03
6401^	-	0.133	0.002	0.019	0.003	0.33	0.02	0.56	0.21	23.6	0.1	0.59	0.22	1257	21	3.762	0.069	1.46	0.04
Grosmont																			
DS46-00	14-5-88-19W4	0.132	0.001	0.010	0.002	0.21	0.01	0.49	0.18	23.9	0.1	0.42	0.16	1304	12	3.961	0.040	1.57	0.02
DS47-00	14-5-88-19W4	0.168	0.001	0.060	0.011	5.40	0.32	8.06	3.02	29.9	0.1	0.67	0.25	1283	11	3.950	0.035	1.60	0.02
DS48-00	14-5-88-19W4	0.139	0.001	0.011	0.002	0.38	0.02	0.57	0.21	24.6	0.1	0.66	0.25	1192	11	3.696	0.034	1.51	0.02
Lloydminster																			
656^	03-14-49-27W3	0.147	0.002	0.010	0.002	1.11	0.07	1.33	0.50	22.2	0.1	0.83	0.32	1028	17	3.303	0.007	1.42	0.02
664^	A12-19-50-24-W3	0.136	0.002	0.060	0.011	8.03	0.47	6.95	2.61	24.0	0.1	1.2	0.4	1260	25	3.976	0.011	1.66	0.03
666^	A13-35-49-24W3	0.150	0.002	0.018	0.003	4.44	0.26	0.74	0.28	24.2	0.1	6.0	2.28	1134	19	3.650	0.075	1.56	0.04
Peace River																			
DS28-00	4-21-85-18W5	0.064	0.001	0.009	0.002	1.20	0.07	0.11	0.04	12.4	0.1	11	4	1404	44	4.018	0.13	1.44	0.07
DS29-00	4-21-85-18W5	0.058	0.001	0.074	0.014	5.87	0.35	7.27	2.73	11.3	0.1	0.81	0.31	1428	38	4.077	0.11	1.46	0.06
DS30-00	4-21-85-18W5	0.070	0.001	0.006	0.001	0.29	0.02	1.04	0.39	13.7	0.1	0.28	0.11	1429	34	4.102	0.10	1.48	0.05

Table 5.3 cont. West Canadian Tar Sands Re and PGE results.

Sample[a]	Well/Core	Os (ppb)	±	Ir (ppb)	±	Pt (ppb)	±	Pd (ppb)	±	Re (ppb)	±	Pt/Pd	±	$^{187}Re/^{188}Os$	±	$^{187}Os/^{188}Os$	±	Os_g[b] (112 Ma)	±
Provost																			
DS42-00	5-20-37-1W4	0.041	0.001	0.001	0.000	0.07	0.00	1.65	0.62	2.78	0.03	0.04	0.02	372	14	1.204	0.076	0.52	0.04
DS43-00	5-20-37-1W4	0.045	0.001	0.024	0.004	0.24	0.01	8.37	3.14	2.88	0.02	0.03	0.01	354	10	1.200	0.058	0.55	0.03
DS45-00	5-20-37-1W4	0.057	0.001	0.006	0.001	0.33	0.02	1.49	0.56	3.92	0.03	0.22	0.08	383	13	1.312	0.070	0.60	0.04
Wabasca																			
DS31-00	2-24-84-22W4	0.133	0.002	0.134	0.025	6.62	0.39	7.01	2.63	23.1	0.1	0.95	0.36	1230	23	3.693	0.096	1.44	0.05
DS32-00	2-24-84-22W4	0.127	0.001	0.005	0.001	0.19	0.01	1.22	0.46	21.7	0.1	0.15	0.06	1200	13	3.641	0.004	1.44	0.02
DS34-00	2-24-84-22W4	0.227	0.002	0.007	0.001	0.22	0.01	1.18	0.44	40.2	0.1	0.19	0.07	1259	11	3.791	0.035	1.48	0.02
650^	14-28-81-22W4	0.225	0.003	0.006	0.001	0.31	0.02	1.17	0.44	41.2	0.1	0.27	0.10	1359	18	4.252	0.067	1.76	0.04

[a] Re - Os data from Selby and Creaser, (2005)

[b] Os_g - $^{87}Os/^{188}Os$ calculated at the time of oil generation (112 Ma; Selby and Creaser, 2005)

Table 5.4 USGS Devonian Ohio Shale Standard PGE results.

Run	Ir (ppb)	± [a]	Pt (ppb)	± [a]	Pd (ppb)	± [a]
1	0.049	18%	1.45	5.4%	2.22	14%
2	0.051	20%	1.43	4.4%	3.41	11%
3	0.041	17%	1.45	2.4%	2.30	12%
4	0.050	13%	1.50	3.7%	2.66	13%
5	0.044	18%	1.39	3.6%	2.87	16%
Mean	**0.047**	**17%**	**1.44**	**3.9%**	**2.69**	**13%**
2 Standard Deviations	0.009		0.09		0.96	
2 Standard Deviations percentage of Mean	18.4%		5.9%		35.7%	

[a] Measured individual run uncertainties

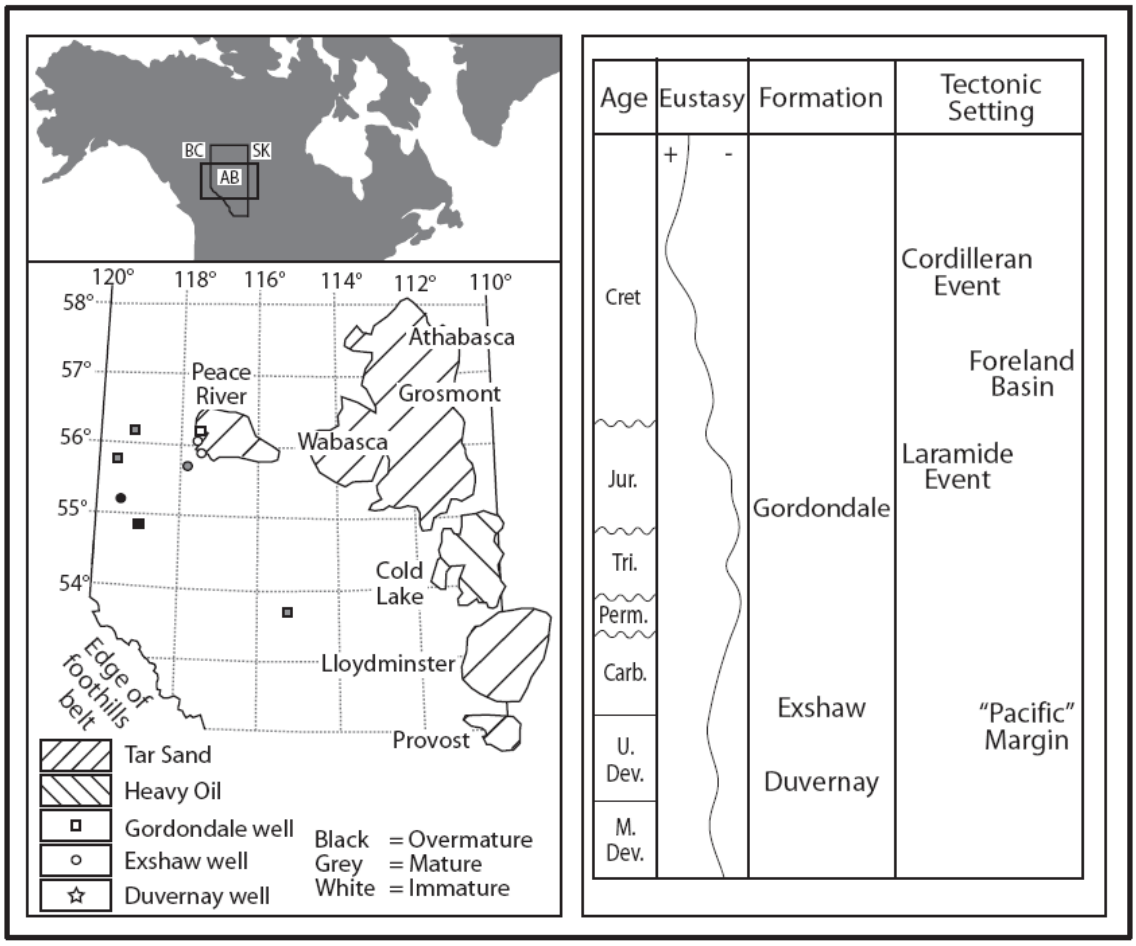

Figure 5.1 Location Map of the West Canadian Tar Sands, Gordondale and Exshaw Fm samples utilised in this study. Abreviations; Sk = Saskatewan; AB = Alberta; BC = British Columbia (modified from Selby and Creaser 2005a; Creaser et al., 2002; Riediger et al., 1995).

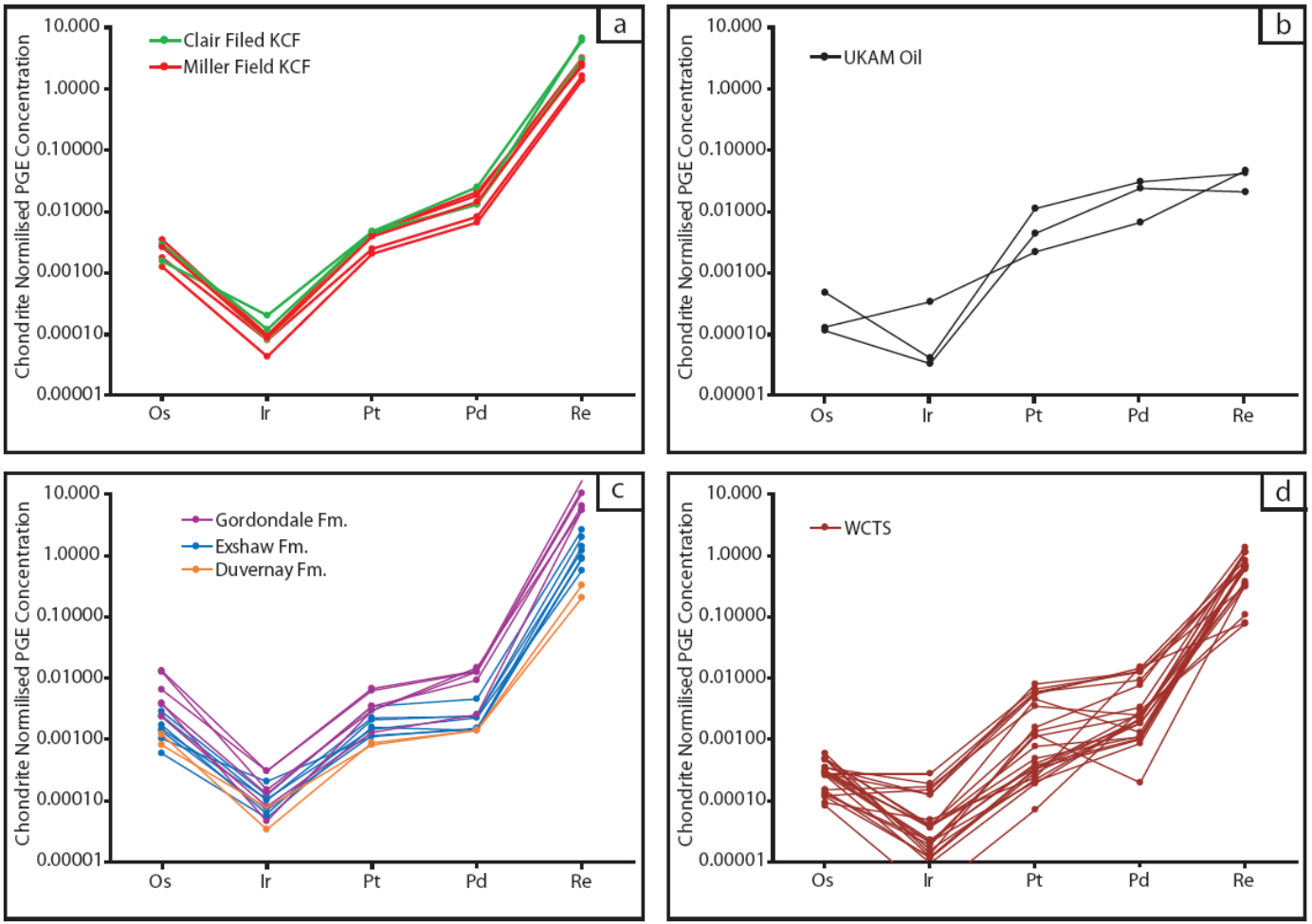

Figure 5.2 Chondrite normalised PGE and Re values for a) Kimmeradge Clay Fm. Shales; b) UKAM oil; c) Gordondale, Exshaw and Duvernay Shales; d) West Canadian Tar sands. Condrite values are 486 ppb Os; 481 ppb Ir; 990 ppb Pt; 560 ppb Pd 36.1 ppb Re; (Siebert et al., 2005). See text for discussion.

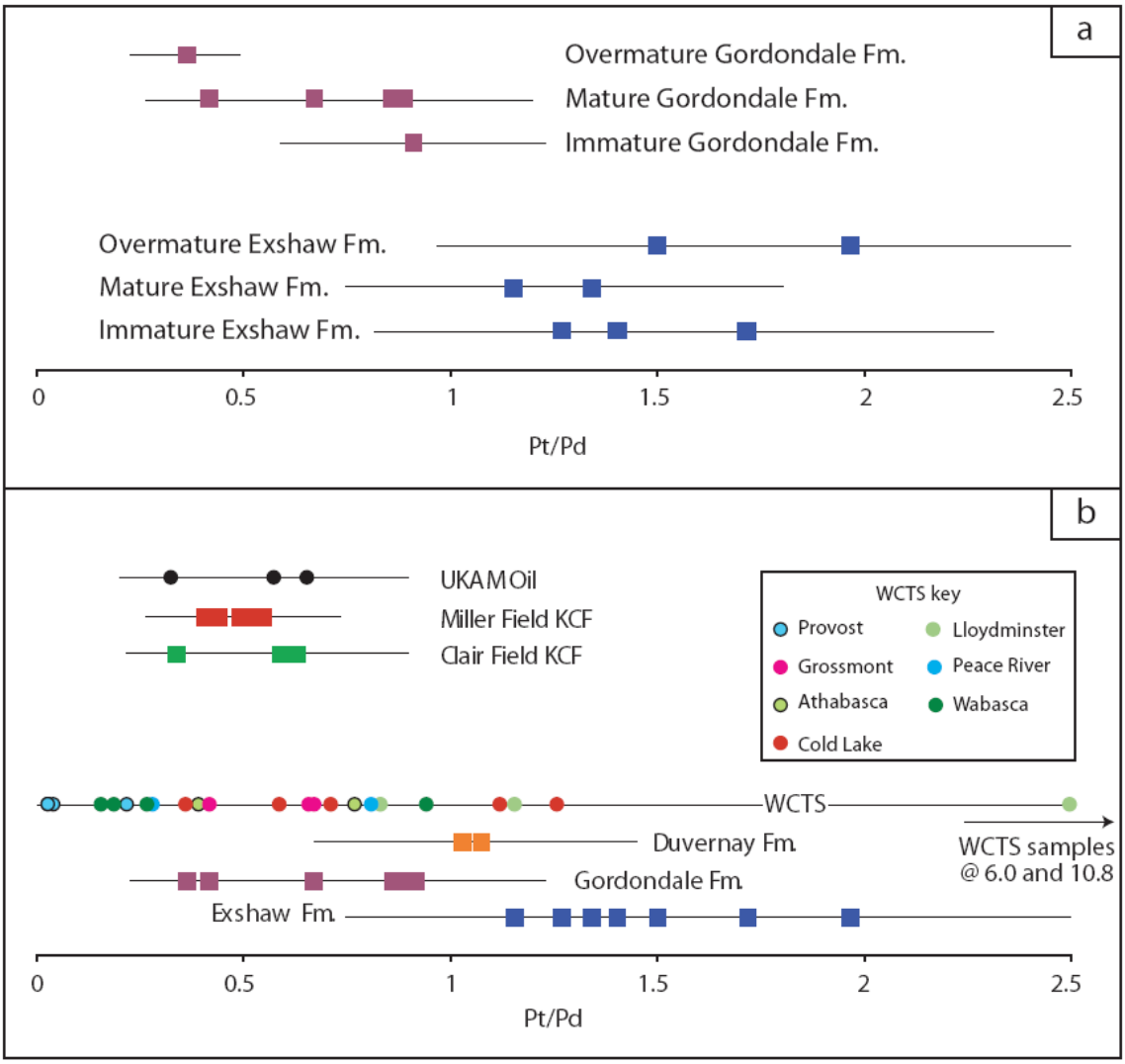

Figure 5.3 Platinum/Pd values for a) oils and source units; b) Gordondale and Exshaw Fm samples of different maturities. See text for discussion.

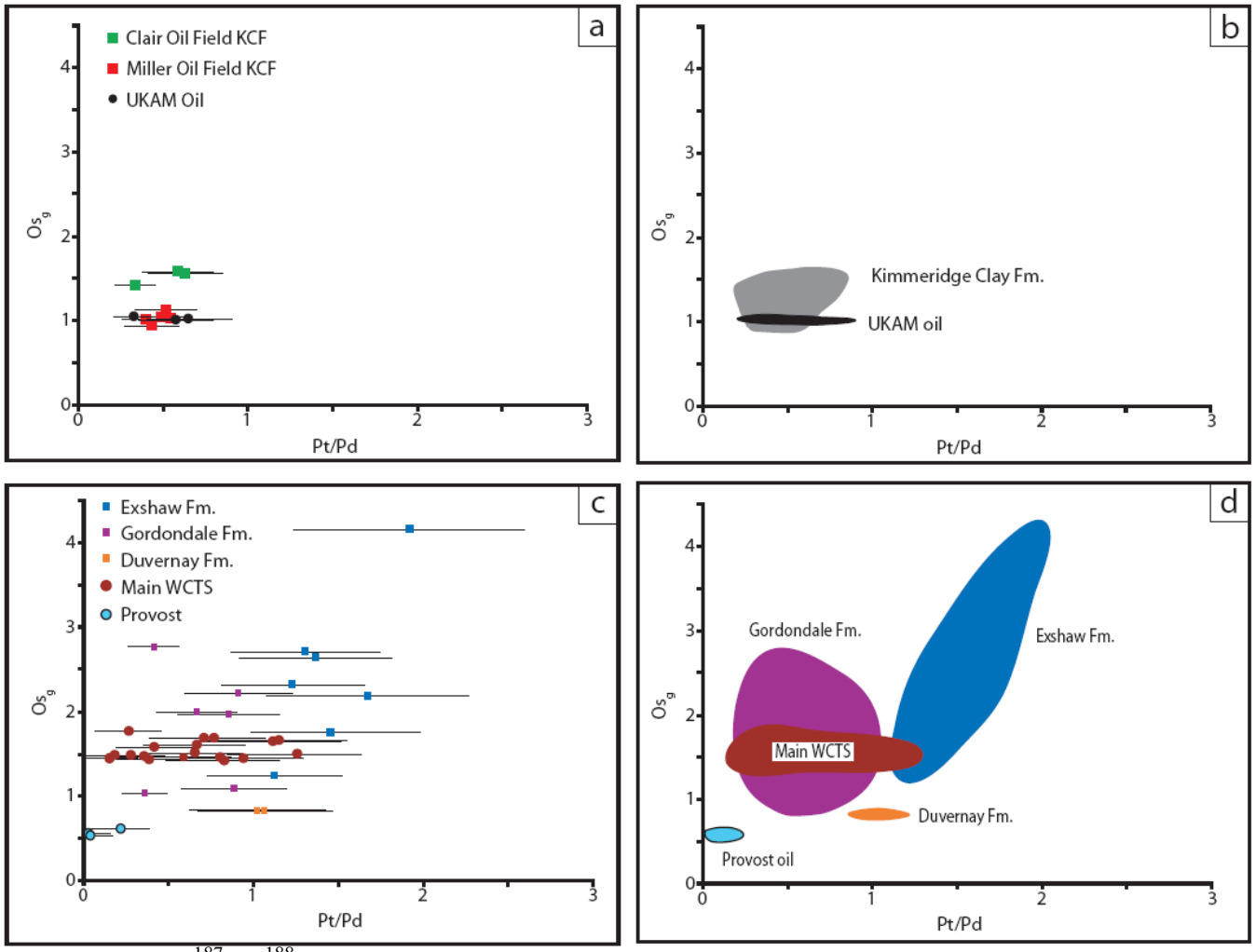

Figure 5.4 Os_g vs Pt/Pd (where Osg is $^{187}Os/^{188}Os$ at the time of petroleum generation) calplots for; a) UKAM raw data; b) UKAM source rock and oil PGE data; c) WCSB and WCTS raw data; d) WCSB and WCTS source unit and oil PGE data. Pt/Pd uncertainty bars are 2 S.D., Os_g uncertainties are smaller than data points. See text for discussion.

CONCLUSIONS AND FUTURE WORK

6.1 Conclusions

The research presented in this thesis has increased the knowledge of Platinum Group element (PGE) and Rhenium – Osmium systematics in petroleum systems. Specifically it is demonstrated that the Re – Os geochronometer absolutely dates the timing of oil generation. Furthermore a new geochemical technique enables the isolation of Platinum Group Elements (PGEs) which, combined with Os isotopes, has enabled the development of a new oil – source fingerprinting tool unaffected by biodegradation. This demonstrates the applicability of utilising Rhenium and the PGEs to further both the spatial and temporal constraints on global petroleum systems.

In Chapter 2 eighteen oils from the UK Atlantic Margin have provided a Re – Os age of 68 ± 13 Ma. This age is in excellent agreement with both basin modelling and $^{39}Ar/^{49}Ar$ feldspar cement ages. To date Re – Os geochronology of petroleum has been confined to oils with an uncertain source unit and, therefore, it is uncertain if the ages produced record oil generation, migration or emplacement. The oils studied in this chapter have a well constrained source, an Upper Jurassic marine shale, equivalent to the North Sea Kimmeridge Clay Fm. Through the use of HPLC, $\delta^{13}C$, GC and GCMS the source of the oils is confirmed to be the Upper Jurassic marine shale. Also the hypothesis that the Os isotopic composition of oils and source units at the time of generation can be used as an oil – source fingerprinting tool is demonstrated to be valid. Therefore, using this data, it is concluded that the Re – Os ages record the timing of oil generation. This provides important temporal constraints for future basin modelling and petroleum exploration in the UK Atlantic Margin and worldwide petroleum systems.

In chapter 3 the controversial hypothesis that unradiogenic Os isotope values reported from the Brent Oil Field, UK North Sea, are inherited from a previously unknown late Jurassic source unit has been investigated. It is demonstrated that wells in the Viking Graben and main East Shetland Basin contain oils with an unradiogenic Os isotope composition (0.13 – 0.40). However, oils from the Moray Firth and Central Graben contain radiogenic Os isotope compositions (1.02 – 3.15). Re – Os analysis of 5 Kimmeridge Clay core samples demonstrates that the radiogenic values associated with oils from the Central Graben and Moray Firth are as expected from a Kimmeridge Clay Fm. However, the unradiogenic values from the Viking Graben and main East Shetland Basin can not be inherited from the Kimmeridge Clay Fm. The overwhelming body of evidence that the Kimmeridge Clay Fm. is the source unit for North Sea oil makes the hypothesis that the unradiogenic Os isotope values are inherited from an unknown

source unlikely. An alternative hypothesis is proposed that the oils have had their Os isotope systematics altered by unradiogenic hydrothermal fluids either sourced from intrusive mafic igneous units or the mantle. This hypothesis is supported by studies of the Miller and Sliepner oil fields (Viking Graben) which demonstrate that they contain up to 30 mol% CO_2 with a mantle/mafic igneous $\delta^{13}C$ signature. Furthermore Noble gas studies of the Magnus oil field (East Shetland basin) demonstrate that there has to have been a mantle component to these oils. Structural analysis of the Viking Graben and main East Shetland basin demonstrate that they have undergone increased stretching and strain localisation along the main basin bounding faults when compared to the Moray Firth and central graben. This has caused increased Cenozoic intrusive mafic volcanism within the Viking Graben and East Shetland Basin and also possibly has enabled the main basin bounding faults and shear zones in the to propagate to sufficient depth to act as a conduit for mantle fluids. This demonstrates that Os isotopes can be used to track crustal scale fluid dynamic processes as well as acting as a tool to identify oil migration pathways in extensional basins, therefore increasing the spatial understanding of petroleum systems.

Chapters 2 and 3 both demonstrate that it is possible to use Os isotopes to fingerprint an oil to its source if the Os isotope signature of the oil and source are known. In chapter 4 the potential variability of Os isotopes within a global source unit, the Ordovician/Silurian shales found at the Ordovician/Silurian boundary GSSP at Dob's Linn, Scotland, is investigated. The late Ordovician was affected by a glacial episode which caused the second largest mass extinction. Initial $^{187}Os/^{188}Os$ (Os_i) values integrated with new $\delta^{13}C_{org}$ data for this section to track this glaciation, are presented. Increasingly radiogenic Os values at the base of the section (~0.3 to ~1.1) track increased silicate weathering which is thought to have draw down enough CO_2 to cause global cooling and the glaciation. The Hirnantian glaciation is reflected by the global positive Hirnantian Isotopic Carbon Excursion. The Os_i at Dob's Linn over this period is relatively unradiogenic (~0.6), reflecting a reduced input of radiogenic Os into sea water due to reduced chemical weathering rates and ice cover. There is a rapid increase to radiogenic Os isotopic values during the period of deglaciation as increased chemical weathering rates combined with easily leached glacial material lead to a sudden increase in radiogenic Os to sea water. Before this study the Hirnantian glaciation has been identified by $\delta^{13}C$ chemostratigraphy. This study has demonstrated the first use of $^{187}Os/^{188}Os$ chemostratigraphy for the Paleozoic as a proxy for reconstructing the Earth's climate system, particularly palaeoceanography. This study

also demonstrates that source rocks can have significantly different Os isotope compositions within a small amount of stratigraphy (e.g. 0.6 – 1.1 over 19 cm of stratigraphy).

In cases such as Chapter 4, where a source unit has a significant spread in Os isotopic values, the usefulness of Os isotopes as an oil source fingerprint is diminished. In Chapter 5 therefore it is demonstrated that combining the $^{187}Os/^{188}Os$ value at the time of hydrocarbon generation (Os_g) with other PGEs, specifically Pt/Pd, can be used to fingerprint oil source. It is demonstrated that Pt/Pd values are: Unaffected by petroleum maturation; similar within individual source units; distinct between differing source units within a petroleum system; and within the UK Atlantic margin, similar between oils and the known source. Therefore this study applies this technique to a petroleum system with a highly debated source, the West Canadian Tar Sands. The majority of oils from within the West Canadian Tar Sands contain Pt/Pd and Os_g values that correlate well with the Lower Jurassic Gordondale Fm. There is also a slight overlap with data from the Exshaw Fm. Therefore, the Gordondale Fm. is proposed to be the major source unit for the West Canadian Tar Sands with minor inputs from the Devonian/Carboniferous Exshaw Fm.

In conclusion, the aims of this project have been achieved through:

1. Demonstrating that the Re – Os petroleum geochronometer records the timing of petroleum generation.
2. Demonstrating that the $^{187}Os/^{188}Os$ value at the time of hydrocarbon generation can be used to help constrain the source of petroleum.
3. Demonstrating that the Re – Os petroleum system can be disturbed by natural processes, yet, still provide important information about petroleum systems.
4. Demonstrated that $^{187}Os/^{188}Os$ value at the time of deposition can vary dramatically within a small stratigraphic interval (Dcm scale)
5. Demonstrate that the $^{187}Os/^{188}Os$ value at the time of deposition can act as a weathering proxy and so provide increased paleoclimate and palaeogeodynamic understanding.
6. Demonstrating that Re and the PGEs, can be a powerful oil source fingerprinting tool.

6.2 Future Work

The studies that form this thesis do raise some further questions. Chapter 1 produces two robust ages for generation in the UK Atlantic Margin. However the Re – Os data from two samples do not form part on these ages. It is possible that these samples relate to an oil generation event hinted at by $^{40}Ar/^{39}Ar$ K feldspar cement bearing oil and aqueous fluid inclusions, in a single Foinaven well (~113 Ma; Mark et al., 2010). Further analysis of extra samples from other fields within the UK Atlantic margin (e.g. Loyell) and Faroes (e.g. Longan well; 6005/15-1) may identify any further oil generation events within the petroleum system.

Chapter 3 records disturbance to the Re – Os geochronometer through contamination by mantle like fluids, hypothesised to have propagated up large scale basin bounding faults. Rhenium – Os analysis of pyrite mineralisation within basin bounding faults could help prove this hypothesis. If fluid related pyrite within these faults contained a mantle like initial Os isotope composition then it would be likely that the fluid is mantle sourced, however if the pyrite produces an age that corresponds to the Cenozoic intrusive volcanism, then that would be the probable source. This is not possible in the Viking Graben, however, large scale carboniferous basin bounding faults outcrop within the UK (e.g. Ninety Fathom Fault; Knott et al., 1996).

Chapter 4 demonstrates how Os_i can record changes in silicate weathering over the Hirnantian glaciation. This study only covers one section, the Ordovician/Silurian GSSP at Dob's Linn, Scotland. Therefore, whether the Os_i signal recorded in Dob's Linn is recording global sea water Os_i or just the Os_i of the Iapetus Ocean is open to debate. It is unlikely that the Global and Iapetus Oceanic Os_i profiles would differ in shape; however they may differ in absolute Os_i values (Du-Vivier, 2010). Analysis of a Ordovician/Silurian section outside of Iapetus (e.g. South China; Fan et al., 2009) would answer this. However, unaltered Ordovician/Silurian shale sections are rare.

Chapter 5 applies Rhenium and the PGEs as an oil source fingerprinting tool within well and poorly constrained petroleum systems and identified the Gordondale Fm. as the likely main source of the WCTS. However, the source of the Provost oil deposit was also not identified. Further analysis of other West Canadian Sedimentary Basin source units (e.g. Doig Fm., Manville Ostracode Fm.; Higley et al., 2009) could enable the identification of the source of this deposit. Furthermore to confirm that the PGEs can be used as an oil source fingerprint several more studies should be undertaken. For example, analysing KCF from Kimmeridge bay, Dorset, and, Staffin, Skye will provide a full Pt/Pd variation within regional KCF of different maturities.

Also needed are further repeat analyses of the SDO-1 standard (n > 15) to constrain PGE uncertainty and achieve robust PGE SDO-1 values. Furthermore, analysis of other well understood petroleum systems with known source units would confirm that the PGEs can be used for oil source fingerprinting.

The application of PGE fingerprinting also provide avenues of exciting new research outside of Geology, namely, Archaeology and Forensic Science. Archaeologically, I wish to test if Re, PGEs, Major and Trace elements can be utilised to identify where Ceramic Building Material (CBM; pottery, brick and other ceramics) were made, i.e. the source of clay. The applicability of this elemental tracing is hinted at in figure 6.1 where a CaO – MgO plot shows that CBM made by the VI legion in the UK has distinct values to those of Roman CBM from The Netherlands, Belgium and Germany (De Clercq et al., 2008) and Southern Italy (Eramo et al., 2004) as well as typical kaolinite and illite (Deer et al., 1992). To further investigate this, samples of Roman CBM and the known source clay have been collected from the York Archaeoological Trust (YAT; Hungate site). An aliquot of clay will be air dried and a second aliquot will be baked in conditions similar to those hypothesised to have been used during the roman period (Eramo et al., 2004). By analysing this large suite of elements (Major, Trace, Re and PGEs), and comparing the results, it will be possible to identify the level of analysis needed to fulfil the aims of this study. For example, if major element compositions, analysed quickly and cheaply by XRF, are shown to be sufficient then there will be no need to apply the complex, time consuming and expensive PGE analysis in future studies. If successful I will seek to develop these methods further to geochemically identify the sources of pottery within Medieval York and Roman Britian, through collaborative research with the YAT.

A second area I wish to develop uses of the Re and PGE fingerprinting tool is Forensic Science. Lead isotopes have been applied to demonstrate the applicability of utilising isotopic and elemental analysis to shooting incident investigations (Zeichner et al., 2006). However, lead isotopes are easily contaminated, e.g. skin oil). I aim to analyse and fingerprint ammunition from different batches and makes of .22 rimfire ammunition (Eley Tenex, Match, Sport and Club; RWS R50 and Rifle match; Lapua X-Act, Midas+ and Centre X. .22 rimfire ammunition has been chosen for analysis because I may legally purchase and store it under my firearms licence). It has been demonstrated that considerable variability exists amongst lead sources (Koons and Grant, 2002), making it likely that they will be amenable to PGE fingerprinting, which are less likely to be contaminated than lead isotopes. If it can be shown that bullet

heads, cartridge cases, powder and powder residues are distinct between differing batches and makes of ammunition it will be possible to fingerprint a bullet removed from a crime scene to it's batch. Furthermore, Zeichner et al. (2006) demonstrate that thorough cleaning of firearms does not completely remove lead deposits, therefore it may be possible to fingerprint a bullet to the weapon it was fired from.

References

De Clercq, W and Degryse, P. 2008. The mineralogy and petrography of Low Lands Ware 1 (Roman lower RhineeMeuseeScheldt basin; the Netherlands, Belgium, Germany). J. Arch. Sci. 23, 448-458

Deer, W.A., Howie, R.A. and Zussman, J. An introduction to the rock forming minerals. 2nd ed. (pearson Education Ltd.)

Du Vivier, A.D.C., 2010 Progression of seawater 187Os/188Os throughout the Oceanic Anoxic Event (OAE) 2: Implications for mechanisms driving global ocean anoxia and ocean palaeocirculation. Unpublished MSci thesis (Department of Earth Sciences, Durham University).

Eramo, G., Laviano, R., Muntoni, I.M. and Volpe, G. 2004. Late Roman cooking pottery fro m the Tavoliere area (Southern Italy): raw materials and technological aspects. J. Cult. Heratige. 5, 157 – 165.

Fan, J., Peng, P., Melchin, M.J., 2009. Carbon isotopes and event stratigraphy near the Ordovician–Silurian boundary, Yichang, South China. Palaeogeogr. Palaeoclimatol. Palaeoecol. 276, 160–169.

Higley, D.K., Lewan, M.D., Roberts, L.N.R., Henry, M. 2009, Timing and petroleum sources for the Lower Cretaceous Mannville Group oil sands of northern Alberta based on 4-D modelling. AAPG Bull.

Knott, S.D., Beach, A., Brockbank, P.J., Brown, L., McCallum, J.E., Welbon, A.I. 1996. Spatial and mechanical controls on normal fault populations. J. Struct. Geol. 18 359-372.

Mark, D.F., Parnell, J., Kelley, S.P., Lee, M.R., Sherlock, S.C. 2010. 40Ar/39Ar dating of oil generation and migration at complex continental margins. Geology 38, 75 – 78.

Zeichner, A., Ehrlich, s., Shoshiani, E. and Halicz, L. 2006. Application of lead isotope analysis in shooting incident investigations. For. Sci. Int. 158, 52 – 64.

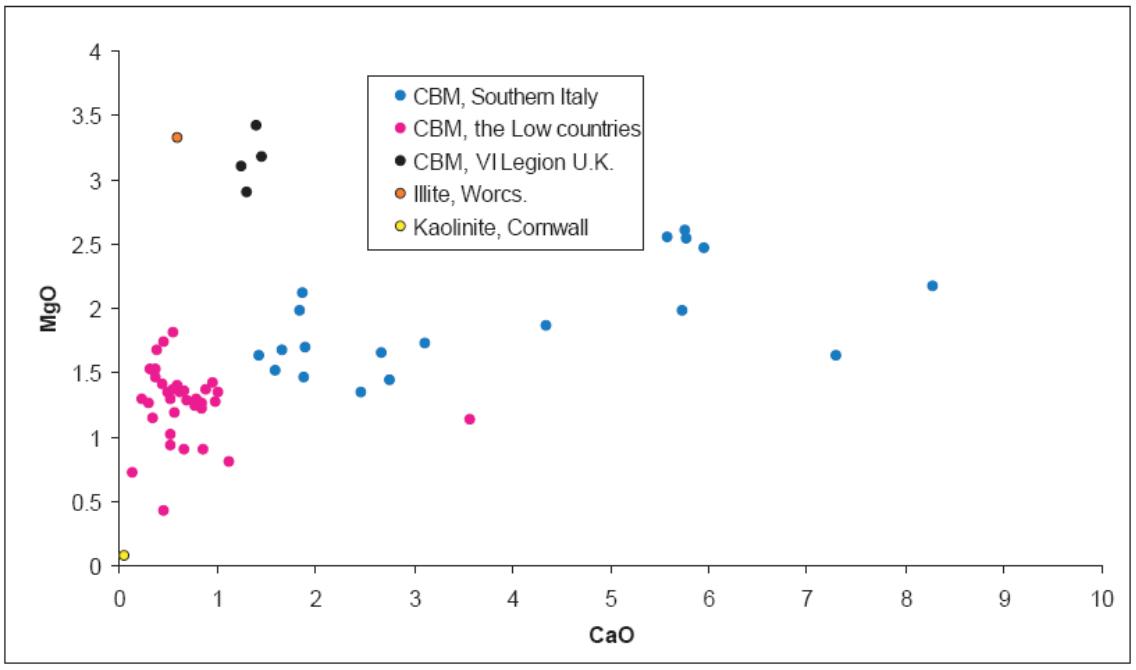

Figure 6.1 CaO vs MgO plot of Ceramic Building Material (CBM) and Clays from the VI Legion, UK (Finlay, unpublished data). The Low Countries (The Netherlands, Belgium and Germany; De Clercq et al., 2008), Southern Italy, (Eramo et al., 2004) as well as typical kaolinite and illite (Deer et al., 1992). The CBM material from different sources appear distinct.

APPENDIX 1

TRACKING THE HIRNANTIAN GLACIATION USING OS ISOTOPES

ALEXANDER J. FINLAY , DAVID SELBY, DARREN R. GRÖCKE

Earth and Planetary Science Letters 293 (2010) 339–348

Contents lists available at ScienceDirect

Earth and Planetary Science Letters

journal homepage: www.elsevier.com/locate/epsl

Tracking the Hirnantian glaciation using Os isotopes

Alexander J. Finlay *, David Selby, Darren R. Gröcke

Department of Earth Sciences, Durham University, Science Laboratories, Durham, DH1 3LE, UK

ARTICLE INFO

Article history:
Received 4 December 2009
Received in revised form 16 February 2010
Accepted 26 February 2010
Available online 23 March 2010

Editor: R.W. Carlson

Keywords:
osmium isotopes
carbon isotopes
glaciation
weathering
Hirnantian
Ordovician

ABSTRACT

Here we present initial $^{187}Os/^{188}Os$ (Os_i) values integrated with $\delta^{13}C_{org}$ for the first Paleozoic section — the Ordovician/Silurian boundary GSSP at Dob's Linn, Scotland. Our $^{187}Os/^{188}Os$ data tracks major changes in climate that occurred during the Late Ordovician (Hirnantian glaciation), which coincides with the second largest known mass extinction. During the *complanatus* and early *anceps* Biozones Os_i values increase from 0.28–1.08. This provides evidence for a period of increased silicate weathering of radiogenic continental crust, likely from the Caledonian Orogen. This increase in weathering was likely the driving mechanism for the drawdown in atmospheric CO_2 and global cooling that resulted in the onset of the Hirnantian Glaciation. A decrease to less radiogenic Os_i occurs at the base Hirnantian *extraordinarius* Biozone and coincides with the trend to more positive $\delta^{13}C_{org}$ values that mark the onset of the Hirnantian Glaciation. The trend in Os_i during this interval is ascribed to Hirnantian ice cover and reduced chemical weathering rates cutting the supply of radiogenic material to the Iapetus Ocean. The reduction in silicate weathering enabled atmospheric CO_2 to return back to greenhouse levels, causing rapid deglaciation during the mid *persculptus* Biozone. This period is marked by an abrupt increase in Os_i values from 0.6 to 1.08 over 19 cm of stratigraphy and coincides with the deglacial limb of the $\delta^{13}C_{org}$ profile. We interpret the Os_i data to reflect the leaching of exposed radiogenic $^{187}Os/^{188}Os$ bearing glacial deposits and increased weathering of radiogenic $^{187}Os/^{188}Os$ silicate terrane during the deglaciation. Previous workers have identified the Hirnantian glaciation primarily through $\delta^{13}C$ stratigraphy. However, our Os isotope data indicate that an initial mechanism (i.e. increased silicate weathering) was the driving mechanism behind the Hirnantian Glaciation and subsequent mass extinction. Thus, by coupling Os_i and $\delta^{13}C_{org}$ proxies we provide the most direct evidence for the initiation and cessation of the Hirnantian glaciation. Furthermore, this study demonstrates the first use of $^{187}Os/^{188}Os$ chemostratigraphy for the Paleozoic as a proxy for reconstructing the Earth's climate system, particularly palaeoceanography.

1. Introduction

The Late Ordovician Hirnantian stage records the second largest mass extinction of the Phanerozoic Eon (Sheehan, 2001). This extinction eradicated 85% of species, 61% of genera and 12–24% of families (Brenchley et al., 2001 and references therein). The extinction occurs during an abrupt change in climate (Hirnantian Glaciation) that culminated in ice-sheet growth over Gondwana and a global fall in sea-level that drained large areas of previously submerged marine shelf (Brenchley et al., 2001; Finney et al., 2007; Trotter et al., 2008).

Global Hirnantian sections (Anticosti Is. Quebec, Long, 1993; Dob's Linn, Underwood et al., 1997; South China, Wang et al., 1997, Yan et al., 2009, Fan et al., 2009; Nevada, Finney et al., 1999; Estonia/Latvia, Brenchley et al., 2003; Arctic Canada, Melchin and Holmden, 2006; North America and China, Young et al., 2008; Fig. 1) record positive inorganic and organic carbon-isotope excursions at the onset of the glaciation (Fig. 2), which have been attributed to increased weathering of ^{13}C-enriched carbonates exposed during the glacio-eustatic lowstand (e.g. Kump et al., 1999; Melchin and Holmden, 2006; LaPorte et al., 2009). The major positive $\delta^{13}C_{org}$ excursion during the Late Ordovician is referred to as the Hirnantian Isotopic Carbon Excursion (HICE; Bergstrom et al., 2008), which broadly coincides with the phases of the Hirnantian extinction.

During the Cenozoic, osmium isotope ($^{187}Os/^{188}Os$) values of organic-rich marine sediments have been used to reconstruct changes in seawater $^{187}Os/^{188}Os$ (Pegram et al., 1992; Ravizza et al., 2001; Ravizza and Peucker-Ehrenbrink 2003; Dalai et al., 2006; Oxburgh et al., 2007). During the Pleistocene interglacial, seawater $^{187}Os/^{188}Os$ ratios are more radiogenic (~1.04) than during the glacial period (~0.94; Oxburgh et al., 2007). This has been interpreted to reflect the reduction in weathering of radiogenic continental crust in response to burial beneath ice sheets and decreased rates of chemical weathering. However, following deglaciation increased chemical weathering combined with exposure of easily leached glacial deposits releases more radiogenic $^{187}Os/^{188}Os$ into the oceans (Peucker-Ehrenbrink and Blum, 1998), thus causing a rise in seawater $^{187}Os/^{188}Os$. In contrast to

* Corresponding author.
E-mail addresses: a.j.finlay@durham.ac.uk (A.J. Finlay), david.selby@durham.ac.uk (D. Selby), d.r.grocke@durham.ac.uk (D.R. Gröcke).

0012-821X/$ – see front matter © 2010 Elsevier B.V. All rights reserved.
doi:10.1016/j.epsl.2010.02.049

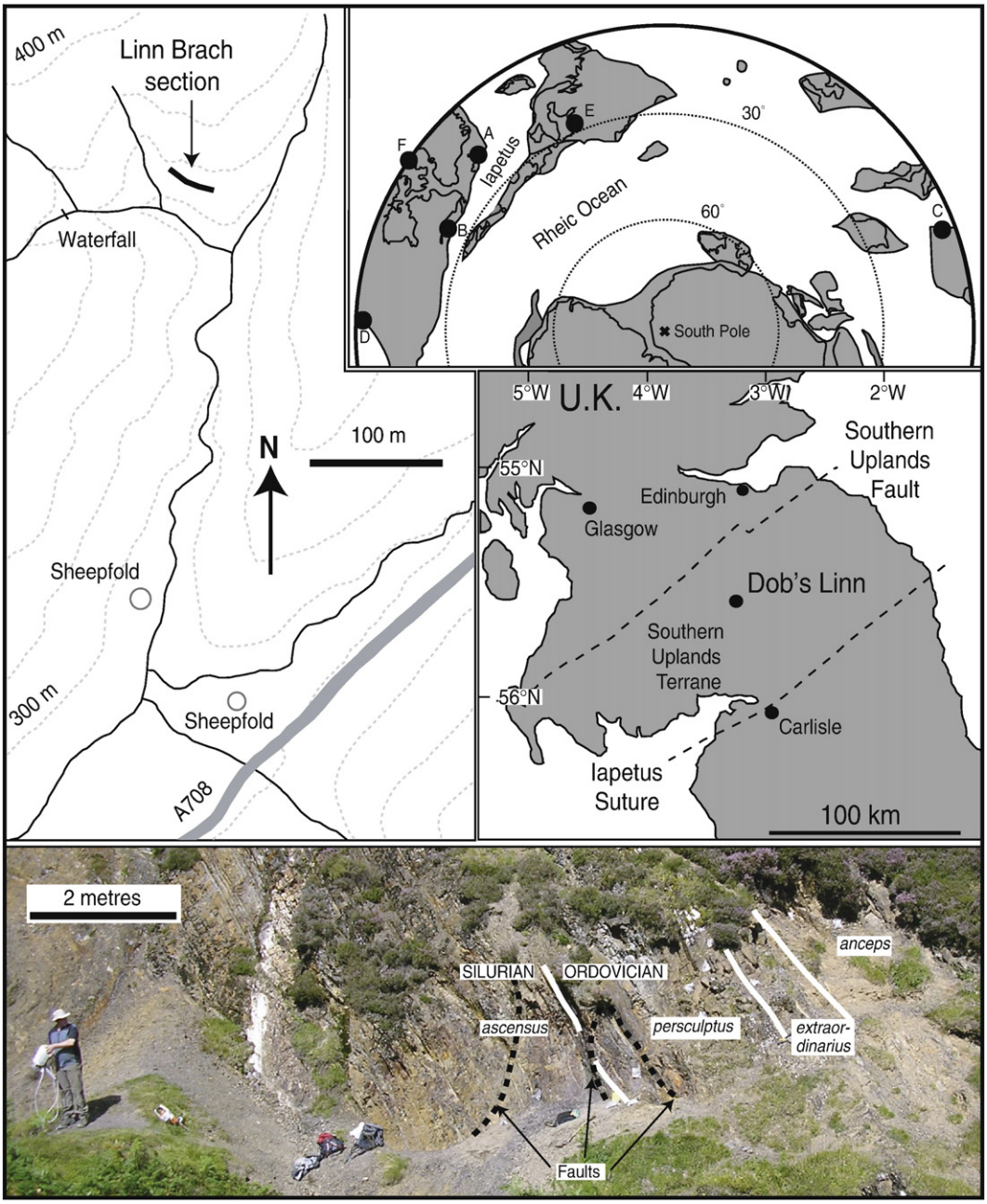

Fig. 1. Location maps for the study area, Dob's Linn, Scotland. Palaeogeographic map for 440 Ma (modified from Cocks and Torsvik, 2006) showing locations discussed in text; A — Dob's Linn, Scotland; B — Anticosti Island, Quebec; C — South China; D — Nevada, USA; E — Estonia/Latvia; and F — Arctic Canada. Linn Branch Section at Dob's Linn location; 55°25′ 47.56″N 003°16′72.91″W (OSGB-36), UK National Grid NT 1962, 1584. Contour lines represent 25 m elevation. Photograph of Linn Branch section taken facing North East.

the Cenozoic glaciations, the $^{187}Os/^{188}Os$ profile of the Hirnantian glaciation (recorded in the Dob's Linn section) reflects a much more dramatic change (~0.4; this study).

Herein, we document similar climatically driven shifts in silicate weathering through the application of initial $^{187}Os/^{188}Os$ (Os_i) from ocean basin sediments preserved at Dob's Linn (Point Linn Branch section) in the Southern Uplands of Scotland — the Global Stratotype Section and Point (GSSP) for the basal Silurian. We discuss how Os isotopes track events prior to, during and after the Hirnantian glaciation and the associated implications for Earth processes during this time. In addition to the Os_i data, we present a new $\delta^{13}C_{org}$ profile for the GSSP. The two complimentary proxies track changes in continental weathering to the Iapetus Ocean throughout the Hirnantian glaciation. During the Hirnantian the Iapetus Ocean was connected to the Rheic Ocean (Cocks and Torsvik, 2006). Climatic events that drive silicate weathering are global (c.f. Sheehan, 2001), and as the Iapetus and Rheic Oceans were interconnected (Fig. 1) it is feasible that, although absolute the Os isotope composition may vary globally, the general trend in Os isotope compositions during the Late Hirnantian presented here may reflect that of a global oceanic signature. This study also demonstrates the application of Os isotopes for understanding palaeoceanographic and geological processes. Furthermore, we present the first use of Os_i stratigraphy for a Paleozoic sedimentary succession.

2. Geological setting

The base Silurian GSSP is found in the Linn Branch section, Dob's Linn, which is located in the Central Zone of the Southern Uplands Terrane, Scotland (Williams, 1983; Cocks, 1985; Fig. 1; location,

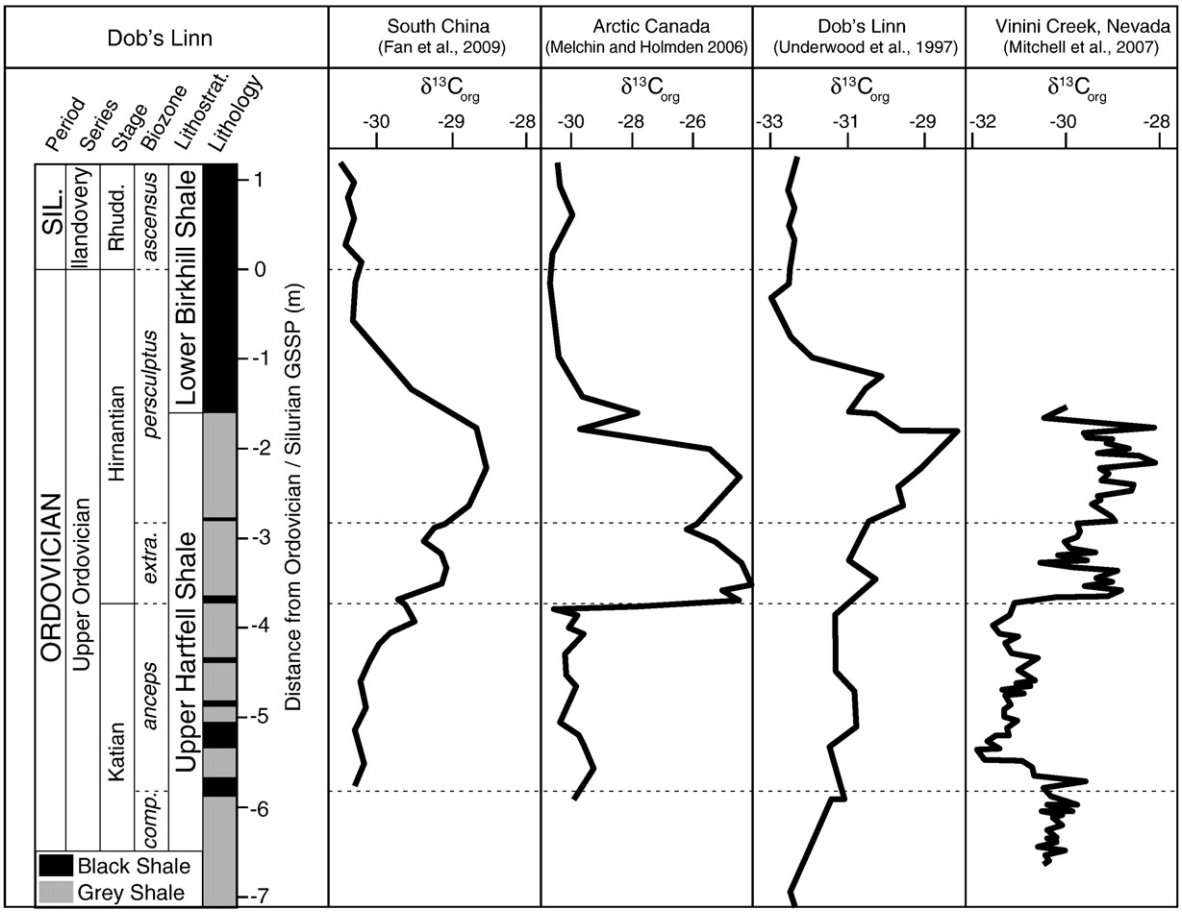

Fig. 2. Stratigraphic column for the Linn Branch Section at Dob's Linn. Periods, series and stages from Ogg et al. (2008). Biozones taken from Melchin et al. (2003). Lithostratigraphy and broad lithological changes taken from Williams (1986); Melchin et al. (2003); and field observations (this study). The $\delta^{13}C_{org}$ profiles modified from Fan et al. (2009) to fit Dob's Linn biostratigraphy. Abbreviations; Sil. — Silurian; Rhudd. — Rhuddanian; *comp.* — *complanatus*; *extra.* — *extraordinarius*.

55°25′47.56″N 003°16′72.91″W (OSGB-36), UK National Grid NT 1962, 1584). The Linn Branch section is comprised of two geological formations of the Moffat Shale Group: the stratigraphically lower Upper Hartfell Shale, which is overlain by the Lower Birkhill Shale (Fig. 2). The Upper Hartfell Shale is comprised of two lithologies (Fig. 2). The major lithology is an organic-poor (~0.1–0.4% Total Organic Carbon [TOC]) grey shale, with no preserved graptolites or sedimentary structure and minor amounts of disseminated pyrite. In the studied area this unit is interbedded with six, ~5 to 20 cm thick bands of organic-rich (~1–2% TOC) black to dark grey shale. These bands are laminated and contain abundant graptolites and disseminated pyrite (Armstrong and Coe, 1997).

The Lower Birkhill Shale is a black, organic-rich (TOC = 0.63 to 1.69%), laminated, and graptolite-rich. Disseminated pyrite is abundant throughout the unit and pyrite also forms regular sub mm layers parallel to lamination (Armstrong and Coe, 1997). Both units are interbedded with numerous <1 cm to ~5 cm scale bentonite horizons. This study also observed a poorly developed low angle cleavage through the section.

The stratigraphy of the GSSP section represents a distal microturbidite that was deposited on the eastern continental margin of Laurentia during the closure of the Iapetus Ocean (Armstrong and Coe, 1997; Armstrong and Owen, 2002). The Hirnantian, specifically the *extraordinarius* and *persculptus* Biozones (Figs. 1–3) records the glaciation that covered Gondwana up to ~30°S (Cocks and Torsvik, 2006). The end of this glacial period is marked by the global deposition of black anoxic shales as the climate returned to greenhouse conditions (Armstrong and Coe, 1997).

The black shale units of the Hartfell and Birkhill Shale Formations are rich in numerous species of graptolites that are used as the main criteria for defining the biostratigraphy of the Ordovician and Silurian (cf. Lapworth, 1878; Williams, 1983; Cocks, 1985; Fan et al., 2009; Figs. 1–3). Graptolites within these bands define the *Dicellograptus anceps* Biozone (Lapworth, 1878), that have been further subdivided into the *Dicellograptus complexus* and *Paraorthograptus pacificus* Subzones, and the younger *Normalograptus extraordinarius* Biozone (Melchin et al., 2003; Figs. 1 and 2). The graptolites, *Climacograptus hastus* and *Glyptograptus posterus* within the *anceps* Biozone of the Hartfell Shale are correlated with Australian and Chinese Ordovician/Silurian sections (Williams, 1988). The first occurrence of *Akidograptus ascensus* within the Birkhill Shale, which is used to define the base of the Silurian, occurs 1.6 m above the base of the Lower Birkhill Shale units (Melchin et al., 2003; Rong et al., 2006). The base Silurian is not marked by any major lithological change.

It is important to note that there is a small fault, not discussed in detail in the published literature, ~50 cm below the GSSP (Fig. 1). The displacement from this fault is masked by two bentonite horizons, smeared into each other. The exact loss of stratigraphy is unknown, but is likely to be ~15 cm from field observations (this study). This likely accounts for the different measured distances between the GSSP and Upper Hartfell/Lower Birkhill Shale formation contact of 1.72 m (Verniers and Vandenbroucke, 2006) and 1.6 m (Cocks, 1985; this study).

There are numerous bentonites within the Upper Hartfell Shale and the Lower Birkhill Shale at Dob's Linn, however they are rare in the *extraordinarius* to mid-*persculptus* Biozone, which span the glacial

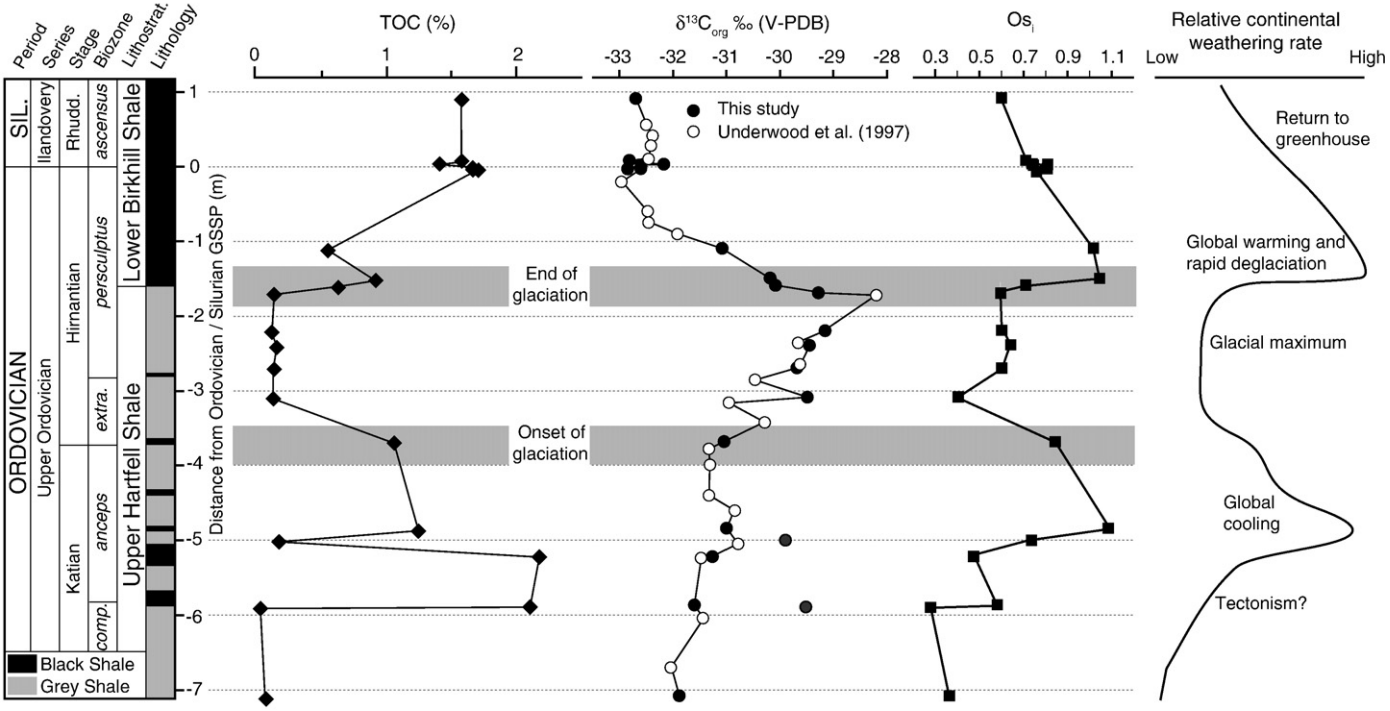

Fig. 3. Stratigraphic column as in Fig. 2. The onset and end of glaciation placed as given for the Hirnantian (Brenchley et al., 2003). The $\delta^{13}C_{org}$ profile comprise data from this study and Underwood et al. (1997). The Os_i (calculated at 443 Ma) profile from the Dob's Linn is used to produce a relative weathering rate. Note $\delta^{13}C_{org}$ and Os_i symbol sizes are greater than uncertainty for each point. See text for discussion.

maximum (Figs. 1–3). The rarity of bentonite horizons may relate to the suppression of eruptions in response to the ice cover of the Hirnantian glaciation. The numerous bentonite units within the Linn Branch section are suggested to be the product of subduction-related, explosively erupted ashes of intermediate to acid composition (Batchelor and Weir, 1988; Huff et al., 1988; Merriman and Roberts, 1990; Huff et al., 1991; Cameron and Anderson, 2007). Multi-grain U–Pb zircon geochronology of bentonites ~4.5 m below and ~6 m above the Ordovician/Silurian boundary yield dates of 445.7 ± 2.4 and 438.7 ± 2 Ma, respectively (Tucker et al., 1990). Mathematical fitting of these dates gives an age of 443 ± 1.5 Ma for the Ordovician/Silurian boundary (Geologic Time Scale 2008, Ogg et al, 2008).

The bentonite units are dominated by illite and smectite with minor chlorite that formed during anchizone (prehnite–pumpellyite/low greenschist facies) metamorphism (Huff et al., 1991). Peak metamorphism occurred at ~340 °C during the Wenlock (428–422 Ma; Oliver and Leggett, 1980), which coincides with the Scandian orogeny (435–425 Ma; Trewin and Rollin, 2002). However, determining the absolute timing of metamorphism at Dob's Linn is challenging because of the low blocking temperature of the K–Ar systematics in illite/smectite (I/S; ~200 °C; Huff et al., 1991). The <0.5 μm I/S fraction from nine bentonites in the lower Llandovery at Dob's Linn and correlated sections in County Down, Ireland, yield a mean age of 390 ± 10 Ma. The K–Ar dates from Dob's Linn are 406 ± 10 Ma and 383 ± 10 Ma, suggesting that metamorphism and cooling to ~200 °C occurred by the early-mid Devonian (Huff et al., 1991).

3. Samples and analytical methods

Samples ($n = 23$) were collected from within the Linn Branch Stratotype Section, Dobs Linn, for $\delta^{13}C_{org}$ and $^{187}Os/^{188}Os$ analysis during the summers of 2007 and 2008. The samples were approximately 10 cm × 10 cm × 3 cm (stratigraphic height) in size, weighing ~50–80 g, and were collected from both black and grey shale horizons, 0.9 m above to 7.1 m below the GSSP.

Carbon isotope analysis was conducted on decalcified bulk sediment powders by mixing 3 M HCl with ~1 g powder in 50 ml centrifuge tubes for 24 h, after which they were thoroughly washed using ultra pure water (Milli-Q) until neutralised. The samples were dried in an oven at 60 °C for 48 h. The residue was then reground to homogenise the sample and loaded into tin capsules. Stable isotope measurements were performed at Saskatchewan and Durham using a Costech EA coupled to a ThermoFinnigan DeltaPlus XL and a Costech EA coupled to a ThermoFinnigan Delta V Advantage, respectively. Carbon-isotope ratios are corrected for ^{17}O contribution (Craig, 1957) and reported in standard delta (δ) notation in per mil (‰) relative to the VPDB scale. Carbon-isotope data is calibrated against international standards, L-SVEC ($\delta^{13}C = -46.6$‰ VPDB) and IAEA-CH6 ($\delta^{13}C = -10.45$‰ VPDB; Coplen et al., 2006). An intermediate international standard (IAEA-CH7) yielded a $\delta^{13}C$ value of -32.14 ± 0.03‰ VPDB ($n = 12$), which is within uncertainty of the accepted value ($\delta^{13}C = -32.15 \pm 0.10$‰ VPDB; Coplen et al., 2006). Data accuracy is monitored through routine analyses of in-house standards, which are stringently calibrated against the international standards noted above. Analytical uncertainty for $\delta^{13}C_{org}$ measurements is typically better than ±0.1‰. Total organic carbon (TOC) data was obtained as part of this method.

Prior to crushing, all samples were polished to remove cutting and drilling marks to eliminate any contamination. The samples were dried at 60 °C for ~12 h and then crushed to a fine powder ~30 μm. The samples of ~50–80 g represent ~3 cm of stratigraphy and were broken into chips with no metal contact and powdered in a ceramic mill. Rhenium–Osmium isotope analysis was carried out at Durham University's TOTAL laboratory for source rock geochronology and geochemistry at the Northern Centre for Isotopic and Elemental Tracing (NCIET) using Cr^{VI}–H_2SO_4 digestion and solvent extraction ($CHCl_3$), micro-distillation and anion chromatography methods and negative ionisation mass spectrometry (cf. Creaser et al., 1991; Selby and Creaser, 2003; Selby 2007).

Rhenium–Os analysis of organic-rich rocks involves whole-rock digestion. Previous research has shown that the Re and Os abundances and isotopic compositions for organic-rich sediments

predominantly reflect the hydrogenous uptake of Re and Os from seawater (Ravizza and Turekian, 1989; Cohen et al., 1999; Selby and Creaser, 2003). Further, the Re and Os are complexed by organic matter (Ravizza and Turekian, 1989; Cohen et al, 1999; Selby and Creaser, 2003). The detrital fraction of the sediment may also contain a minor abundance of Re and Os (~0.2 to 2 ppb Re and ~50 ppt Os; Esser and Turekian, 1993; Peucker-Ehrenbrink and Jahn, 2001). However, the CrO_3–H_2SO_4 digestion method employed here principally dissolves the organic fraction of a shale, thus principally liberates the hydrogenous Re–Os load of the sediment (Selby and Creaser, 2003; Kendall et al., 2004).

Total procedural blanks for Re and Os are 12 and <0.5 pg, respectively, with an average $^{187}Os/^{188}Os$ value of ~0.4 ($n=2$). Raw Re and Os oxide values were corrected for oxygen contribution and mass fractionation. The Re and Os isotopic values and elemental abundances are calculated by full propagation of uncertainties from Re and Os mass spectrometer measurements, blank abundance and isotopic composition, spike calibration, and sample and spike weights. Throughout the period of this study, in-house Re and Os standard solutions were repeatedly analysed to monitor instrument reproducibility. The NCIET Re standard is made from 99.999% zone-refined Re ribbon and is considered to be identical to the AB1 Re standard of the Department of Earth Sciences, University of Alberta. The Re standard runs produced average $^{185}Re/^{187}Re$ values of 0.5980 ± 0.0019 (1S.D. $n=20$) identical to 0.5977 ± 0.0012 (Selby, 2007 and references therein). The measured difference between the $^{185}Re/^{187}Re$ values and the accepted $^{185}Re/^{187}Re$ value of Gramlich et al. (1973) is used to correct for sample mass fractionation. The Os (AB2) standard is made from ammonium hexachloro-osmate. The average $^{187}Os/^{188}Os$ AB2 ratio, using an electron multiplier, is 0.10681 ± 0.00022 (1S.D. $n=24$), identical to reported AB2 values (0.10679 ± 0.00007, Selby, 2007 and references therein).

Initial $^{187}Os/^{188}Os$ compositions (Os_i) are calculated for the time of deposition using the age of the basal Silurian (443 ± 1.5 Ma; Ogg et al, 2008) and the ^{187}Re decay constant of $\lambda=1.666\times10^{-11}$ a^{-1} (Smoliar et al., 1996). The calculated initial is taken to represent the Iapetus oceanic $^{187}Os/^{188}Os$ composition at the time of sediment deposition.

4. Results

A $\delta^{13}C_{org}$ profile of the Dob's Linn section was determined by Underwood et al. (1997) for chemostratigraphic correlation of Late Ordovician successions. However, no explanation of the excursion was given and no TOC data was reported. The TOC contents for our samples range between 0.03 and 2.18%, which reflect lithological variations of the Upper Hartfell Shale and Lower Birkhill Shale (Table 1; Fig. 3). For example, the Upper Hartfell Shale black shale bands have TOC values between 1.06 and 2.18%, whereas grey shale units of the Upper Hartfell Shale are between 0.03 to 0.17% (Table 1). From the base of the Lower Birkhill Shale at 1.6 m below the GSSP within the *persculptus* Biozone TOC values increase from ~0.6% to a maximum of ~1.7%, 0.05 m below the GSSP. Above the GSSP the TOC values are similar (~1.6%).

Our $\delta^{13}C_{org}$ data range between −29.15 and −32.86‰ and fit the observed trend reported by Underwood et al. (1997; Figs. 2, 3; Table 1). Throughout the Katian (*complanatus* to top of the *anceps* Biozone; 7.1 to 3.69 m below the GSSP) $\delta^{13}C_{org}$ values display a relative stable profile, with a minor (~0.5‰) shift to more positive $\delta^{13}C_{org}$ values. Throughout this interval the mean $\delta^{13}C_{org}$ value is −30.9‰ (S.D. = 0.95, $n=14$; Fig. 3). From the base of the Hirnantian (*extraordinarius* Biozone), $\delta^{13}C_{org}$ values become less negative, peaking at −28.2‰ at 1.72 m below the GSSP (mid-*persculptus* Biozone). From here to 0.75 m below the GSSP (upper-*persculptus* Biozone) $\delta^{13}C_{org}$ values shift to more negative values after which they become relatively constant at ~−32.5‰ (S.D. = 0.2, $n=14$).

The Re and Os abundances and $^{187}Re/^{188}Os$ and $^{187}Os/^{188}Os$ ratios are variable throughout the studied section (Re = 0.14 to 81 ppb; Os = 29 to 6393 ppt; $^{187}Re/^{188}Os = 14.23$ to 832.54 and $^{187}Os/^{188}Os = 0.551$ to 6.972, Table 1). The uncertainty in Re and Os abundance varies from varies from 0.12–6.92%, 0.22–1.98% and $^{187}Re/^{188}Os$ and $^{187}Os/^{188}Os$ varies from 0.34–6.80% and 0.12–5.99% respectively. The Os_i values range from 0.28–1.08 and have uncertainties of 0.41–1.08% (Fig. 3; Table 1).

From 7.1 to 4.85 m below the GSSP, within the *complanatus* and *anceps* Biozones, the Os_i increases from 0.37 to 1.08. From 4.85 to

Table 1
Total organic carbon, $\delta^{13}C_{org}$ and Re–Os data for the Dob's Linn Basal Silurian GSSP.

Sample	Distance from O/S GSSP (m)	TOC[a] (wt.%)	$\delta^{13}C_{org}$ (‰, V-PDB)	Re (ppb)	Os (ppt)	$^{187}Re/^{188}Os$	$^{187}Os/^{188}Os$	Os_i[b]
AF20-07	0.90	1.57	−32.70	59.33 ± 0.20	692.9 ± 2.8	728.4 ± 2.8	5.995 ± 0.013	0.598 ± 0.003
DS03-04	0.07	1.57	−32.82	58.15 ± 0.19	671.4 ± 2.8	753.0 ± 2.9	6.291 ± 0.014	0.713 ± 0.003
DS01-04	0.03	1.41	−32.17	63.20 ± 0.21	835.9 ± 3.1	607.5 ± 2.2	5.243 ± 0.009	0.744 ± 0.003
DS05-04	0.03	1.41	−32.17	50.05 ± 0.17	571.1 ± 2.6	769.8 ± 3.1	6.437 ± 0.016	0.730 ± 0.003
AF03-07	0.00	1.66	−32.60	66.27 ± 0.22	726.9 ± 3.2	831.5 ± 3.2	6.972 ± 0.016	0.812 ± 0.004
DS02-04	−0.03	1.66	−32.86	64.03 ± 0.21	701.7 ± 3.1	832.3 ± 3.2	6.972 ± 0.016	0.806 ± 0.026
AF04-07	−0.05	1.69	−32.60	66.44 ± 0.22	1043 ± 6	472.2 ± 2.1	4.259 ± 0.020	0.761 ± 0.004
AF07-07	−1.10	0.54	−30.77	19.94 ± 0.07	505.1 ± 1.8	260.1 ± 1.0	2.944 ± 0.007	1.018 ± 0.005
AF08-07	−1.51	0.91	−30.17	29.03 ± 0.10	465.3 ± 2.0	474.8 ± 1.9	4.567 ± 0.012	1.050 ± 0.005
AF32-07	−1.60	0.63	−30.08	11.71 ± 0.04	318.0 ± 1.1	230.3 ± 0.9	2.407 ± 0.006	0.702 ± 0.009
AF23-07	−1.70	0.14	−29.26	0.31 ± 0.01	89.8 ± 1.8	17.8 ± 0.8	0.729 ± 0.042	0.600 ± 0.042
AF24-07	−2.20	0.11	−29.15	0.16 ± 0.01	57.1 ± 1.1	14.2 ± 0.8	0.710 ± 0.041	0.604 ± 0.048
AF25-07	−2.40	0.15	−29.45	0.15 ± 0.01	48.1 ± 1.0	15.8 ± 0.9	0.758 ± 0.044	0.641 ± 0.052
AF26-07	−2.70	0.13	−29.92	0.27 ± 0.01	47.5 ± 0.9	29.5 ± 1.4	0.823 ± 0.048	0.605 ± 0.045
AF27-07	−3.10	0.12	−29.49	0.28 ± 0.01	37.4 ± 0.7	37.4 ± 1.8	0.685 ± 0.040	0.404 ± 0.030
AF11-07	−3.69	1.06	−31.02	6.71 ± 0.03	1349 ± 9	26.9 ± 0.2	1.047 ± 0.016	0.850 ± 0.014
AF13-07	−4.85	1.25	−30.99	81.01 ± 0.27	6393 ± 14	73.0 ± 0.3	1.625 ± 0.002	1.084 ± 0.005
AF29-07	−5.00	0.17	−29.87	8.10 ± 0.01	102.6 ± 1.2	46.8 ± 1.0	1.069 ± 0.031	0.726 ± 0.026
AF14-07	−5.22	2.18	−31.26	16.45 ± 0.06	578.0 ± 1.7	165.4 ± 0.6	1.702 ± 0.004	0.477 ± 0.002
AF15-07	−5.88	2.11	−31.59	20.25 ± 0.29	914 ± 5	126.1 ± 1.9	1.517 ± 0.010	0.583 ± 0.009
AF30-07	−5.90	0.03	−29.53	0.80 ± 0.01	44.5 ± 0.4	96.7 ± 2.1	0.983 ± 0.017	0.279 ± 0.007
AF30 rpt	–	–	–	0.80 ± 0.01	44.5 ± 0.4	96.7 ± 2.1	0.983 ± 0.017	0.280 ± 0.006
AF31-07	−7.10	0.08	−31.88	0.14 ± 0.01	29.6 ± 0.6	24.9 ± 1.7	0.551 ± 0.033	0.381 ± 0.033

Uncertainties are given as 2σ. Samples are held by Alexander Finlay.

[a] Total organic carbon.

[b] Os_i — initial $^{187}Os/^{188}Os$ composition calculated at time of deposition (443 Ma). Os_i uncertainties are calculated through full propagation of calculated $^{187}Re/^{188}Os$ and $^{187}Os/^{188}Os$ uncertainties.

3.10 m below the GSSP within the late *anceps* to early *extraordinarius* Biozones Os_i becomes less radiogenic (~0.4) and then remains constant at ~0.6 to 1.7 m below the GSSP within the *persculptus* Biozone. Between 1.7 and 1.5 m below the GSSP there is an abrupt increase to more radiogenic Os_i compositions (0.6 to 1.1; Fig. 3). From 1.6 m below to 0.9 m above the GSSP within the *persculptus* and *ascensus* Biozones Os_i values decrease to 0.60 (Fig. 3).

5. Discussion

5.1. Updated Dobs Linn $\delta^{13}C_{org}$ profile and $\delta^{13}C$ throughout the Hirnantian Glaciation

The new $\delta^{13}C_{org}$ profile for Dob's Linn shows the same general trend as other global late Ordovician/early Silurian profiles (Quebec, Long, 1993; South China, Wang et al., 1997; Yan et al., 2009; Fan et al., 2009; Nevada, Finney et al., 1999; Estonia/Latvia, Brenchley et al., 2003; Kaljo et al., 2004; Arctic Canada, Melchin and Holmden, 2006; North America and China, Young et al., 2008; Figs. 2 and 3). During this interval the $\delta^{13}C_{org}$ values change from being very similar throughout the Katian to becoming less negative values from the base of the Hirnantian until the mid-late Hirnantian *persculptus* Biozone. At this point the $\delta^{13}C_{org}$ becomes abruptly more negative and return to values similar to those prior to the excursion over ~1 m. This $\delta^{13}C_{org}$ profile is known as HICE (Bergstrom et al., 2008).

The HICE is proposed to have been triggered by the increased weathering of silicate terrains during the Caledonian Orogeny, which resulted in the drawdown of atmospheric CO_2 (Kump et al., 1999). This reduction in greenhouse gas drove global cooling that resulted in a glaciation and marine regression during the Hirnantian. The marine regression caused significant areas of shallow marine carbonate to be exposed to weathering, increasing the flux of ^{13}C into the oceans. At Dob's Linn this event occurs in the *extraordinarius* and early–mid *persculptus* Biozones, 3.69 to 1.72 m below the GSSP, where $\delta^{13}C_{org}$ values become less negative peaking at −28.2‰. As global temperatures fell the chemical weathering rates decreased reducing silicate weathering and associated atmospheric CO_2 drawdown. In response atmospheric CO_2 levels increased back to pre glaciation greenhouse levels. This drove rapid deglaciation and a marine transgression, which flooded previously exposed carbonates, thus limiting the flux of ^{13}C to the oceans.

5.2. Re–Os systematics in the Dob's Linn section

Although not collected specifically for Re–Os geochronology, samples spanning the GSSP (DS03-04, DS01-04, DS05-04, AF03-07, DS02-04 and AF04-07) possess similar Os_i (0.71–0.81; Table 1; Fig. 3) when calculated at the age of the Ordovician/Silurian boundary (443 Ma; Ogg et al., 2008). These samples, similar to the majority of samples from organic-rich black shale horizons from the Dobs Linn stratigraphy, are enriched in Re and Os (6.71 to 81.01 ppb Re, 317.96 to 6393.04 ppt Os; Table 1). The Re–Os data for samples DS03-04, DS01-04, DS05-04, AF03-07, DS02-04 and AF04-07 yield a Re–Os age (449 ± 22 Ma, MSWD = 15, *Isoplot* v.3 Model 3, Ludwig, 2003, Fig. 4a). This Re–Os age is within uncertainty of the determined GSSP age given by U–Pb zircon geochronology (443 ± 1.5 Ma; Ogg et al., 2008). Given the positive correlation of $^{187}Re/^{188}Os$ with $^{187}Os/^{188}Os$ and the agreement of the determined Re–Os age with the known age of the stratigraphic interval, we are confident that our Re–Os analyses reflect the hydrogenous Re–Os load and that the Re–Os systematics have not been significantly affected by weathering or Silurian lower greenschist metamorphism (Oliver and Leggett, 1980). This conclusion is consistent with previous studies (e.g. Peucker-Ehrenbrink and Hannigan, 2000; Jaffe et al., 2002; Kendall et al., 2004; Kendall et al., 2009a,b). As a result we infer the Os_i values to record that of Iapetus Ocean contemporaneous with sediment deposition.

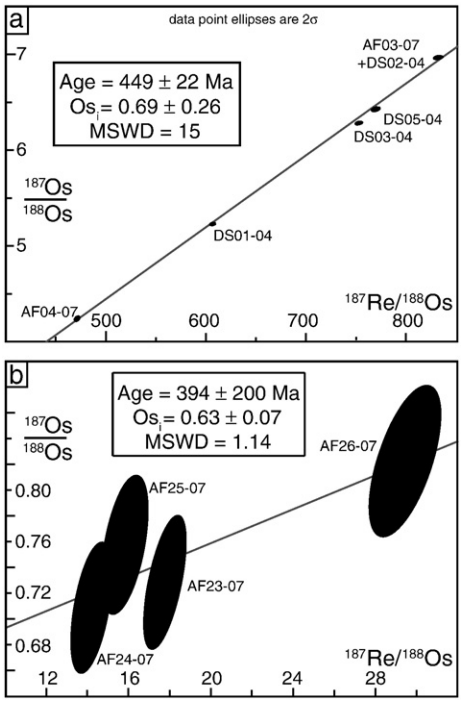

Fig. 4. Re–Os isochrons for the Linn Branch section. a — area surrounding the GSSP, b — area spanning Hirnantian glaciation. Uncertainty ellipses are at the 2σ level. See text for discussion.

In contrast to the organic-rich black shales of the Dobs Linn stratigraphy, grey shales from the Upper Hartfell Shale are less enriched in Re and Os (0.14 to 0.89 ppb Re; 29.58 to 102.64 ppt Os; Table 1). These samples have similar Re and Os abundances to the average upper continental crust (Esser and Turekian, 1993; Peucker-Ehrenbrink and Jahn, 2001; Sun et al., 2003). As a result, a minor contribution of detritus with average upper continental radiogenic $^{187}Os/^{188}Os$ composition (~1.4) during the whole rock digestion process could modify the hydrogenous $^{187}Os/^{188}Os$ composition of the grey shale. However, we consider our Os_i grey shale data to record the hydrogenous $^{187}Os/^{188}Os$ composition as explained below.

Firstly, four grey shale samples (AF23-07, AF24-07, AF25-07 and AF26-07) with similar Os_i (0.6–0.64; Table 1) show a positive correlation of $^{187}Re/^{188}Os$ and $^{187}Os/^{188}Os$ values. The Re–Os age derived from the Re–Os data is imprecise (394 ± 200 Ma) because of the limited spread in the Re–Os data (~15 $^{187}Re/^{188}Os$ units; ~0.11 $^{187}Os/^{188}Os$ units; Table 1; Fig. 4b). However, the nominal agreement of the Re–Os age to the known age of the Dobs Linn section, suggests that the grey shale Re–Os data predominantly reflect the hydrogenous Re–Os load.

It is beyond the scope of this research to identify every source of sediment shedding into the Iapetus Ocean during the Late Ordovician. However, we suggest that the majority of the detritus entering into the Iapetus Ocean was predominantly from radiogenic continental crust from the Laurentian, Avalonia–Baltican and Siberian cratons, with only minor mafic inputs (Wilde et al., 1986; McCaffrey and Kneller, 1996; Oliver et al., 2000; Cocks and Torsvik, 2006). Thus, any detrital Re and Os contribution to the grey shales should result in radiogenic Os_i compositions. In contrast, we observe significantly less radiogenic Os_i compositions (0.4 to 0.64; Fig. 3; Table 1). To generate non hydrogenous Os_i compositions of 0.4 and 0.6 would require detrital input from less radiogenic material (e.g., ultramafic/mafic or cosmic components), however there is no evidence for a major increase in sourcing of unradiogenic material during the Hirnantian (Wilde et al., 1986; Oliver et al., 2000; Shields et al., 2003).

The Os_i of samples AF23-07 and AF32-07 (1.7 and 1.6 m below the GSSP), which border the stratigraphic interval between the Upper Hartfell shale and Lower Birkhill are similar (0.6 and 0.7, respectively). Despite similar Os_i for samples AF23-07 and AF32-07 they contain significantly different Re and Os abundances (0.31 and 11.71 ppb Re; 89.81 and 317.96 ppt Os; Table 1). This suggests that the Re–Os grey shale data reflects predominantly the hydrogenous Re and Os load and by inference the Os_i is that of Iapetus Ocean at the time of sediment deposition.

Across the Eocene–Oligocene transition (including the first Oligocene glaciation), oxic organic-poor sediments (TOC not given; DSDP site 522; Angola basin; Ravizza and Peucker-Ehrenbrink, 2003) are shown to yield the same hydrogenous Os_i trends as sub-oxic organic-rich (TOC = ~0.5 to 4%) sediments from the same correlative stratigraphic interval (ODP site 959; eastern equatorial Atlantic; Ravizza and Paquay, 2008). The organic-poor sediments contain similar Re and Os abundances to the grey shales of Dob's Linn (6 to 256 ppt; Ravizza and Peucker-Ehrenbrink, 2003; Dalai et al., 2006; Oxburgh et al., 2007). Also, similar to the Dob's Linn grey shales, the Cenozoic sediments predominantly comprise a matrix that does not host hydrogenous Re and Os (e.g. carbonates and silicates). The hydrogenous Re and Os is complexed by organic matter (Selby and Creaser, 2003). From this we can suggest that the Re and Os contents for both Dob's Linn and the Cenozoic sediments are similar and do not reflect detrital contamination. Given the above discussion we consider the Os_i data for the grey shales at Dobs Linn to record the hydrogenous Os_i signal of the contemporaneous Iapetus Ocean.

5.3. Tracking the Hirnantian glaciation using initial $^{187}Os/^{188}Os$ (Os_i)

Throughout the *complanatus* and *anceps* Biozones, from 7.1 to 4.85 m below the GSSP, Os_i compositions become more radiogenic increasing from ~0.37 to 1.08. The Os_i abruptly increase (0.48 to 1.08) over a short time interval (<40 cms of the *anceps* Biozone, 5.22 to 4.85 m below the GSSP; Fig. 3). The most radiogenic Os_i (1.08) is typically more radiogenic than the $^{187}Os/^{188}Os$ for seawater for the entire Phanerozoic, until the last 2 Myrs, and is comparable to present day sea water (~1.06; Peucker-Ehrenbrink and Ravizza, 2000 and references there in; Selby and Creaser, 2003; Ravizza and Peucker-Ehrenbrink, 2003; Widom et al., 2004; Williams and Turekian, 2004; Dalai et al., 2005; Dalai et al., 2006; Poirier, 2006; Burton, 2006; Turgeon et al., 2007; Ravizza, 2007; Selby, 2007; Oxburgh et al., 2007; Turgeon and Creaser, 2008; Selby et al., 2009). Within the same stratigraphic interval (7.1 to 4.85 m below the GSSP) the $\delta^{13}C_{org}$ shows only a minor (~0.5‰ increase to heavier values; Fig. 3).

The increasingly radiogenic Os_i across the late Katian suggest that the Os influx to the Iapetus Ocean became dominated by a radiogenic crustal component. This is supported by observed concordant increasingly radiogenic $^{87}Sr/^{86}Sr$ compositions (Shields et al., 2003). Throughout the Early and Middle Ordovician seawater $^{87}Sr/^{86}Sr$ decreased (0.7090 to 0.7088) with a sudden decrease across the Middle to Late Ordovician (Late Darwillian, Sandbian and Early Katian) to 0.7078. From this point to near the End Ordovician $^{87}Sr/^{86}Sr$ remains stable at ~0.7078 before becoming more radiogenic throughout the Silurian (Shields et al., 2003). The Ordovician unradiogenic $^{87}Sr/^{86}Sr$ values are attributed to low continental erosion rates and an increased submarine hydrothermal exchange rate (Shields et al., 2003). The change to radiogenic $^{87}Sr/^{86}Sr$ is coincident with the increasingly radiogenic Os_i values (~0.3 to ~0.6). The source of Os to the global ocean is similar to Sr, suggesting that the Iapetus Ocean became increasingly dominated by a radiogenic crustal component from the Katian. Thus, we consider the predominant detritus shed into the Iapetus Ocean to be from the radiogenic Laurentian, Avalonia–Baltican and Siberian cratons, with only minor mafic inputs (Wilde et al., 1986; McCaffrey and Kneller, 1996; Oliver et al., 2000; Cocks and Torsvik, 2006). We suggest that the significant increase in Os_i relates to increased silicate weathering of the Caledonian Orogen.

From the peak of Os_i (1.08) at 4.85 m below the GSSP, Os_i compositions become abruptly less radiogenic within the *extraordinarius* Biozone (0.85; 3.69 m below the GSSP and 0.4, 3.1 m below the GSSP), and then remain stable (~0.6) until 1.70 m below the GSSP in the *persculptus* Biozone. This stratigraphic interval coincides with the positive, glacial, limb of the $\delta^{13}C_{org}$ excursion ($\delta^{13}C_{org} = -31.3$ to -28.2‰; Fig. 3). Between 1.7 and 1.51 m below the GSSP there is a very abrupt increase to more radiogenic Os_i compositions (0.6 to 1.05), which coincides with the negative, deglacial limb of the $\delta^{13}C_{org}$ excursion. From 1.6 m below the GSSP to the top of the studied section within the *persculptus* and *ascensus* Biozones Os_i values decrease to ~0.6.

Given the radiogenic $^{187}Os/^{188}Os$ input into the Iapetus Ocean from the Laurentian, Avalonia–Baltican and Siberian Cratons, unradiogenic Os_i (0.4 to 0.64) would not be expected during the *persculptus* Biozone, as observed here (Fig. 3). To generate Os_i compositions of 0.4 and 0.6 would require detrital input from less radiogenic material (e.g., ultramafic/mafic or cosmic components), however there is no evidence for a major increase in sourcing of unradiogenic material during the Hirnantian (Wilde et al., 1986; Oliver et al., 2000; Shields et al., 2003).

The decrease in Os_i coincides with the ~4‰ increase to heavier $\delta^{13}C_{org}$ values during the same interval that globally marks the onset of the Hirnantian glaciation. This shift in $\delta^{13}C_{org}$ is attributed to the flux of ^{13}C into the oceans from the weathering of exposed marine carbonates as a result of sea level fall (Kump et al., 1999; Melchin and Holmden, 2006; LaPorte et al., 2009). The less radiogenic Os_i compositions recorded during the glacial period are likely to have been caused by a decrease in chemical weathering rates, caused by a reduction in global temperatures coupled with glacial ice cover that diminished the flux of radiogenic $^{187}Os/^{188}Os$ material into both the Iapetus and global oceans (Trotter et al., 2008). Intriguingly the Os_i during the glacial maximum (~0.6) are higher than at the start of the section (~0.3). We attribute this to the weathering of radiogenic marine sediments exposed during glacial low stand.

The observed Os_i trend at Dobs Linn is similar to that associated with Cenozoic glacial periods and is related to a marine regression causing the exposure and weathering of young, unradiogenic, continental shelf material (Williams and Turekian, 2004). An increased flux of unradiogenic $^{187}Os/^{188}Os$ will cause the seawater $^{187}Os/^{188}Os$ to decrease during glacial periods, as observed at Dob's Linn (Fig. 3). Given the short residence time of Os in the ocean (5–50 kyrs; Oxburgh et al., 2007), we interpret the change in the Os_i at Dob's Linn to capture the time when the Hirnantian glaciation and deglaciation caused drastic changes in continental weathering. Global cooling and the onset of the Hirnantian Glaciation are proposed to be caused by the drawdown of atmospheric CO_2 driven by a period of high silicate weathering (Kump et al., 1999). This hypothesis is supported by the trend towards more radiogenic Os_i (0.37 to 1.08) during the Katian (7.1 to 4.85 m below the GSSP; Fig.3), indicating that increased silicate weathering was the driving process for the onset of the Hirnantian glaciation.

The rapid increase to radiogenic Os_i (0.6 to 1.05 over 19 cm) during the mid *persculptus* Biozone occurs at the correlative stratigraphic interval, in addition to the $\delta^{13}C_{org}$ deglacial limb, as field evidence for deglaciation in North Africa (Le Heron et al., 2008). Post-glacial erosion of glacial deposits provides an easily leachable source of radiogenic Os into the oceans (Peucker-Ehrenbrink and Blum, 1998). Consequently, erosion of glacial deposits, combined with an increase in chemical weathering rates, rapidly increases the flux of radiogenic Os into the Iapetus and Rheic Oceans as reflected in the rapid shift to radiogenic Os_i compositions seen at Dob's Linn. The Hirnantian spans 1.9 Ma and covers ~3.75 m of stratigraphy at Dob's Linn. If a constant rate of sedimentation across the Hirnantian is assumed the compacted

sedimentation rate is 2 m/Ma. Therefore, the rapid increase in $^{187}Os/^{188}Os$ (over 19 cms) spans 95 ka across the deglacial period. However, the sedimentation rate across the Hirnantian was not constant, minor deposition occurred during the glacial maximum and maximum deposition occurring with the deglaciation. Therefore the 19 cm of stratigraphy which covers the deglacial period likely has a duration <95 ka.

5.4. Comparing the Hirnantian glacial Os_i profile with Cenozoic glaciations

Osmium isotope analysis of global Eocene/Oligocene and Pleistocene sediments show a correlation between $^{187}Os/^{188}Os$ compositions and glacial/interglacial climatic conditions (Ravizza et al., 2001; Ravizza and Peucker-Ehrenbrink, 2003; Williams and Turekian, 2004; Dalai et al., 2006; Oxburgh et al, 2007). These correlations highlight radiogenic values occurring during interglacial periods and less radiogenic values occurring during glacial periods. The changes seen in the Os_i compositions during the Hirnantian glaciation (~0.6 to 1.1) are greater than that observed in the Pleistocene glacial/interglacial periods (~0.94 to 1.04; Williams and Turekian, 2004). This difference relates to the climatic and geographic conditions of the glacial and interglacial cycles of the Hirnantian and Pleistocene.

Although the Hirnantian glaciation was smaller in area than the Pleistocene (30,000,000 km^2 as opposed to 44,000,000 km^2; Sheehan, 2001) it was centred near the South Pole and thus covered a large proportion of the Gondwanan craton and little of the global ocean (Le Heron et al., 2008). In contrast, the Pleistocene glacial maximums covered large areas of open ocean as well as the Canadian and Fennoscandinavian craton. However, significant areas of Archean cratons with highly evolved radiogenic signatures remained exposed e.g. Australasian, South American, African and Indian (Mercer, 1983; Clark and Mix, 2002; Pearson and Wittig, 2008). From this tectonic setting/scenario the extensive cratonic glacial cover during the Hirnantian would have reduced the radiogenic $^{187}Os/^{188}Os$ flux into the oceans. Furthermore, sea level fall resulting from the Hirnantian glaciation is estimated to be <100 m compared to 100–150 m for the Pleistocene glacial maximum (Sheehan, 2001; Brenchley et al., 2003; Williams and Turekian, 2004). Thus, Hirnantian glaciation lead to less exposure and reworking of radiogenic anoxic deep marine ORS (e.g. black shales) than the Pleistocene.

Finally, CO_2 levels at ~440 Ma were ~14 times higher than present (Berner, 2006). This indicates, with oxygen isotopes (Trotter et al., 2008), that global temperatures and therefore chemical weathering rates were higher during the late Ordovician than in the Pleistocene. Therefore, the reduction in chemical weathering rates as a result of the Hirnantian icehouse would have been greater than during the Pleistocene, further decreasing the input of radiogenic Os to the Iapetus Ocean. This has been observed during the Toarcian OAE where a similar magnitude Os_i shift of ~0.6 is attributed to an increase in chemical weathering rates caused by a rise in temperature of ~10 °C (Cohen et al., 2004; Waltham and Gröcke, 2006). This temperature rise is identical to that determined during the Hirnantian glaciation (Trotter et al., 2008).

6. Conclusions

Through the integration of Os_i and $\delta^{13}C_{org}$ profiles at Dob's Linn it has proved possible to track the onset and cessation of the Hirnantian glaciation (Fig. 3). We interpret the Os_i stratigraphy at Dob's Linn to record the evolution in seawater Os isotopic composition of the Iapetus Ocean. However, given that this seaway was connected to the global ocean it may also reflect that of global seawater. The changes in climate that force the trends in the profile described for Dob's Linn are global and therefore will have the same effect on both Iapetus and the global oceans. Thus, we hypothesise that although absolute data may vary between Iapetus and other global Ordovician/Silurian oceans (e.g. Rheic) the trends in the profile will be similar.

Throughout the Katian, Os_i becomes increasingly radiogenic, as a result of increased silicate weathering of radiogenic orogenic material associated with the Caledonian Orogen. As a result of atmospheric CO_2 drawdown, global cooling ensued, causing the onset of the Hirnantian Glaciation. Reduced chemical weathering rates and growth of continental ice cover significantly reduced the input of radiogenic Os into the oceans. Increased ice volume resulted in falling sea levels, thus exposing marine carbonates and unradiogenic shelf to weathering. These new weathering regimes lead to an increased flux of ^{13}C and unradiogenic Os into the oceans. As a direct result of the decrease in silicate weathering during the Hirnantian, atmospheric CO_2 returned to greenhouse levels, causing rapid deglaciation during the Late Hirnantian mid *persculptus* Biozone. This de-glacial period is recorded by a dramatic rise in Os_i (0.6–1.05) over 19 cm of stratigraphy at Dob's Linn. We interpret this dramatic rise to be a consequence of the leaching of radiogenic $^{187}Os/^{188}Os$ from glacial deposits and increased weathering of radiogenic $^{187}Os/^{188}Os$ silicate terrane.

The results of this study further highlight the use of Os_i as a powerful tool for understanding the Earth climate system and, in particular, aid in monitoring changes in weathering and its affect on palaeoceanography (e.g. Cohen et al., 1999; Ravizza and Peucker-Ehrenbrink, 2003; Cohen et al., 2004; Oxburgh et al., 2007; Ravizza and Paquay, 2008). In addition, the short residence time of Os (5–50 kyrs) in comparison to Sr (1–4 Ma) allows for a greater resolution for enhancing our understanding of palaeoenvironmental processes (cf. Cohen et al., 1999; Peucker-Ehrenbrink and Ravizza, 2000; Turgeon and Creaser, 2008; Selby et al., 2009; this study). For example, diachronous Neoproterozoic Sturtian deglacial sediments have been shown to have highly radiogenic Os_i (0.82–1.00; Kendall et al., 2006, 2009a,b). These values are remarkably similar to that reported here for the Hirnantian deglaciation. Thus, suggesting an increased continental weathering rate associated with deglaciation. However, we have no known values of seawater Os_i for pre/syn Neoproterozoic Sturtian glaciation. Therefore, Os_i data could provide increased understanding of weathering rates associated with Neoproterozoic global glaciations.

Acknowledgements

We wish to thank Tom Challands for the invaluable help in sample collection and associated fieldwork. Also, we wish to thank Mike Melchin, Howard Armstrong, Bernard Peucker-Ehrenbrink, Greg Ravizza and an EPSL anonymous reviewer for their insightful comments on the manuscript. This work was made possible through a NERC/BP Case studentship and permission from Scottish National Heritage for sample collection at Dob's Linn. Bill Patterson at the Saskatchewan Isotope Lab provided assistance with isotopic measurements.

References

Armstrong, H.A., Coe, A.L., 1997. Deep-sea sediments record the geophysiology of the late Ordovician glaciation. J. Geol. Soc. (Lond.) 154, 929–934.
Armstrong, H.A., Owen, A.W., 2002. Euconodont paleobiogeography and the closure of the Iapetus Ocean. Geology 30, 1091–1094.
Batchelor, R.A., Weir, J.A., 1988. Metabentonite geochemistry: magmatic cycles and graptolite extinctions at Dob's Linn, southern Scotland. Trans. R. Soc. Edinburgh 79, 19–41.
Bergstrom, S.M., Chen, X., Gutierrez-Marco, J.C., Dronov, A., 2008. The new Chronostratigraphic classification of the Ordovician System and its relations to major regional series and stages and to $\delta^{13}C$ chemostratigraphy. Lethaia 42, 97–107.
Berner, R.A., 2006. GEOCARBSULF: a combined model for Phanerozoic atmospheric O2 and CO2. Geochim. Cosmochim. Acta 70, 5653–5664.
Brenchley, P.J., Marshall, J.D., Underwood, C.J., 2001. Do all mass extinctions represent an ecological crisis? Evidence from the Late Ordovician. Geol. J. 36, 329–340.
Brenchley, P.J., Carden, G.A., Hints, L., Kaljo, D., Marshall, J.D., Martma, T., Meidla, T., Nolvak, J., 2003. High-resolution stable isotope stratigraphy of Upper Ordovician

sequences: constraints on the timing of bioevents and environmental changes associated with mass extinction and glaciation. Geol. Soc. Am. Bull. 115, 89–104.
Burton, K.W., 2006. Global weathering variations inferred from marine radiogenic isotope records. J. Geochem. Explor. 88, 262–265.
Cameron, T.D.J., Anderson, T.B., 2007. Silurian metabentonites in County Down, Northern Ireland. Geol. J. 15, 59–75.
Clark, P.U., Mix, A.C., 2002. Ice sheets and sea level of the last glacial maximum. Quat. Sci. Rev. 21, 1–7.
Cocks, L.R.M., 1985. The Ordovician–Silurian boundary. Episodes 8, 98–100.
Cocks, L.R.M., Torsvik, T.H., 2006. European geography in a global context from the Vendian to the end of the Palaeozoic. Geol. Soc. (Lon) Mem. 32, 83–95.
Cohen, A.S., Coe, A.L., Bartlett, J.M., Hawkesworth, C.J., 1999. Precise Re–Os ages of organic-rich mudrocks and the Os isotope composition of Jurassic seawater. Earth Planet. Sci. Lett. 167, 159–173.
Cohen, A.S., Coe, A.L., Harding, S.M., Schwark, L., 2004. Osmium isotope evidence for the regulation of atmospheric CO_2 by continental weathering. Geology 32, 157–160.
Coplen, T.B., Brand, W.A., Gehre, M., Groning, M., Meijer, H.A.J., Toman, B., Verkouteren, R.M., 2006. New guidelines for $\delta^{13}C$ measurements. Anal. Chem. 78, 2439–2441.
Craig, H., 1957. Isotopic standards for carbon and oxygen and correction factors for mass-spectrometric analysis of carbon dioxide. Geochim. Cosmochim. Acta 12, 133–149.
Creaser, R.A., Papanastassiou, D.A., Wasserburg, G.J., 1991. Negative thermal ion mass-spectrometry of osmium, rhenium, and iridium. Geochim. Cosmochim. Acta 55, 397–401.
Dalai, T.K., Suzuki, K., Minagawa, M., Nozaki, Y., 2005. Variations in seawater osmium isotope composition since the last glacial maximum: a case study from the Japan Sea. Chem. Geol. 220, 303–314.
Dalai, T.K., Ravizza, G.E., Peucker-Ehrenbrink, B., 2006. The Late Eocene $^{187}Os/^{188}Os$ excursion: chemostratigraphy, cosmic dust flux and the Early Oligocene glaciation. Earth Planet. Sci. Lett. 241, 477–492.
Esser, B.K., Turekian, K.K., 1993. Anthropogenic osmium in coastal deposits. Environ. Sci. Technol. 27, 2719–2724.
Fan, J., Peng, P., Melchin, M.J., 2009. Carbon isotopes and event stratigraphy near the Ordovician–Silurian boundary, Yichang, South China. Palaeogeogr. Palaeoclimatol. Palaeoecol. 276, 160–169.
Finney, S.C., Berry, W.B.N., Cooper, J.D., Ripperdan, R.L., Sweet, W.C., Jacobson, S.R., Soufiane, A., Achab, A., Noble, P.J., 1999. Late Ordovician mass extinction: a new perspective from stratigraphic sections in central Nevada. Geology 27, 215–218.
Finney, S.C., Berry, W.B.N., Cooper, J.D., 2007. The influence of denitrifying seawater on graptolite extinction and diversification during the Hirnantian (latest Ordovician) mass extinction event. Lethaia 40, 281–291.
Gramlich, J.W., Murphy, T.J., Garner, E.L., Shields, W.R., 1973. Absolute isotopic abundance ratio and atomic weight of a reference sample of rhenium. J. Res. Nat. Bur. Stand. 77, 691–698.
Huff, W.D., Whiteman, J.A., Curtis, C.D., 1988. Investigation of a K-bentonite by X-ray powder diffraction and analytical transmission electron microscopy. Clays Clay Miner. 36, 83–93.
Huff, W.D., Anderson, T.B., Rundle, C.C., Odin, G.S., 1991. Chemostratigraphy, K–Ar ages and illitization of Silurian K-bentonites from the Central Belt of the Southern Uplands-Down-Longford Terrane, British Isles. J. Geol. Soc. (Lond) 148, 861–868.
Jaffe, L.A., Peucker-Ehrenbrink, B., Petsch, S.T., 2002. Mobility of rhenium, platinum group elements and organic carbon during black shale weathering. Earth Planet. Sci. Lett. 198, 339–353.
Kaljo, D., Hints, L., Martma, T., Nolvak, J., Oraspold, A., 2004. Late Ordovician carbon isotope trend in Estonia, its significance in stratigraphy and environmental analysis. Palaeogeogr. Palaeoclimatol. Palaeoecol. 210, 165–185.
Kendall, B.S., Creaser, R.A., Ross, G.M., Selby, D.S., 2004. Constraints on the timing of Marinoan "Snowball Earth" glaciation by $^{187}Re–^{187}Os$ dating of a Neoproterozoic, post-glacial black shale in Western Canada. Earth Planet. Sci. Lett. 222, 729–740.
Kendall, B.S., Creaser, R.A., Selby, D.S., 2006. Re–Os geochronology of postglacial black shales in Australia: constraints on the timing of "Sturtian" glaciation. Geology 34, 729–732.
Kendall, B.S., Creaser, R.A., Calver, C.R., Raub, T.D., Evans, A.D., 2009a. Correlation of Sturtian diamictite successions in southern Australia and northwestern Tasmania by Re–Os black shale geochronology and the ambiguity of "Sturtian"-type diamictite-cap carbonate pairs as chronostratigraphic marker horizons. Precambrian Res. 172, 301–310.
Kendall, B.S., Creaser, R.A., Selby, D., 2009b. $^{187}Re–^{187}Os$ geochronology of Precambrian organic-rich sedimentary rocks. Geol. Soc. (Lond). Spec. Publ. 326, 85–107.
Kump, L.R., Arthur, M.A., Patzkowsky, M.E., Gibbs, M.T., Pinkus, D.S., Sheehan, P.M., 1999. A weathering hypothesis for glaciation at high atmospheric pCO_2 during the Late-Ordovician. Palaeogeogr. Palaeoclimatol. Palaeoecol. 152, 173–187.
LaPorte, D.F., Holmden, C., Patterson, W.P., Loxton, J.D., Melchin, M.J., Mitchell, C.E., Finney, S.C., Sheets, H.D., 2009. Local and global perspectives on carbon and nitrogen cycling during the Hirnantian glaciation. Palaeogeogr. Palaeoclimatol. Palaeoecol. 276. 1–4, 182–195.
Lapworth, C., 1878. The Moffat series. Q. J. Geol. Soc. 34, 240–346.
Le Heron, D.P., Khoukhi, Y., Paris, F., Ghienne, J.F., Le Herisse, A., 2008. Black shale, grey shale, fossils and glaciers: Anatomy of the Upper Ordovician–Silurian succession in the Tazzeka Massif of eastern Morocco. Gondwana Res. 14, 483–496.
Long, D.G.F., 1993. Oxygen and carbon isotopes and event stratigraphy near the Ordovician–Silurian boundary, Anticosti Island Quebec. Palaeogeogr. Palaeoclimatol. Palaeoecol. 104, 49–59.
Ludwig, K.R., 2003. ISOPLOT: A Plotting and Regression Program for Radiogenic-Isotope Data, version 3.
McCaffrey, W.D., Kneller, B.C., 1996. Silurian turbidite provenance on the north Avalonian margin. J. Geol. Soc. (Lond) 153, 437–450.
Melchin, M.J., Holmden, C., 2006. Carbon isotope chemostratigraphy in Arctic Canada: sea-level forcing of carbonate platform weathering and implications for Hirnantian global correlation. Palaeogeogr. Palaeoclimatol. Palaeoecol. 234, 186–200.
Melchin, M.J., Holmden, C., Williams, S.H., 2003. In: Albanesi, G.L., Beresi, M.S., Peralta, S. H. (Eds.), Ordovician from the Andes – Proceedings of the 9th International Symposium on the Ordovician System: INSUGEO, Serie Correlación Geológica, 17, pp. 101–104.
Mercer, J.H., 1983. Cenozoic glaciation in the southern hemisphere. Annu. Rev. Earth Planet Sci. 11, 99–132.
Merriman, R.J., Roberts, B., 1990. Metabentonites in the Moffat Shale Group, Southern Uplands of Scotland — geochemical evidence of ensialic marginal basin volcanism. Geol. Mag. 127, 259–271.
Ogg, J.G., Ogg, G., Gradstein, F.M., 2008. The Concise Geologic Time Scale. Cambridge University Press.
Oliver, G.J.H., Leggett, J.K., 1980. Metamorphism in an accretionary prism: prehnite–pumpellyite facies metamorphism of the Southern Uplands of Scotland. Trans. R. Soc. Edinburgh Earth Sci. 71, 235–246.
Oliver, G.J.H., Chen, F., Buchwaldt, R., Hegner, E., 2000. Fast tectonometamorphism and exhumation in the type area of the Barrovian and Buchan zones. Geology 28, 459–462.
Oxburgh, R., Pierson-Wickmann, A.C., Reisberg, L., Hemming, S., 2007. Climate-correlated variations in seawater 187Os/188Os over the past 200,000 yr: evidence from the Cariaco Basin, Venezuela. Earth Planet. Sci. Lett. 263, 246–258.
Pearson, D.G., Wittig, N., 2008. Formation of Archaean continental lithosphere and its diamonds: the root of the problem. J. Geol. Soc. (Lond) 165, 895–914.
Pegram, W.J., Krishnaswami, S., Ravizza, G.E., Turekian, K.K., 1992. The record of sea water $^{187}Os/^{186}Os$ variation through the Cenozoic. Earth Planet. Sci. Lett. 113, 569–576.
Peucker-Ehrenbrink, B., Blum, J.D., 1998. Re – Os isotope systematics and weathering of Precambrian crustal rocks: implications for the marine osmium record. Geochim. Cosmochim. Acta 62, 3193–3203.
Peucker-Ehrenbrink, B., Hannigan, R.E., 2000. Effects of black shale weathering on the mobility of rhenium and platinum group elements. Geology 28, 475–478.
Peucker-Ehrenbrink, B., Jahn, B., 2001. Rhenium–osmium isotope systematics and platinum group element concentrations: loess and the upper continental crust. Geochem. Geophys. Geosyst. 2, 1061.
Peucker-Ehrenbrink, B., Ravizza, G., 2000. The marine osmium isotope record. Terra Nova 12, 205–219.
Poirier, A., 2006. Re–Os and Pb isotope systematics in reduced fjord sediments from Saanich Inlet (Western Canada). Earth Planet. Sci. Lett. 249, 119–131.
Ravizza, G., 2007. Reconstructing the $^{187}Os/^{188}Os$ record and the particulate flux of meteoric osmium during the late Cretaceous. Geochim. Cosmochim. Acta 71, 1355–1369.
Ravizza, G., Paquay, F., 2008. Osi isotope chemostratigraphy applied to organic-rich marine sediments from the Eocene–Oligocene transition on the West African margin (ODP Site 959). Paleoceanography 23, PA2204.
Ravizza, G., Peucker-Ehrenbrink, B., 2003. The marine ^{187} $Os/^{188}Os$ record of the Eocene–Oligocene transition: the interplay of weathering and glaciation. Earth Planet. Sci. Lett. 210, 151–165.
Ravizza, G., Turekian, K.K., 1989. Application of the $^{187}Re–^{187}Os$ system to black shale geochronometry. Geochim. Cosmochim. Acta 53, 3257–3262.
Ravizza, G., Norris, R.N., Blusztajn, J., Aubry, M.-P., 2001. An osmium isotope excursion associated with the late Paleocene thermal maximum: evidence of intensified chemical weathering. Paleoceanography 16, 155–163.
Rong, Jia-yu, Boucot, A.J., Harper, D.A.T., Ren-bin, Zhan, Neuman, R.B., 2006. Global analyses of brachiopod faunas through the Ordovician and Silurian transition: reducing the role of the Lazarus effect. Can. J. Earth Sci. 43, 23–39.
Selby, D., 2007. Direct Rhenium–Osmium age of the Oxfordian–Kimmeridgian boundary, Staffin bay, Isle of Skye, U.K., and the Late Jurassic time scale. Norw. J. Geol. 87, 291–299.
Selby, D., Creaser, R.A., 2003. Re–Os geochronology of organic rich sediments: an evaluation of organic matter analysis methods. Chem. Geol. 200, 225–240.
Selby, D., Mutterlose, J., Condon, D.J., 2009. U–Pb and Re–Os geochronology of the Aptian/Albian and Cenomanian/Turonian stage boundaries: implications for timescale calibration, osmium isotope seawater composition and Re–Os systematics in organic-rich sediments. Chem. Geol. 265, 394–409.
Sheehan, P.M., 2001. The Late Ordovician mass extinction. Annu. Rev. Earth Planet. Sci. 29, 331–364.
Shields, G.A., Carden, G.A.F., Veizer, J., Meidla, T., Rong, J.Y., Li, R.Y., 2003. Sr, C, and O isotope geochemistry of Ordovician brachiopods: a major isotopic event around the Middle-Late Ordovician transition. Geochim. Cosmochim. Acta 67, 2005–2025.
Smoliar, M.I., Walker, R.J., Morgan, J.W., 1996. Re–Os ages of group IIA, IIIA, IVA, and IVB iron meteorites. Science 23, 1099–1102.
Sun, W., Bennett, V.C., Eggins, S.M., Kamenetsky, V.S., Arculus, R.J., 2003. Enhanced mantle-to-crust rhenium transfer in undegassed arc magmas. Nature 422, 294–297.
Trewin, N.H., Rollin, K.E., 2002. Geological history and structure of Scotland. In: Trewin, N.H. (Ed.), The Geology of Scotland. The Geological Society, London, pp. 1–25.
Trotter, J.A., Williams, I.S., Barnes, C.R., Lecuyer, C., Nicoll, R.S., 2008. Did cooling oceans trigger Ordovician biodiversification? Evidence from conodont thermometry. Science 321, 550–554.
Tucker, R.D., Krogh, T.E., Ross Jr., R.J., Williams, S.H., 1990. Time-scale calibration by high-precision U–Pb zircon dating of interstratified volcanic ashes in the Ordovician and Lower Silurian stratotypes of Britain. Earth Planet. Sci. Lett. 100, 51–58.
Turgeon, S.C., Creaser, R.A., 2008. Cretaceous oceanic anoxic event 2 triggered by a massive magmatic episode. Nature 454, 323–326.

Turgeon, S.C., Creaser, R.A., Algeo, T.J., 2007. Re–Os depositional ages and seawater Os estimates for the Frasnian–Famennian boundary: implications for weathering rates, land plant evolution, and extinction mechanisms. Earth Planet. Sci. Lett. 261, 649–661.

Underwood, C.J., Crowley, S.F., Marshall, J.D., Brenchley, P.J., 1997. High-resolution carbon isotope stratigraphy of the basal Silurian stratotype (Dob's Linn, Scotland) and its global correlation. J. Geol. Soc. (Lond) 154, 709–718.

Verniers, J., Vandenbroucke, T.R.A., 2006. Chitinozoan biostratigraphy in the Dob's Linn Ordovician–Silurian GSSP, Southern Uplands, Scotland. GFF 128, 195–202.

Waltham, D., Gröcke, D.R., 2006. Non-uniqueness and interpretation of the seawater $^{87}Sr/^{86}Sr$ curve. Geochim. Cosmochim. Acta 70, 384–394.

Wang, K., Chatterton, B.D.E., Wang, Y., 1997. An organic carbon isotope record of Late Ordovician to Early Silurian marine sedimentary rocks, Yangtze Sea, South China: implications for CO_2 changes during the Hirnantian glaciation. Palaeogeogr. Palaeoclimatol. Palaeoecol. 132, 147–158.

Widom, E., Gaddis, S.J., Wells Jr., N.E., 2004. Re–Os isotope systematics in carbonates from Serpent Mound, Ohio: implications for Re–Os dating of crustal rocks and the osmium isotopic composition of Ordovician seawater. Geochem. Geophys. Geosyst. 5, Q03006.

Wilde, P., Berry, W.B.N., Quinbyhunt, M.S., Orth, C.J., Quintana, L.R., Gilmore, J.S., 1986. Iridium abundances across the Ordovician –Silurian Stratotype. Science 233, 339–341.

Williams, S.H., 1983. The Ordovician–Silurian boundary graptolite fauna of Dob's Linn, southern Scotland. Palaeontology 26, 605–639.

Williams, S.H., 1986. Top Ordovician and lowest Silurian of Dob's Linn. Geol. Soc. (Lond.) Spec. Publ. 20, 165–171.

Williams, S.H., 1988. Dob's Linn—the Ordovician–Silurian boundary stratotype. In: Cocks, L.R.M., Rickards, R.B. (Eds.), A Global Analysis of the Ordovician–Silurian Boundary: Bull. Brit. Mus. (Nat. Hist.) Geol., 43, pp. 17–30.

Williams, G.A., Turekian, K.K., 2004. The glacial–interglacial variation of seawater osmium isotopes as recorded in Santa Barbara Basin. Earth Planet. Sci. Lett. 228, 379–389.

Yan, D., Chen, D., Wang, Q., Wang, J., Wang, Z., 2009. Carbon and sulphur isotopic anomalies across the Ordovician–Silurian boundary on the Yangtze Platform, South China. Palaeogeogr. Palaeoclimatol. Palaeoecol. 274, 32–39.

Young, S.A., Saltzman, M.R., Bergström, S.M., Leslie, S.A., Chen, Xu, 2008. Paired $\delta^{13}C_{carb}$ and $\delta^{13}C_{org}$ records of Upper Ordovician (Sandbian–Katian) carbonates in North America and China: implications for paleoceanographic change. Palaeogeogr. Palaeoclimatol. Palaeoecol. 270, 166–178.